Galaxy Assembly through Mergers

Uncovering Dry and Non-dry Mergers in the SDSS

Paula Brochado

Departamento de Física e Astronomia da
Faculdade de Ciências da Universidade do Porto

December 2012

Galaxy Assembly through Mergers

Uncovering Dry and Non-dry Mergers in the SDSS

Paula Brochado

Thesis Advisors
Dr. Jarle Brinchmann and Dr^a. Catarina Lobo

Thesis submitted to the Faculdade de Ciências da
Universidade do Porto to complete the degree of Ph.D. in Astronomy

Departamento de Física e Astronomia da
Faculdade de Ciências da Universidade do Porto

December 2012

To my mom, my dad and my husband.

Acknowledgments

"Not everything that can be counted counts, and not everything that counts can be counted."

W. B. Cameron, 1963

Simply put, and as romantic as it sounds, this project would not have been possible without the people that I thank in the following lines. They have been here with me, in many ways, since the very beginning of this journey.

First and foremost, I am deeply grateful to my supervisors Jarle Brinchmann and Catarina Lobo from whom I have learned much more than I can possibly grasp. Catarina has been a part of my path ever since I took my first steps in astronomy, as a young undergraduate. I thank her dedication and support throughout these years, while I tried to find my way through science.

More than a supervisor, Jarle has been a mentor. I feel lucky to have had the guidance of such a brilliant scientist and a wonderful person. The invaluable lessons he has taught me from day one, never settling and always questioning, are the cornerstone of the astronomer I aim to become. His endless patience, enthusiasm and care when teaching me, from the most basic lines of code to the most complex scientific analysis, is something I will definitely nurture for years to come, along with the sense of wonderment he embedded in me. Thank you Jarle.

I thank my parents from the bottom of my heart. They have always, unconditionally, encouraged me to follow my dreams, especially this precious dream of becoming an astronomer. They have taught me where there is a will there is a way, always cherishing my silliest ideas and showing me how to make the best out of them. Thank you for your tremendous support and above all for your inspiration.

I thank Rupes, who has been holding my hand for more than a decade now. He has always been there, challenging me, dreaming with me, every step of the this bumpy

way. I imagine that putting up with me when I started rambling about galaxies was sometimes not easy, but you always listened. I treasure how you always found a way to make me smile and a word to comfort me. Thank you for being my safe haven.

My friends have been the backbone of my life, especially in the last few years. Ana and Pedro, my partners in crime, thank you for bearing with me in the most turbulent of times, never leaving my side. I thank you for the care, for the non-sense, for fighting against and with me never scratching our friendship and for those memorable moments – whether on stage, at a dinner table or in the middle of a forsaken road with our helmets on. My Twine Luísa, with whom I have been sharing the ups and downs of this learning process ever since I started my academic voyage, and João, have kept me anchored to what really matters in the later stages of this work. I am eagerly looking forward to fulfill our long-lasting goal of raising a glass in Times Square, as I am to break ice with a spoon for many more winter drinks. I have also been lucky to have made new friends during this time – with whom would I discuss astronomy as passionately as football if not with my Italian friend Daniele? – and to have deepen ties with old ones, seeing them grow inside and outside astronomy – I believe we will be sharing stories over many RENA dinners yet to come. I am truly surrounded by beautiful people, places and stories, including an angel, a warmhearted city, a half-smile and a wonderfully crazy family.

I also want to leave a heartfelt thank you to Doctor Alice Marques. With her help, I am here, now, presenting this work and I am finally able to look back with a smile.

I acknowledge CAUP, my host institution, and I thank Sterrewacht Leiden for the valuable support during my stays in the Netherlands. In particular, I would like to thank Professora Teresa Lago for pointing me towards the right direction ever since I had my very first astronomy class and my collaborator Mercedes Filho with whom I expect to be working and sharing successes in the coming years. I thank in a very special way Joana Ascenso who has been not only a great friend but a teacher, and Joana Sousa, with whom I started this experience a few years ago and have seen our friendship grow much more beyond astronomy. Along with Joana and Joana, I also shared my office with Rui, Bruno and Jorge. I will certainly miss our time together, our conversations, our shared fears and our unbeatable certainties. I also thank my very good friend Nelma for her support in critical moments, being a right-hand throughout this time.

Without music, life would be a mistake, Nietzsche once wrote, and indeed music, like astronomy, is part of what I am. I thank Coral de Letras da Universidade do Porto

for allowing me to sing some of the best music ever composed and for giving me great moments of joy after a day's work. I would also like to thank my good friend and composer Daniel for one of the most exquisite experiences that came out of this thesis: a music made from Figure 2.16. Inspiration definitely comes in many forms, shapes and colors. Just like galaxies.

The last few years have been nothing short of a roller coaster ride – they have taught me more about science, myself and others, than I could possibly imagine. I cannot wait for the rides that are still yet to come.

Abstract

The assembly of new galaxies through mergers of galaxies already in place has been long studied as a path of galaxy formation. Within this hierarchical model, where larger structures are built from smaller ones, more massive galaxies can then be assembled from less massive galaxies, thus contributing to shape the galaxy mass function. However, disentangling the role of mergers in the build up of this mass function is a complex process, not only due to the short timescales involved, at a cosmic scale, but to the nature of the phenomenon itself. On one hand, in the case of spiral, gas-rich mergers, the encounter can give rise to a series of events, from bursts of star formation to severe morphological changes. On the other hand, for mergers between elliptical, gas-poor galaxies, the apparent absence of strong perturbations poses another challenge, even though, given their massive nature, they may be responsible for the high mass end of the mass function. Understanding the latter in the local universe, dubbed dry mergers, constitutes the basis of this work.

With the availability of large dedicated surveys such as the Sloan Digital Sky Survey (SDSS), the sheer amount of information obtained for millions of galaxies, over years of operation, has allowed to take the first steps in understanding the role of mergers in galaxy assembly, mainly because they are able to provide data on different types and stages of interaction.

To build a sample of potential merging systems for the redshift interval $0.005 < z < 0.2$, we have made use of the spectroscopic catalogue of galaxies from the 6^{th} Data Release (DR6) of the SDSS, since having information on the spectroscopic redshift of the galaxies was paramount to establishing their potential merging status. Nevertheless, the photometric catalogue of galaxies from the SDSS DR6 was later added for completeness, dramatically increasing the number of presumed mergers and, therefore, the quality of our results.

Using a set of proximity criteria based on spectroscopy – a projected separation

between galaxies no larger than 30 h^{-1} kpc and a velocity offset of at most 800 km/s – a sample of ∼4000 potential mergers was obtained, including ∼ 700 dry mergers, the biggest sample of these type of mergers known to date. The study of this set of galaxies, unravelled the role of gas-poor mergers, which are typically mergers between the highest mass galaxies known, in the galaxy mass function – up to 15% of the most massive end of the mass function, with stellar masses above $10^{11} M_{\odot}$, has been involved in dry mergers since $z = 0.2$. We have also shown that the putative remnants of these mergers have stellar masses consistent with the most massive galaxies in the SDSS DR6 and their combined stellar populations are similar to those of isolated galaxies of the same (combined) mass.

Taking advantage of a merger sample of this magnitude, we have also analysed other properties of galaxies with neighbours, but now focusing not only on gas-poor but on also gas-rich mergers. As expected we find a significant increase in the star formation activity when the galaxies are close together, but, contrary to what could have been expected, we find a decrease in the fraction of AGN host galaxies. We interpreted both results as a classification issue, as the *veiling* of the AGN emission lines by the star forming component.

Probing the central parts of galaxies, we have also studied the gas dynamics of these regions when galaxies are nearby, usually below 10 kpc, by comparing them to a set of isolated, yet similar, galaxies. Surprisingly, we have found that they appear to behave as closed boxes where the increased star formation activity gives rise to an increase of metallicity and a decrease in the ratio of gas-to-stars. A subsequent blind analytical study has confirmed the observed trends, further supporting this scenario.

Contents

List of Tables

List of Figures

Chapter 1

Introduction

Out of the many sciences encompassing the most diverse fields of knowledge known to us, astronomy is the only one where the object of study is, literally, outside our world. From asteroids to clusters of galaxies, the wide variety of disciplines inside astronomy have this peculiar property - out of what we see in a very short instant of the cosmic history, a complete story is built hoping to explain a single snapshot. The field of extragalactic astronomy is no different and understanding how the galaxies we observe came to be as we see them today is a story still to be completed.

Attempting to tell this story is, by itself, a daunting task. The overwhelming number of galaxies we know by now and the astonishing differences between them, from red to blue, from dwarf satellites to giant cannibals, from young and star forming to old and dead, there are no two galaxies alike. Nevertheless, because we are curious beings by nature, this has not stopped us, nor will it for the next decades, from trying to understand why the galaxies are the way they are, how and when were they formed, what is their story as a whole and what makes each one different.

One of the discoveries made in the last few decades is that one of the paths leading to the assembly of new galaxies is the merger between already existing galaxies: the study of this process has shed some light into theories concerning galaxy formation and, simultaneously, has given rise to other questions.

In this PhD project, an attempt is made to answer some remaining questions, inevitably raising further ones, about galaxy assembly through mergers and, in particular, of mergers between old, red and dead galaxies.

1.1 Galaxies in the universe

Even when the Earth was the center of the universe, the different points of light in the celestial sphere were already arising curiosity among sky gazers. Long before Galileo made use of a telescope to establish that the Milky Way is composed of a very large number of stars in 1610, the Andromeda galaxy and the Magellanic Clouds were subject of scrutiny due to their nebulous nature. With the development of new telescopes, what seemed to be a blank space between stars and nebulae seen with the naked eye, started to be filled with other stars, other planets, their moons and even other nebulae. When Edwin Hubble observed some of those nebulae in 1936 and realized that not only were they not part of the Milky Way but they were also made of stars, the classical definition of galaxy was born and with it ended the debate regarding the reality of "island universes".

Less than 20 years ago, the Hubble Space Telescope gave us a glimpse of that blank space creating the Hubble Deep Field North (HDF, Williams et al. 1996) image, seen in Figure 1.1, where, with few exceptions, every point of light is neither a star nor a planet, but in fact a galaxy when the Universe was 1 billion years old. As the emergence of other powerful instruments ended up proving, the galaxies are indeed the building blocks of our universe and, regardless the direction we look at, their distribution is quite similar.

The myriad of galaxies shown in the HDF image range from high to low luminosity galaxies, from blue to red and, even more interestingly, from very young galaxies in the early stages of their formation to fully assembled galaxies. Galaxies with spiral and disky structures, alongside galaxies without any particular recognizable pattern, can both be easily identified through their bright blue colors indicating the presence of newly formed stars. Large red galaxies evolving quietly and small galaxies with their colors reddened by their always growing distance, are also clearly spotted among the thousands of objects. Even though there are not two galaxies alike, these general

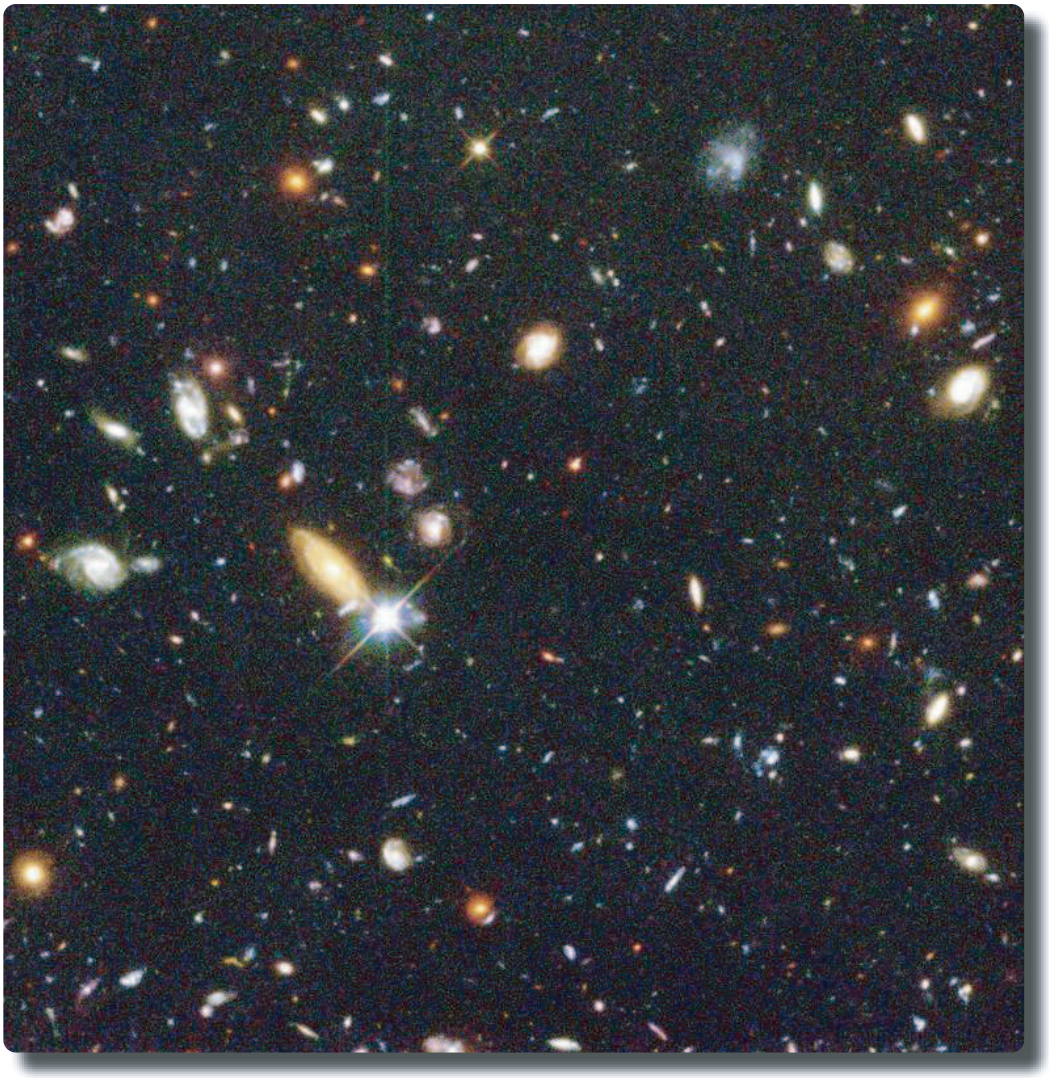

Figure 1.1: The Hubble Deep Field taken with the Wide Field Planetary Camera 2 from the Hubble Space Telescope (Williams et al. 1996). *Credit: R. Williams (STScI), the Hubble Deep Field Team and NASA*

properties were noticed by Edwin Hubble. He designed a morphological classification, the so-called Hubble Sequence (illustrated in Figure 1.2, where galaxies are divided into four broad classes: ellipticals, lenticulars, spirals (barred and non-barred) and irregulars. The first two are commonly referred to as early-type galaxies and the latter two are known as late-type galaxies, a useful reference to their position on the diagram.

In fact, the diversity of galaxies in the Universe becomes even greater considering that the Hubble sequence of the present-day Universe may have not always been like this, Figure 1.2. Hammer et al. (2009) found that 6 billion years ago the number of peculiar galaxies was much higher and suggest that, interestingly, mergers and interactions were responsible for the shape of the galaxies in the actual Hubble Sequence.

The similarity between the way galaxies are arranged in the sky regardless of the direction we observe, is illustrated in HDF and its subsequent counterpart, the HDF-South (Williams et al. 2000), as well as the Hubble Ultra Deep Field (HUDF Beckwith et al. 2006), a much deeper version of the HDF going up to redshifts between z=7 and z=12(Bouwens et al. 2010, 2011), taken in yet another direction. Designated as the cosmological principle, this *uniformity* of the Universe is also present in the cosmic microwave background (CMB) radiation (Penzias & Wilson 1965), created during the first moments of the universe as explained by the Big Bang model. The CMB radiation has been shown to have a thermal black body spectrum peaking at the low temperature of 2.725 K in the microwave range. The structure in the map, seen in Figure 1.3 as measured by the Wilkinson Microwave Anisotropy Probe (WMAP [1]) satellite (Bennett et al. 2003), is due to minute variations in the temperature distribution. In turn, these differences in temperature are the imprint of the fluctuations in the density of the early universe that later gave rise to the structure observed today. This pattern represents the backbone of the distribution of matter of the observable universe, as most of the galaxies are placed along this structure, making up the walls, filaments and voids known as the large-scale structure of the cosmos.

1.2 Galaxy formation and evolution

Despite our knowledge of the importance of galaxies in the universe, how exactly a galaxy is formed is a question that, so far, no one can answer. Many theories have been

[1] http://map.gsfc.nasa.gov/

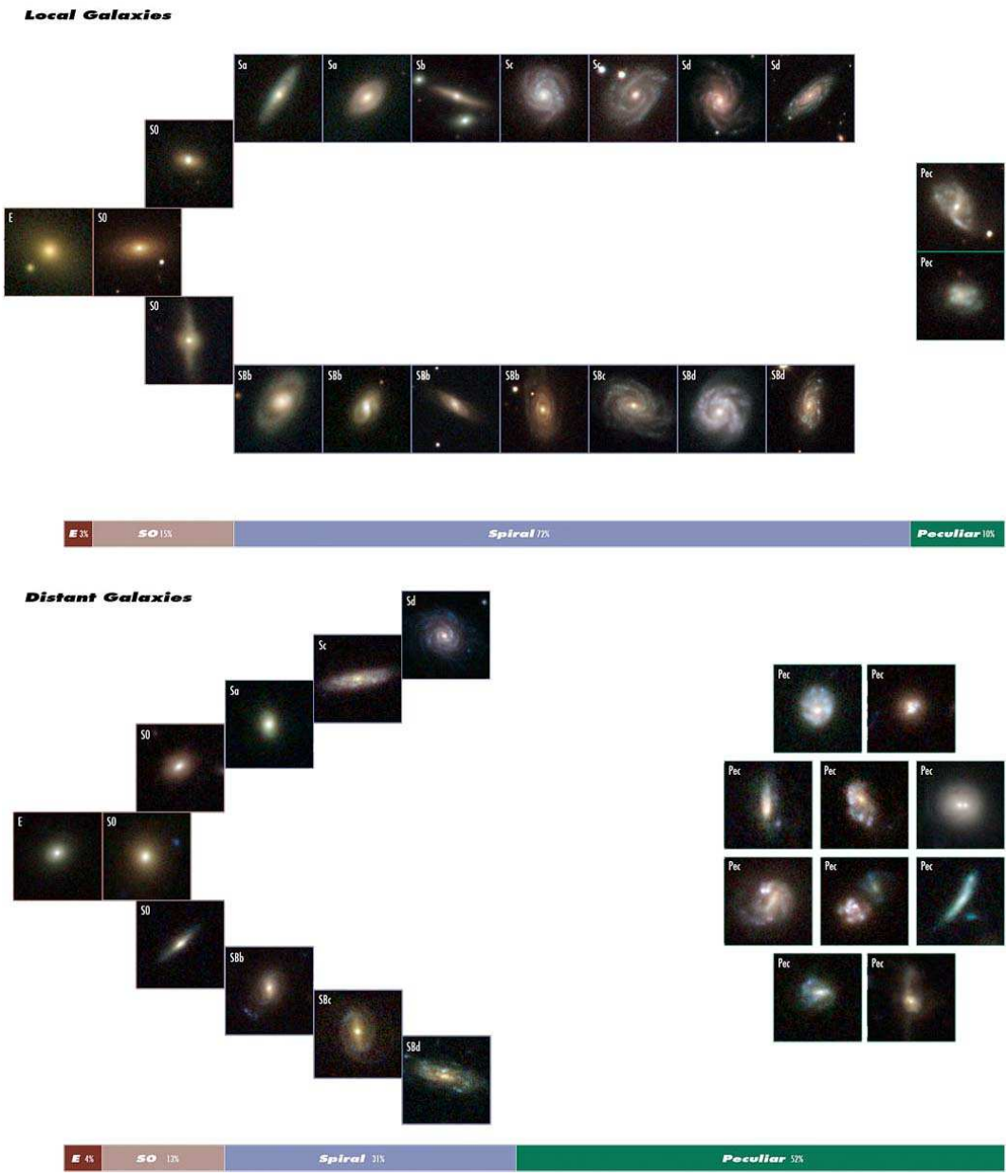

Figure 1.2: The evolution of the Hubble Sequence. The upper diagram represents the Hubble Sequence for the present-day Universe. The lower diagram illustrates the galaxy distribution 6 billion years ago - peculiar galaxies, much more common in the past, must have become the spiral galaxies of today (Hammer et al. 2009). *Credit: NASA, ESA, SDSS.*

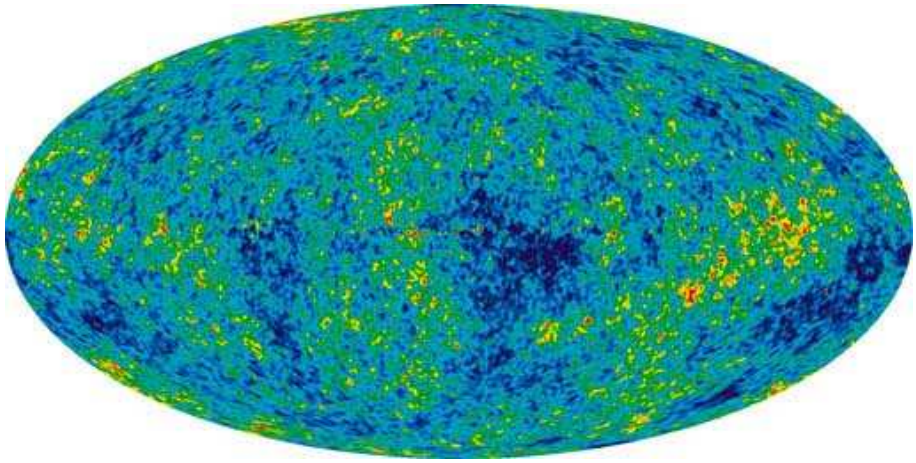

Figure 1.3: Image of the microwave sky created from seven years of WMAP data, after subtraction of the signal of our Galaxy. The different colors represent the temperature variations in the early stages of the universe. Red regions, indicating higher temperature, correspond to what would later become overdense regions whereas the blue and green colors indicate what would later become less dense regions, however within both galaxies will be formed . *Credit: NASA and the WMAP Science Team.*

proposed over the years and some have been refined through time and endured against cutting-edge data. A galaxy formation theory should be able to account not only for the galaxies themselves - e.g. their gas and stellar contents, their morphologies - but also for the known properties of groups and even clusters of galaxies. Moreover, it should reconcile the long known disparity between high- and low-luminosity galaxies and be able to include what in fact has been shown to be the dominant component in the universe: non-luminous, or dark, matter.

1.2.1 The ΛCDM paradigm

The existence of dark matter has been postulated to account for the disparity between the measured luminous matter of the galaxies and its dynamical behaviour - e.g. orbital velocities in clusters and the galactic rotation curve (Bertone et al. 2005). The majority, approximately 80% of the total mass (e.g. Jarosik et al. 2011), of the gravitating matter in the Universe is made up of non-baryonic matter that could theoretically be composed by particles with a wider range of velocities. What is most commonly done is to assume that the dark matter is made up of a single type, or at most a mixture of a couple. The most common is to assume that dark matter is either hot or cold (e.g. Kolb & Turner 1990). Hot dark matter is envisaged to be made up

by very small mass particles which stayed relativistic until the epoch of decoupling, in contrast to hot dark matter, particles in cold dark matter are more massive with lower velocities. The Hot Dark Matter (HDM) model was however unable to reproduce the known structures of the Universe because the high velocities of the dark matter particles meant that they would stream out of any perturbations smaller than the horizon scale at the time of decoupling (when ordinary matter could start to collapse gravitationally free from the influence of photons). This meant that any perturbations smaller than this scale would be washed out. The success of the Lambda-Cold Dark Matter (ΛCDM) model (where the Λrefers to the cosmological constant associated with the dark energy component) resulted from the ability of describing the Universe seen today, since the lower velocity particles of the CDM would be able to cluster together and start forming larger structures from smaller ones (e.g. Springel et al. 2008).

Nowadays, there is general consensus that the process of structure formation follows this path as predicted by the ΛCDM where structure formation and growth happens in a hierarchical manner, with larger objects being formed at later times. This "standard model of cosmology" states that the foundation of the cosmic structure is based on non-baryonic cold dark matter and that baryons, i.e. normal matter, trace the dark matter. The gravitational collapse of the baryons, namely gas, gives rise to galaxies inside a DM halo and, for larger scales, to groups and clusters that, linked together, form the sheets and filaments of the large scale structure of the universe (Springel et al. 2006, 2008; Diemand & Moore 2009). This model has been very successful in reproducing the nearby observed structure. Recent observational extragalactic surveys, such as the Sloan Digital Sky Survey (SDSS York et al. 2000) and the 2dF Galaxy Redshift Survey (2dFGRS Colless et al. 2003), bear incredible resemblance to mock galaxy surveys, such as the Millennium simulation (Springel et al. 2005c), as seen in Figure 1.4.

The diverse nature of the galaxies seen in the local universe has however inspired different theories through the years. The so-called monolithic collapse scenario (e.g. Larson 1975), for instance, emerged first to explain the structure of the bulge of the Milky Way (Eggen et al. 1962) and gained some strength due to the apparent simplicity of elliptical galaxies - these systems seem to have their stars formed early on in a single burst of star formation and now appear to be passively evolving. This hypothesis, however, not only was confined to elliptical galaxies but it was also not supported

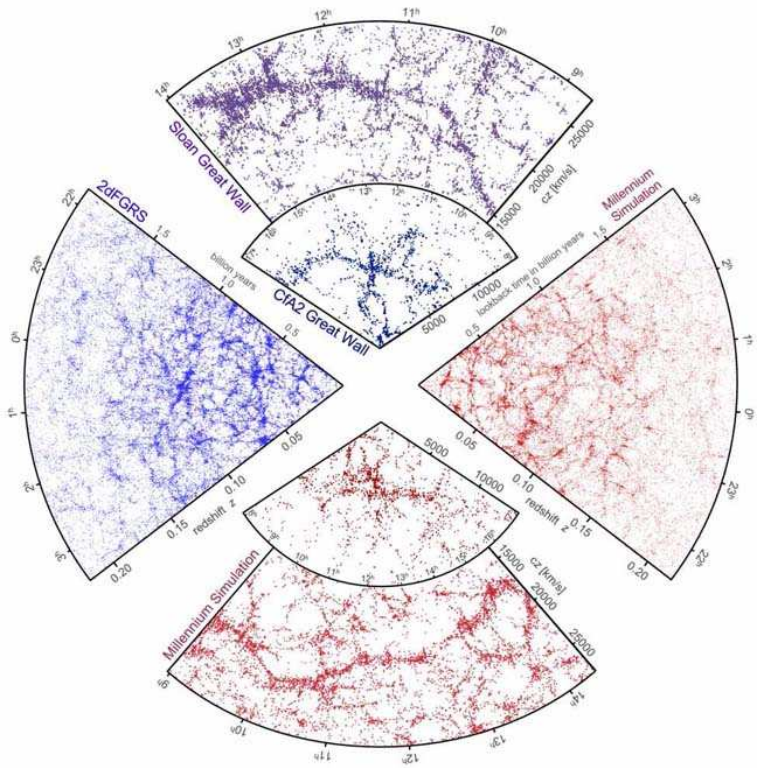

Figure 1.4: The galaxy distribution obtained from spectroscopic redshift surveys and from mock catalogues constructed from cosmological simulations. The red slices indicate the mock galaxy surveys built using the Millennium Simulation and the blue slices the observed distribution of galaxies. The top and bottom slices show the structure at lower redshifts (up to z∼0.08) and consist of (top slice) a small section of the SDSS and of the CfA2; and (bottom slice) of the mock survey. The right and left slices illustrate the distribution at higher redshifts taken from the 2dFGRS and from the Millennium Simulation, respectively. (Springel et al. 2006)

by any cosmological model. Nonetheless, adding to a hierarchical model a dissipative stage at smaller scales (specially to form the inner parts of the galaxies), White & Rees (1978) reproduced the observed luminosity function, showing that a galaxy formation theory is a complex process. More recent efforts to construct a comprehensive theory of galaxy formation within the frame work of ΛCDM structure formation, have been focused on reproducing the observations in the present-day universe, in particular the galaxy luminosity function.

1.2.2 Reproducing the Galaxy Luminosity Function

The galaxy luminosity function (GLF) is the distribution of the number of galaxies, per unit volume, in a given luminosity interval (Schechter 1976). Since a luminosity distribution implies a mass distribution as well, the information enclosed in the GLF, i.e. how many galaxies of a given mass have been formed, is crucial to build any galaxy formation theory. Schechter (1976) proposed an analytic expression (Equation 1.1) to fit the luminosity function of a set of clusters composed of a power law, dominating at low luminosities, and an exponential function for the higher luminosities.

$$\phi(L)dL = \phi^*(L/L_*)^\alpha \; e^{-L/L_*} \; d(L/L_*) \tag{1.1}$$

Shown in Equation 1.1 is the analytic expression for the Schechter function, with $\phi(L)dL$ being the number of galaxies per unit volume in the luminosity interval $[L, L+dL]$; and α, ϕ^* and L_* being free parameters to be determined for the particular set of data under analysis. The L_* corresponds to a *characteristic (bright) luminosity*, where the function rapidly changes its slope. The shape of this function, dubbed the Schechter Function, seen in Figure 1.5 for the galaxies in the clusters studied by Schechter (1976), reveals that fainter galaxies are quite common whereas very luminous galaxies are very rare. Schechter obtained a value of -1.24 ± 0.05 for the power-law index α. However, the Schechter function is not universal and LFs for different morphological classes or even environments yield slightly different values for the power-law index, typically between $-1 < \alpha < -2$ (e.g. Binggeli et al. 1988; Marzke et al. 1998; Yagi et al. 2002).

Reproducing the luminosity functions for galaxies in the local universe in a ΛCDM scenario has been challenging (e.g. White & Frenk 1991; Navarro et al. 1996; Heyl

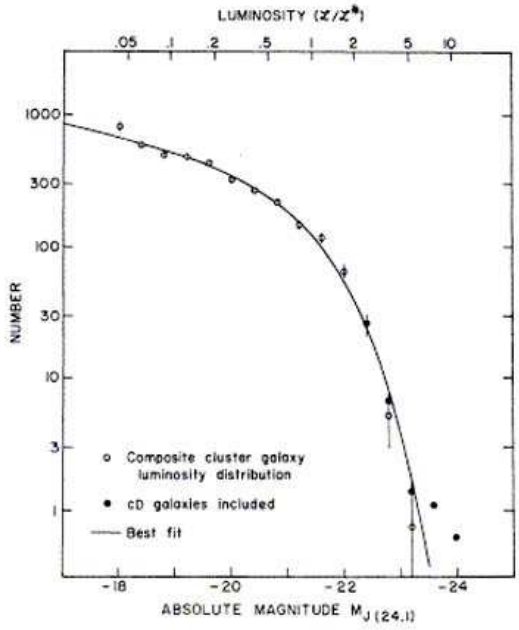

Figure 1.5: Best fit of Equation 1.1 to observed composite galaxy luminosity distribution for 13 clusters. Filled circles show the effect of including cD galaxies in composite. Schechter (1976)

et al. 1995), in particular, models consistently found more blue galaxies than seen in the observations. By tracing in detail the merging histories of an assemble of dark matter halos, Kauffmann et al. (1993) reproduced the observed trends in luminosity, color, gas content and morphology of galaxies, but predicted an excess in the B-band luminosity density of a factor of 2. Either the models were over predicting the number of dark matter halos or some halos were still observationally undetectable. Another possible explanation would be that galaxy properties are not only defined by the large scale merger of dark matter halos, but also by intrinsic processes within the galaxies themselves contributing to their evolution and, as a result, to their place in the luminosity function.

The first clues towards this latter hypothesis were highlighted with studies using semi-analytic models to calculate luminosity functions in the K-band, which is more closely related to the stellar mass than the blue luminosity used previously. Finding evidence that shows that the number of massive galaxies at $z \sim 1$ is already below the local value, the premise of massive galaxies passively evolving since $z = 2$ was refuted and new support of the idea of having massive galaxies still forming nowadays emerged (e.g. Kauffmann & Charlot 1998; Kauffmann & Haehnelt 2000). In other words, the

problem would not be in the number of predicted halos. Moreover, Baldry et al. (2004) found a bimodal behaviour on the (u-r) color vs. M_r absolute magnitude plane of local ($z < 0.08$) galaxies. This bi-modality is composed of blue and red distributions and even more revealing is the clear trend for more massive galaxies occupying the red distribution. The number density per magnitude of the red distribution overtakes the blue distribution at $\sim 3 \times 10^{10} M_{\odot}$, thus indicating that, at bright magnitudes, the majority of the galaxies are on the red sequence and that the early models of galaxy formation tended to predict significant numbers of massive blue galaxies.

These results pointed in the direction of a theory where massive red galaxies are formed through merging of smaller objects along with other processes that would redden the galaxy to the local observed measurements. Processes like feedback from stars and central super-massive black holes have long been thought to play a significant role in galaxy formation (Dopita 1985; Dekel & Silk 1986; Haehnelt 1995; Silk 1997; Kereš et al. 2005; Di Matteo et al. 2005). Stripping the newly assembled galaxy of its gas through feedback would extinguish the formation of new stars and the stellar populations already in place would continue to age into a red massive galaxy, in agreement with Baldry et al. (2004).

In fact, recent studies have come to confirm the importance of these processes - several studies have shown using hydrodynamical simulations that in addition to a burst of star formation during a major gas-rich merger, winds arise from the accreting central super-massive black holes and the gas is swept away resulting in a gas-poor remnant. Because during the merger phase tidal interactions have driven the gas towards the inner regions of the new assembled galaxy, the active galactic nuclei (AGN) outflows, that emerge sensibly 0.5 Gyr after the first passage of the two galaxies, remove sufficient gas to halt star formation activity and the remnant stellar population evolves rapidly to red colors(e.g. Di Matteo et al. 2005; Springel et al. 2005b; Bower et al. 2006; Croton et al. 2006). This is however one possible scenario and it is not very well understood yet.

In the hierarchical context of ΛCDM theory, galaxies form first inside dark matter halos and other larger systems are formed subsequently by accretion and merging (e.g. Hogg 2006). Studying the merger of galaxies - with galaxies being the basic ingredients of the so-called "cosmic web"- is therefore the very first step to directly corroborate the hierarchical nature of the ΛCDM paradigm.

Even though galaxy merging is a path to form new galaxies from two (or more) progenitor galaxies, it is convenient to separate the different processes leading to a new galaxy, namely, the *assembly* of the galaxy and its *formation*. While the first term alludes, in general, to the shape of the new galaxy into which the progenitor galaxies have been transformed, the latter refers to the formation of its stellar population. Regarding the galaxies' stellar populations, they may already be in place without significant transformation during the merger or they can, indeed, be strongly affected by the event.

1.3 Galaxy interaction and merging

Once thought to be "island universes", it is now widely accepted that most of the galaxies known in our universe have undergone some type of interaction at some point of their lives. The consequences of a merger event are controlled by a series of factors from the mass ratio of the galaxies to the relative velocity of the encounter and even their relative position at the time of the first passage - there are thousands of observed interacting galaxies, in very diverse stages of their encounters and in a wide range of shapes, mass ratios and relative velocities.

1.3.1 Dynamical processes

Gravitational interaction between galaxies tends to significantly affect their morphology (e.g. Toomre & Toomre 1972; Schweizer 1986; Mihos 1995; Lotz et al. 2008a,b), sometimes beyond recognition, and if they end up merging, the final galaxy can be of a completely different nature from the progenitors. The study of interacting galaxies started more than half a century ago, with Fritz Zwicky in his study of morphological features of intergalactic matter (Zwicky 1953) and, to this date, the best known type of interaction is between spiral galaxies. Due to their violent transformation during the process of interaction, and eventual merging, the interaction of spiral galaxies is not only likely to change significantly the morphology of the galaxies, with the creation of bridges between the interacting galaxies and tails due to tidal forces, but often produces bursts of star formation (Li et al. 2008). These eye-catching events make this type of mergers suitable for subsequent observations and, until very recently, these

were indeed thought to be the only types of mergers worth of note.

The degree of transformation of a galaxy due to a close encounter is not easy to estimate. The spectrum of galaxy interactions is very wide and if it includes the final merger of the galaxies, is even wider. However, when exactly a system of interacting galaxies ends up merging into a single object, is more often than not determined by the velocity at which they first encountered each other - in the frame of reference of the more massive galaxy, if the velocity of the infalling galaxy is smaller than the escape speed, they become gravitationally bound and more often than not the encounter will end in a merger. With respect to **proximity**, *close* encounters can lead to mergers if, as mentioned, the passing galaxy becomes gravitationally bound to its companion. On the other hand, *distant*, or weak, transits are usually characterised by "flybys", slightly disrupting the galaxies due to tidal effects, but not necessarily leading to a merger (Toomre & Toomre 1972; Park & Hwang 2009; Mihos et al. 1992).

Concerning their **mass ratios**, not all mergers induce significant changes in the galaxy morphologies, as is the case of satellite mergers, *i.e.* mergers between galaxies with very different sizes, or masses. These mergers are usually denoted as *minor* mergers and, by contrast, mergers of galaxies that have relatively similar masses are called *major* mergers. In the literature, the frontier for the mass ratio between the members of a merger is usually set at $\frac{1}{3}$, with minor and major mergers having mass ratios, respectively, below and above this limit (Lin et al. 2004; Bell et al. 2005; Bundy et al. 2007; Ciotti et al. 2007; Bundy et al. 2009).

The **environment** in which galaxies are immersed also determines the nature of the interaction. It might be expected, that interactions and mergers would happen with higher frequency in more crowded environments, as is the case of clusters of galaxies where the greater number of galaxies could enable merger events more easily. However, the high velocities that galaxies experience inside the cluster tend to inhibit slow passages and, as a consequence, potential mergers (e.g. Mihos 2003). Even though the contributions of the different processes inside a high density environment, and how they are intertwined, are far from fully understood, some types of interactions are already well studied. In summary it is possible to categorize some of those types of interaction and/or merger, that produce somewhat significant changes in the galaxies, as follows:

- Cannibalism (e.g. Hausman & Ostriker 1978; Lequeux et al. 1998) - This type of

interaction, and eventual merger, refers to the phenomenon of smaller galaxies being accreted by the central galaxy in a cluster of galaxies. As a consequence of this process, the central galaxy is usually the brightest and it keeps increasing its luminosity and mass with the increasing number of in-falling galaxies. As long as the passing galaxy passes through the outer envelope of the central galaxy at a relatively low velocity it will end up being cannibalized.

- Harassment (e.g. Moore et al. 1996, 1998; Lake & Moore 1999; Barazza et al. 2009) - Frequent (at least once per Gyr) high-speed encounters of several thousand km/s between galaxies, where the largest galaxies with luminosities typically $\geq L_*$ gravitationally act on smaller ones, disrupting the lower luminosity galaxy and removing mass without being significantly altered themselves. After a few rapid encounters the harassed galaxy tends to get a spheroidal shape and, in fact, this process is thought to be responsible for the formation of dwarf ellipticals in clusters. Moore et al. (1996) actually invoked this mechanism to explain the different morphologies seen in cluster at z$\sim$0.4, with a predominance of small disk galaxies, and at z$\sim$0 where dwarf elliptical galaxies are more common.

- Ram Pressure Stripping (RPS) (e.g. Abadi et al. 1999) and Strangulation (e.g. Kawata & Mulchaey 2008; Bekki et al. 2002) - These two processes, most dominant in gas-rich galaxies, like spirals, are not caused by the interaction with other galaxies but with the intracluster medium (ICM). Nonetheless, these interactions lead to spectral transformations of the affected galaxies, where the first signs of the changing stellar populations can be detected, and to morphological transformations as well. In the case of RPS, the ICM exerts a pressure on the interstellar medium of a galaxy moving through the cluster, stripping valuable gas from galactic disk inhibiting the formation of new stars. Strangulation, or starvation, refers to a similar process but the star formation is halted due to the hot gas being removed from the halo of the galaxy, by the interaction with the ICM. The ICM removes the gas due to the pressure it exerts on it and the necessary in-fall of gas from the halo to the disk, that once cooled would transform into stars, is quenched and the galaxy eventually stops its star formation.

These dynamical processes that interacting galaxies go through tend to introduce deep transformations in their physical properties. In fact, one can conjecture that only a very particular set of circumstances of the interaction of galaxies would not lead to significant changes on all galaxies involved. Encounters between galaxies have long been associated with the most extreme processes in galaxies. As mentioned above,

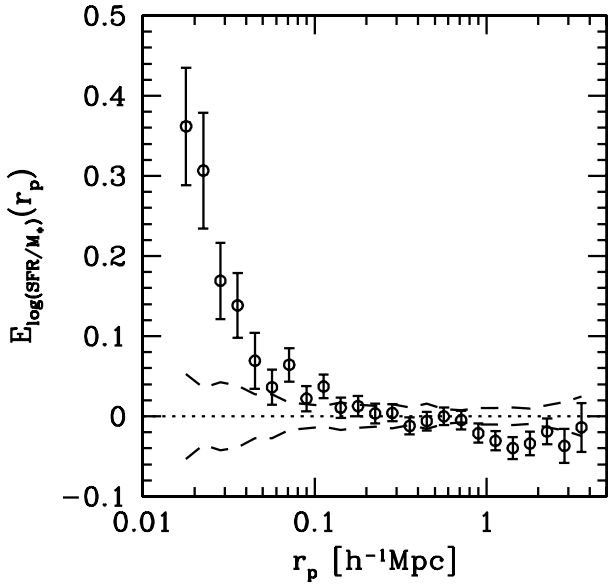

Figure 1.6: Star formation enhancement as a function of the projected separation, r_p from Li et al. (2008). The galaxies in the this sample have been spectroscopically confirmed as galaxies in the SDSS DR4 and have been selected to be star forming according to the classification by Kauffmann et al. (2003). This subset of galaxies shows a clear enhancement in their specific star formation rates at small distances between galaxies.

the triggered star formation induced by the interaction, and even merger, of gas-rich galaxies, usually spirals, is one of the most well studied interacting phenomena. Recent studies have shown that tidal forces generated in the interacting galaxies are efficient in triggering enhanced star formation by causing perturbations in the gas (e.g. de Grijs et al. 2003; Barton et al. 2007; Li et al. 2008), and this enhancement has been proven to be strongly dependent on the distance to the neighbour galaxy, see Figure 1.6.

Famous examples, among quite a few observed also by the Hubble Space Telescope, of this phenomenon is the galaxy M51 (also known as Whirlpool Galaxy) and the Antennae Galaxy, both shown in Figure 1.7. The bright blue and pink regions mark up intense star forming activity, but while in the case of the Antennae Galaxy this is the result of a merger between two spiral galaxies, the Whirlpool Galaxy exhibits this event as a result of the perturbations caused in its gas by the companion galaxy close to it. Other clear examples of interaction induced star formation are some ring galaxies, as illustrated in Figure 1.7 b), easily identified by their shape characterized by a bright ring of extreme star formation.

1.3.2 Transformation of galaxies via merging

The transformation of galaxies through mergers has long been theorized to be of great importance in galaxy evolution. Typically, during a merger event, at least one of the galaxies involved is likely to be completely transformed and since galaxies are thought to suffer a merger event during their life spans it is reasonable to assume that the importance of interactions in galaxy evolution is far from marginal.

Mergers involving gas-rich spiral galaxies are by far the ones that most dramatically change the structure of the galaxies involved. Major mergers of gas-rich, disk galaxies lead to the creation of bridges and tidal tails, inducing perturbations in the gas and creating sites of star formation. As simulations have repeatedly shown, the remnant of a major spiral merger has properties consistent with those of an elliptical galaxy, as the distribution of stars and available gas settles around the center of the already merged nuclei and its stellar populations evolve (e.g. Barnes & Hernquist 1996; Negroponte & White 1983; Barnes 1988; Barnes & Hernquist 1992; Springel et al. 2005a; Richard et al. 2010; López-Sanjuan et al. 2010). A recent study by Hopkins et al. (2009b) investigated the importance of gas (the key ingredient in spiral interactions) on the morphological changes in mergers and showed that mergers between gas-rich low-mass galaxies tend to produce bulgeless systems. On the other hand, minor mergers between spiral galaxies and small satellite galaxies do not tend to significantly disrupt the spiral galaxy but in turn contribute to the increase of the remnant bulge (Eliche-Moral et al. 2006).

Another particular type of transformation involving spiral galaxies is the head-on collision of a relatively small galaxy with the center of a spiral galaxy, producing the ring structures mentioned in Section 1.3.1 and shown in Figure 1.7. These interactions also depend on the relative velocity of the galaxies to define them as a merging system, as mentioned in Section 1.3.1. If they do merge, simulations of these collisions have shown that their late stages are compatible with the properties of giant low surface brightness galaxies (GLSBs), characterized by their unusual large and flat discs, whose origin remain uncertain (Mapelli & Moore 2009).

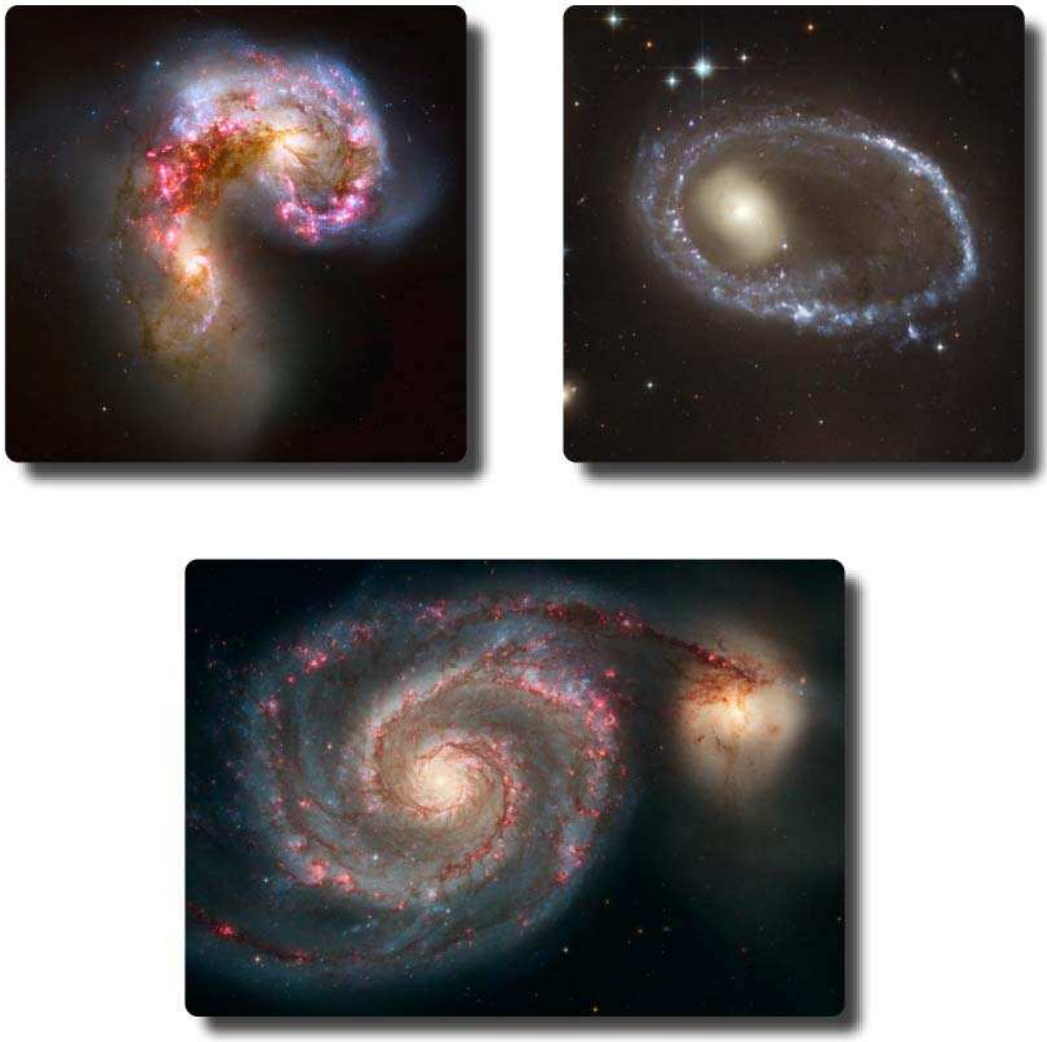

Figure 1.7: Interacting galaxies showing signs of triggered star formation. *Top Left* a) NGC 4038/4039 (Antennae galaxy), image 0.3' wide; *Top Right* b) AM 0644-741 ring galaxy, image 2' wide; *Bottom* c) M51 (Whirlpool galaxy), image 9.6' wide. These images are a composite of separate exposures taken with different filters - Johnson B (blue), Johnson V (green), Hα (pink) and near-infrared (red). The bright blue and pink colors - clearly seen in the Antennae galaxy, in the spiral arms of the Whirlpool galaxy and in the ring of image c) - indicate regions of active star formation, since the blue colors result from the very massive, and short lived, stars and the pink colors from the excited hydrogen atoms in the gas surrounding these sites of star formation. *Credit: NASA, ESA and the Hubble Heritage Team (STScI/AURA) - ESA/Hubble Collaboration*

Either way, the transformation of galaxies throughout a merger event is a complex process and, even though timescales for a complete merger are relatively small, 0.5 Gyr for galaxies separated up to $20\,h^{-1}$kpc (e.g. Lotz et al. 2008b; Patton et al. 1997), each of the several stages alters significantly the involved galaxies.

More than 30 years ago, Toomre (Toomre 1977) defined a sequence of perturbed merging galaxies where the main bodies of the galaxies, with prominent tails, appeared to be close. Adopting the same principle, an illustrative Toomre's Sequence of the galaxies in the merger sample used in this work, taken from the SDSS as described in 2, is shown in Figure 1.8. All of these systems are in obvious interaction and their morphologies are visibly, and severely, altered. Note how the last tile (bottom-right) already resembles an elliptical galaxy, even with the star forming pockets and some noticeable tidal features.

Nowadays, it is widely accepted that elliptical galaxies may be assembled through mergers of spiral galaxies, with their perturbed gas rapidly and massively turned into stars and the merging of the galaxies destroying their disky structure favouring the creation of a spheroidal shaped new galaxy.

1.3.2.1 The case for Milky Way

Our own Galaxy has more than a dozen neighbour satellites (e.g. Strigari et al. 2008). Among them are the well known Large and Small Magellanic Clouds and the Sagittarius dwarf spheroidal galaxy (Sgr dSph) known to be the most dramatic interaction case with the Milky Way. The Sgr dSph is responsible for some stellar streams observed in the Milky Way halo, both in the southern and northern Galactic hemispheres, indicating at least one passage through the Galaxy. However, first thought to have happened without significant disruption of the Milky Way's disk (Belokurov et al. 2006; Niederste-Ostholt et al. 2010), a very recent study by Purcell et al. (2011) suggests, through simulations, that the response of the Milky Way to the infall of the Sgr dSph results in the formation of spiral arms, also influencing the central bar. In recent years, several studies have shown the presence of tidal streams and over densities in the Milky Way disk and halo, suggesting minor interactions with several satellite galaxies in the Local Group (Newberg et al. 2002; Jurić et al. 2008; Newberg et al. 2009). In fact, the bar-shaped core of the Galaxy has been proposed to be the result of a merger event that happened 1.9 Gyr ago (Minchev et al. 2009). These

Figure 1.8: A "Toomre" Sequence of mergers in the SDSS, taken from the merger sample (2). From top-left to bottom-right, the mergers are sorted according to the descending projected distances of their members. Scale is varying in this composition from ∼50 kpc to ∼75 kpc on the side.

interactions should be expected, considering the ΛCDM model where objects like the Milky Way halo would be formed by assembling smaller structures in hierarchical manner, as mentioned previously in Section 1.2.1.

Details about the Milky Way interaction with some of its satellite galaxies will be revealed with the GAIA mission [2] from the European Space Agency (ESA). It will survey the Galaxy and the Local Group at an unprecedented scale obtaining positional and radial velocity measurements for about one billion stars.

1.3.3 Formation of early-type galaxies

Any galaxy formation theory should, obviously, explain the formation of the different types of galaxies seen throughout the sky. Early-type galaxies place crucial constraints on any model of galaxy formation since the bulk of the stellar content of the universe seems to be enclosed in these galaxies now more than ever. In a universe shaped by the ΛCDM model, our understanding of the role of mergers in the assembly of early-type galaxies depends therefore on our understanding of the galaxy mass function and the evolution of the stellar population.

The apparent simplicity of spheroidal galaxies, as is the case of elliptical galaxies, poses several challenges to a formation theory. Their uncomplicated morphology inspired the monolithic collapse model (e.g. Eggen et al. 1962; Larson 1975) where these galaxies would have been formed in a single efficient burst of star formation at high redshift, $z \gg 1$, passively evolving since then. Moreover, consistency in properties like the fundamental plane (e.g. Jorgensen et al. 1996) has strengthened the idea of a basic model for the formation of ellipticals. However, as mentioned in Section 1.2.1, this scenario of monolithic collapse is not reproduced by any cosmological model and this path has been used only as a simple reference model.

Concerning stellar populations, observations suggest that a) red, bulge - dominated and massive galaxies were already in place at redshifts $z = 2 - 3$ (Franx et al. 2003), b) a substantial part of the stars in local elliptical galaxies was already formed by $z = 1$ (Bell et al. 2004; Thomas et al. 2005; Bundy et al. 2006) and c) at very low redshifts, the majority of stars in the local universe is known to be locked up in red

[2] http://www.rssd.esa.int/gaia/

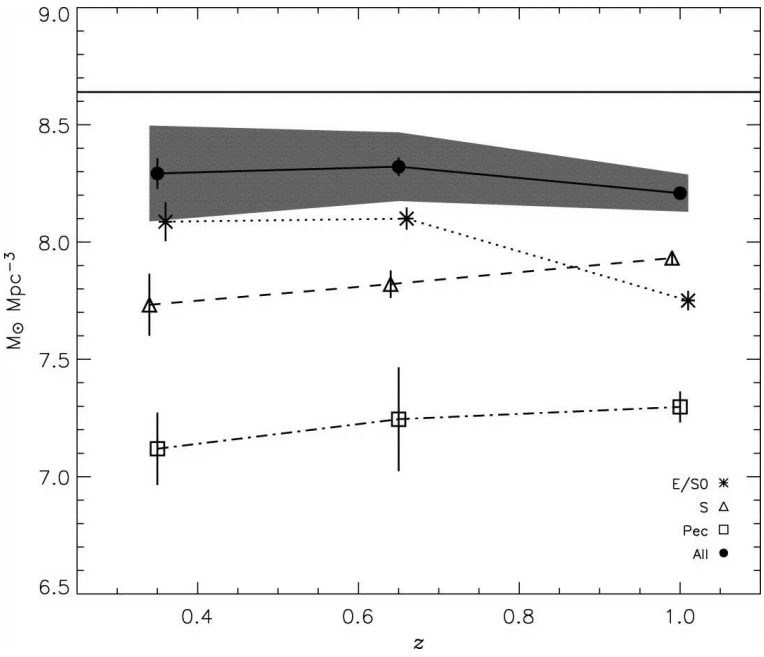

Figure 1.9: Integrated stellar mass density as a function of redshift, split by morphology (as indicated) and with a stellar mass cut of $M_* > 10^{11} M_\odot$ (Bundy et al. 2005).

galaxies (Hogg et al. 2002; Brinchmann et al. 2004). These results do not oppose the monolithic collapse scenario, but considering that star formation histories of early-types indicate they are still building up mass since $z = 1$ (Kaviraj et al. 2008) and that their number is higher now than it is at that redshift (Kauffmann & Charlot 1998), a theory predicting a formation at high redshift with a pure passive evolution is very difficult to reconcile with these results.

Furthermore, following Brinchmann & Ellis (2000), Bundy et al. (2005) found evidence indicating an increase in the total stellar mass enclosed in early-type galaxies since $z = 1$, as shown in Figure 1.9, with a simultaneous decrease in stellar mass density enclosed in spirals and peculiar galaxies. These trends suggest a transformation of blue star forming galaxies at $z = 1$ into the old objects observed in the present epoch and a merger scenario, where red galaxies are built at the expense of blue galaxies, arises as the natural explanation (Brinchmann & Ellis 2000; Bundy et al. 2007).

As mentioned above, mergers between disk galaxies, with young stellar populations, have long been thought to be one of the possible paths of elliptical formation (Toomre

& Toomre 1972; Barnes 1988; Barnes & Hernquist 1996). Such mergers can indeed account for some of the properties of elliptical galaxies: some luminous ellipticals show the presence of a fine structure consistent with a disk-disk merger (Schweizer et al. 1990); disk merger remnants appear kinematically very similar to observed ellipticals (Jesseit et al. 2007) and intermediate- to low-mass giant ellipticals show disky isophotes in good agreement with a binary disk merger (Naab & Burkert 2003). Differences between massive, typically with total masses $M > 10^{11} M_{\odot}$, and lower mass ellipticals, have also been found using early-type galaxies in the SAURON project: slow rotators, i.e. low angular momentum, tend to be bright and massive whereas low mass galaxies, $M_B \gtrsim -20.5$, are fast rotators (Emsellem et al. 2007).

However, there are also some properties not consistent with the creation of ellipticals through mergers of spiral, gas-rich galaxies. Massive ellipticals with boxy isophotes are not compatible with the remnants of a merger between disk galaxies (Naab & Burkert 2003). Furthermore, the mass in metals of elliptical galaxies is conflicting with predictions from models of spiral mergers which would produce an elliptical with low metal masses, and the stellar populations from disk galaxies and present day low and intermediate mass elliptical galaxies are only comparable if they had merged 3.5 Gyrs ago (Naab & Ostriker 2009).

Adding to this evidence, the number density of blue galaxies has remained nearly constant since $z = 1$, whereas the number density of massive red galaxies has increased (Faber et al. 2007) indicating that an important fraction of massive early-type galaxies must have been assembled at late times.

Regarding the formation of early-type galaxies it seems plausible to admit another path besides the merger of disk, gas-rich spiral galaxies. A possible way to reconcile these results is to postulate that some of these massive galaxies have been assembled through early-type, gas-poor, mergers where no new, or very few, stars are formed.

1.4 Mergers between gas-poor galaxies

Mergers between gas-poor galaxies are often called *dry* mergers, in reference to the lack of gas to form new stars during, or as a consequence of, the merger process. By

contrast, mergers between gas-rich galaxies, such as blue, star-forming, disk galaxies, have been dubbed *wet* mergers. The term *moist*, or *damp*, mergers is not as common but describes a merger, usually between early- and late-type galaxies.

In Figure 1.10 a representative set of the dry mergers issued from the merger sample used in this work, as described in Chapter 2, is shown. The contrast between the pairs of Figure 1.8 and Figure 1.10 is evident: the regions of bright blue colors of wet mergers are not seen in dry mergers, which are predominantly red, and there is a clear absence of prominent tidal features as tails and bridges in these pairs.

What exactly constitutes a gas-rich or gas-poor galaxy is somewhat arbitrary and to establish a clear difference between the two types of galaxies would neglect the continuous nature of galaxy properties. The amount of available gas in a galaxy and how much of that gas is available to form new stars is not easy to account for. The formation of new stars depends on the content of cold gas of a galaxy, since the hydrogen needs to be in the molecular form (H_2) for star formation to occur, and even though recent studies have shown that 70% of nearby early-type galaxies contain some amount of atomic hydrogen (HI), they generally show no sign of significant on-going star formation activity (Morganti et al. 2006; Sanchez-Blazquez et al. 2009; Huang & Gu 2009). In fact, the fraction of HI is found to decrease with increasing stellar mass (Catinella et al. 2010), which would point towards a scenario where any mergers of massive, elliptical galaxies would proceed without significant formation of stars.

The process of gas-poor galaxy merging, or mergers between early-type galaxies, with no significant associated star formation (van Dokkum 2005; Bell et al. 2005) was at first thought to be highly unlikely since the median collision between galaxies must be between the "average" type of galaxy, the Sb spirals (Schweizer & Seitzer 1992). Even observationally, mergers between early-type galaxies are not as prominent as mergers between, for instance, spiral galaxies and although evidence of merging of red, bulge-dominated massive galaxies goes back to more than a decade ago (e.g. van Dokkum et al. 1999), only recently the importance of dry mergers in the assembly of massive galaxies has started to surface to explain some properties seen in early-type galaxies.

In fact, ever since van Dokkum et al. (2001) confirmed a triple red merger at $z = 1.27$ (Figure 1.11) in clear contrast with the theory of all massive elliptical galaxies being

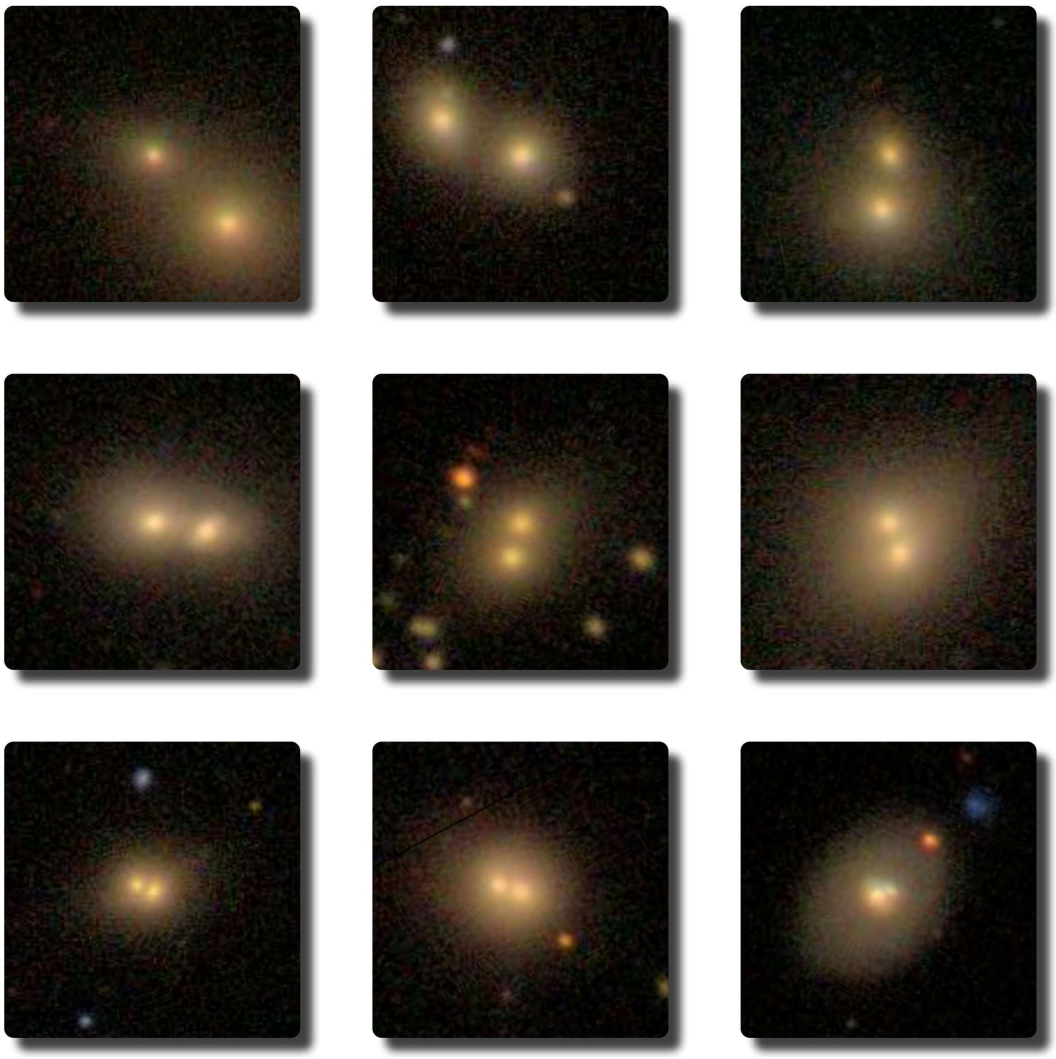

Figure 1.10: A sequence of dry mergers drawn from the SDSS, as described in 2. From top-left to bottom-right, the mergers are sorted according to the descending projected distances of their members.

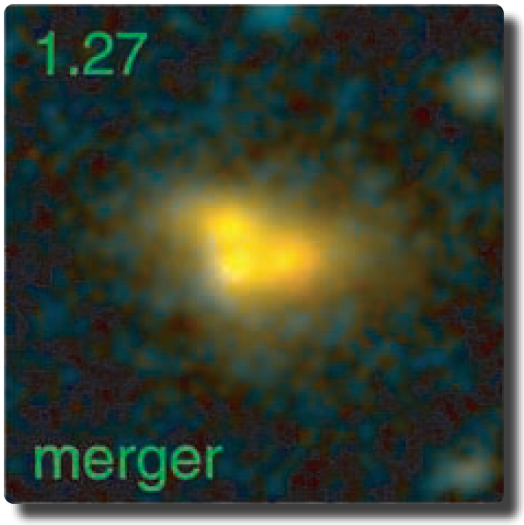

Figure 1.11: Color image from the triple red merger at $z = 1.27$ in van Dokkum et al. (2001)

formed at high redshifts through monolithic collapse, dry mergers have been proposed as the predominant path to the formation of massive elliptical galaxies (Naab et al. 2006; van Dokkum 2005; Bell et al. 2006, 2004; Khochfar & Silk 2009).

The influence of the gas-poor mergers in the formation of elliptical galaxies seems to have been, however, more decisive for massive ellipticals. The properties of high luminosity ellipticals are not compatible with an assembly via a process of merging of spirals with significant associated star formation, since the stellar populations of these progenitor galaxies would have the wrong age and abundance characteristics (Bell et al. 2005).

Low luminosity elliptical galaxies, on the other hand, have characteristics compatible with mergers of gas-rich progenitors. Faint early-type galaxies present diskier isophotes and are characterised by rapid rotation, whereas more luminous ellipticals have more boxy isophotal contours with respect to a perfect ellipse and are basically non-rotating (Kormendy & Bender 1996). Mergers between disky gas-rich galaxies with small bulges and low-mass black holes, have been shown to reproduce quite well the properties of smaller ellipticals but not of more massive ones (Khochfar & Burkert 2003).

This process of gas poor merging is also consistent with the lack of very massive

star-forming galaxies at low redshifts to build the massive non-star-forming early-type galaxies (Bell et al. 2004; Naab & Ostriker 2009). Moreover, observational studies focusing on mergers of early-type galaxies carried out in the last decade showed that the stellar mass density in luminous red galaxies has increased by a factor of $\gtrsim 2$ over the redshift range $0 < z < 1$, possibly explained by mergers of red, bulge-dominated, galaxies (van Dokkum 2005).

Overall, evidence seems to support the scenario of high luminosity elliptical galaxies being the remnants of mergers between early-type galaxies (Naab et al. 2006; Bell et al. 2006). However, this is by no means an accepted fact, for instance, Masjedi et al. (2006) conclude that dry merging of elliptical galaxies is of marginal importance from their study of the correlation function of SDSS luminous red galaxies (LRGs). Likewise, in their study of the mass functions in the COSMOS survey, Scarlata et al. (2007) argue that the massive end of the mass function was in place by $z = 1$ and they find no evidence of significant evolution. These contrasting results on the recent assembly history of the most massive galaxies in the universe are likely in part due to the rare nature of massive galaxies, not allowing statistically significant studies, and in part to different classification schemes used.

1.4.1 Merger, pair or group?

In this work we make a broad use of the word *merger* when referring to the potential merger candidates found as outlined in Chapter 2. In fact, we can not say with certainty that all of the potential mergers, mostly composed by two elements - hence the extensive use of the word *pairs* - in particular for the ones at higher projected distances and velocity offsets. As mentioned before, the merging process depends not only on the ever-changing distance between the galaxies but also on their relative velocities and, e.g., mass ratio. However, for simplicity, we will refer to potential merger candidates, i.e., the pair or group found to be within our initial conditions for merging, simply as *mergers*, unless stated otherwise.

Also, most of these systems are expected, and will turn out to be, made up of two galaxies in its majority but some are made up of more than two elements and the word *pair* would be misleading. Even though in the literature one can find wide use of the word *pair* when referring to a probable merger, the extent of the merger sample built

during the course of this work introduced the need to refer to the potential mergers as *groups*, since some of these systems have indeed more than two elements.

Therefore, we have made use of the word *merger* to refer to the system - either a *pair* or *group* - and not to the actual merging status. We use this word throughout this project unless, for clarity the words *pair* or *group* are better suited.

1.5 Thesis outline

The main goal of this thesis is to understand the overall role of dry mergers in the assembly of massive galaxies and reconcile the different conclusions on the importance of this type of mergers. To that end, a sample of potential groups of merging galaxies with spectroscopic observations from the SDSS DR6 is constructed, building the largest sample of dry mergers to date. Due to their rare nature, only a large set of dry mergers allows understanding their contribution to the assembly of new galaxies. In fact, the access to spectroscopic information makes the merger sample unprecedented both in number of potential mergers and available intrinsic data for these objects.

How the merger sample is defined constitutes a critical part of this work and is fully detailed in Chapter 2. This Chapter also describes the comparison samples drawn from the parent sample, i.e. the SDSS DR6, and the general properties found in the sample of potential mergers. Chapter 3 is dedicated to the properties of dry mergers and their role in the scenarios of galaxy assembly. The gas content of galaxies throughout the merger process is explored in 4. The following Chapter presents some individual dry-merger systems, from the merger sample, in more detail. Finally, Chapter 6 contains the summary of the conclusions from this work, last remarks and some comments on the work yet to be done.

Chapter 2

Data, Sample Selections and Merger Classification

The interaction and merging of galaxies is indeed a remarkable event known, and studied, for several decades. However, to understand how galaxies interact, and what exactly happens during the interaction and how much it affects the overall assembly and evolution of galaxies, one should investigate individual mergers in detail, where the most intrinsic aspects of the merger phenomenon can be explored but also, whenever possible, large sets of merging galaxies in order to have a broader perspective to comprehend the role of this phenomenon and get statistics in a significant way. In any hierarchical model for structure formation, such as the currently favoured ΛCDM, mergers are ubiquitous, but decreasing in frequency with cosmic time, and in the local universe they are found to be quite rare. So, in order to study their impact on galaxy assembly, we would prefer a large sample of mergers since observations of mergers in the local Universe long focused on small samples studied in detail rather than a statistical study.

The emergence of large dedicated surveys, particularly in the last decade, e.g. CFRS (Lilly et al. 1995), SDSS (York et al. 2000), 2dFGRS (Colless et al. 2003), has provided substantial amounts of data, especially of the nearby universe. Samples of galaxies potentially undergoing a merger can be built and studied, even at different

wavelengths, thus contributing to increase our knowledge of the processes behind galaxy assembly and evolution.

This Chapter describes the data used in this project, including the original survey from where it was drawn, the choices made in order to assemble one of the largest samples to date of galaxies potentially undergoing a dry merger and some results concerning the overall properties of the merger sample.

2.1 The Sloan Digital Sky Survey

The Sloan Digital Sky Survey project (SDSS; York et al. 2000)) is one of the major successes of modern astronomy. Being the largest survey of the extragalactic sky thus far undertaken, it covers more than a quarter of the sky, obtaining photometry in five different bands (*u,g,r,i and z*) for 357 million unique objects and spectroscopic information for more than 1 million objects, in its last Data Release, DR7 (Abazajian et al. 2009) [1].

The SDSS survey used a dedicated 2.5 m telescope (Gunn et al. 2006), located at Apache Point Observatory in New Mexico, in the United Stated of America. Since it first started to cover the sky it had two phases of observations, SDSS-I (2000-2005) and SDSS-II (2005-2008), and during those eight years has produced seven data releases(e.g Abazajian et al. 2009; Adelman-McCarthy et al. 2008, 2006), the final one - Data Release 7 (DR7) - was made available in October 2008 (Abazajian et al. 2009). The telescope is composed of two instruments: for the imaging it had a drift-scan CCD camera (Gunn et al. 1998) and a pair of spectrographs, each with 320 optical fibers. The photometry footprint area covered 11663 square degrees of the sky, with the total spectroscopic area covered being, in DR7, 9380 square degrees. The spectroscopy data was obtained within a wavelength range of 3800-9200 Å and in a single run up to 640 spectra can be measured with each fiber having a diameter of 3".

As described in Stoughton et al. (2002), the imaging data was gathered first and, after astrometric and photometric calibrations have been applied, some selected objects are flagged for spectroscopic follow-up. They have their spectra extracted and calibrated,

[1] http://www.sdss.org/dr7

and their redshift information and spectral type derived in a later stage. Based on the photometry, a number of possible spectroscopic samples are identified: Main Galaxy Sample, Luminous Red Galaxies (LRG), Quasars and Stars, among others. The Main Galaxy Sample comprises objects which are selected to have an r-band Petrosian magnitude $r_P \leq 17.77$ after correction for foreground Galactic extinction. In addition there is a r-band Petrosian half-light surface brightness cut at $\mu_{50} \leq 24.5$ mag arcsec^{-2}, as detailed in Strauss et al. (2002) but we will focus on (fairly) high surface brightness objects here so this latter cut is not of importance for our discussion here. The Luminous Red Galaxies sample is acquired through selected cuts in the (g-r, r-i, r) color-color-magnitude cube and corrected for Galactic extinction. The details for selection of the LRG sample are described in Eisenstein et al. (2001), however this sample of galaxies is not relevant for the present work.

The SDSS data are separated into a data archive server DAS[2] and a catalogue archive server. The former stores, among other things, the FITS images, spectra and object detections. The spectroscopic data referred to are based on analysis of the FITS spectra from the DAS analysed as described in Tremonti et al. (2004) and Brinchmann et al. (2004). The Catalog Archive Server Jobs System, or CasJobs[3], allows to search through the SDSS database, using SQL. The `PhotoObjAll` and the `SpecObjAll` tables contain, respectively, the characteristics of each photometric object and the measured parameters for the spectrum of the objects [4].

The spectroscopic pipelines (Schlegel et al. 1998; SubbaRao et al. 2002) produce a classification of the spectra stored in the `specClass` parameter. The categories used are: quasar, high-redshift quasar, star, late-type star, galaxy or unknown. For galaxies, in particular, a quantitative spectroscopic classification is offered by the eClass parameter. This is defined as in Connolly et al. (1995) to be the ratio of the first two eigencoefficients of a given spectrum. Connolly et al. (1995) find it to be a useful spectroscopic classifier, in terms of early- or late-type galaxies, although as discussed by Yip et al. (2004) it is not a complete description of the galaxy spectra.

In the present work, due to the scheduling of the work plan, the catalog of spectroscopically confirmed galaxies used in the first stage was the DR4 release (Adelman-

[2]http://das.sdss.org
[3]http://casjobs.sdss.org
[4]http://cas.sdss.org

McCarthy et al. 2006), with 567 486 galaxies. In a second stage, it was updated with the DR6 release (Adelman-McCarthy et al. 2008), containing 796 912 galaxies. This data release has an imaging footprint area of 9583 square degrees and a spectroscopic area of 7425 square degrees, and the photometric catalog encloses more than 287 million unique objects.

Even though this study is mostly focused on the spectroscopic catalogue, we also make use of the photometric sample from the SDSS DR6, to ensure spatial completeness. The spectroscopic targeting in the SDSS is based on a sophisticated tiling algorithm described in Blanton et al. (2003) and to improve spectroscopic coverage in dense regions these are visited multiple times. That not withstanding there is some spatial incompleteness, particularly likely for late-stage mergers, and we complement the spectroscopic catalogue with data from the photometric catalogue to address this incompleteness. However there will of course be some incompleteness at very late stages in the merging process when the galaxies have fused almost completely. This can to some extent be addressed by looking at faint morphological features (van Dokkum 2005; Darg et al. 2010). This technical issue is of particular importance if one is trying to look for late stage mergers. If the galaxies are very close together they would not be considered because the fiber usually pinpoints the central region of the galaxy, if two galaxies happen to have their central regions very close, as it is the case in very late stage mergers, these would be missed due to the restrictions in fiber placement. Here we will not aim to follow mergers to complete fusion and thus avoid this issue.

The redshift distribution of the SDSS galaxy sample is shown in Figure 2.1, where it is possible to grasp the extent of redshifts covered by the DR6 release of SDSS. Even though there are measurements for redshifts up to z=1, the peak is clearly around z$\simeq$0.1, corresponding to the main galaxy sample. The second peak, occurring for a redshift close to 0.35 is the result of the presence of the LRG sample.

Since this study focuses on the low-redshift universe, the first condition applied to the main sample of spectroscopic galaxies from the SDSS was to set up an upper limit to the redshift. The main galaxy sample consists primarily of galaxies with $z \leq 0.2$ and we adopt this as our upper redshift cut-off.

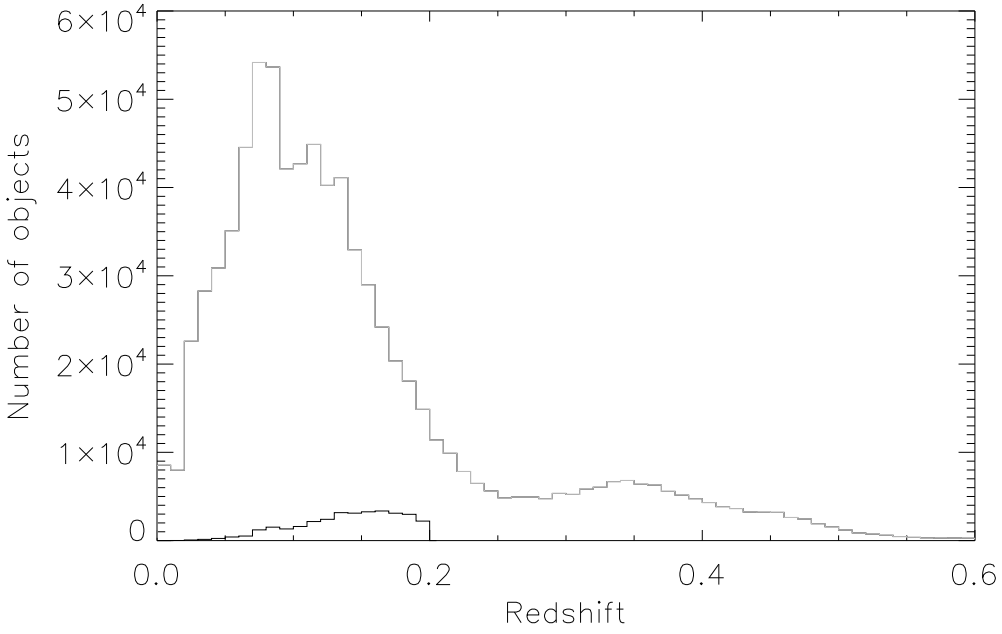

Figure 2.1: The spectroscopic redshift distribution (in grey) for the spectroscopic galaxy sample of SDSS DR6, including the main galaxy sample and the LRG sample. The black histogram refers to the redshift distribution of the galaxy sample with the cuts mentioned in Section 2.1.1.

2.1.1 First constraints on the main galaxy sample from the SDSS

To account for spatial incompleteness the SDSS returns to the same part of the sky more than once if possible. There are two main classes of duplicate observations: one, which is easy to deal with is the re-observation at essentially the same position of an object. This is done as part of the quality assurance in the SDSS. The other type of duplicate occurs because the photometric object detection code, particularly the early version, had a tendency to split large, nearby galaxies into several parts which were taken to be individual objects and hence targeted simultaneously for spectroscopic follow-up (e.g. Blanton et al. 2005). These duplicate observations are not as easy to identify as the re-observations of the same objects. However, this is only a problem at low redshift so a low-redshift cut helps reducing the seriousness of this issue.

Bearing this in mind, and to minimize the need of visual inspection, while keeping the main parent sample of galaxies as untouched as possible, and to avoid the effect of significant deviations from the local Hubble flow, we adopt a lower redshift limit of $z = 0.005$.

The overall quality of SDSS data is high, nevertheless, in the case of the objects with spectroscopic observations, a `sciencePrimary` flag was defined to assure the quality of the data. To be a `sciencePrimary` an object has to fulfill a set of five conditions, relying purely on spectroscopic and geometric considerations, regarding the spectroscopic observation of a given object. In such a case, the object will have `sciencePrimary` = 1. Even though the database includes all spectroscopic objects, under `specObjAll`, it also contains a separate table for objects with `sciencePrimary` = 1 stored in the `specObj` table. This condition of `sciencePrimary` = 1 was also a requirement in the selection of galaxies making up the parent sample from which the pair sample would be extracted.

- Objects within a spectroscopic redshift interval of $0.005 < z < 0.2$
- Objects flagged as science primary, *i.e.* with `sciencePrimary` = 1.

The final parent sample, from which the pair sample is built, contains 549 572 galaxies with the redshift distribution shown in Figure 2.1. The distribution of a subset of this sample is shown in Figure 2.2.

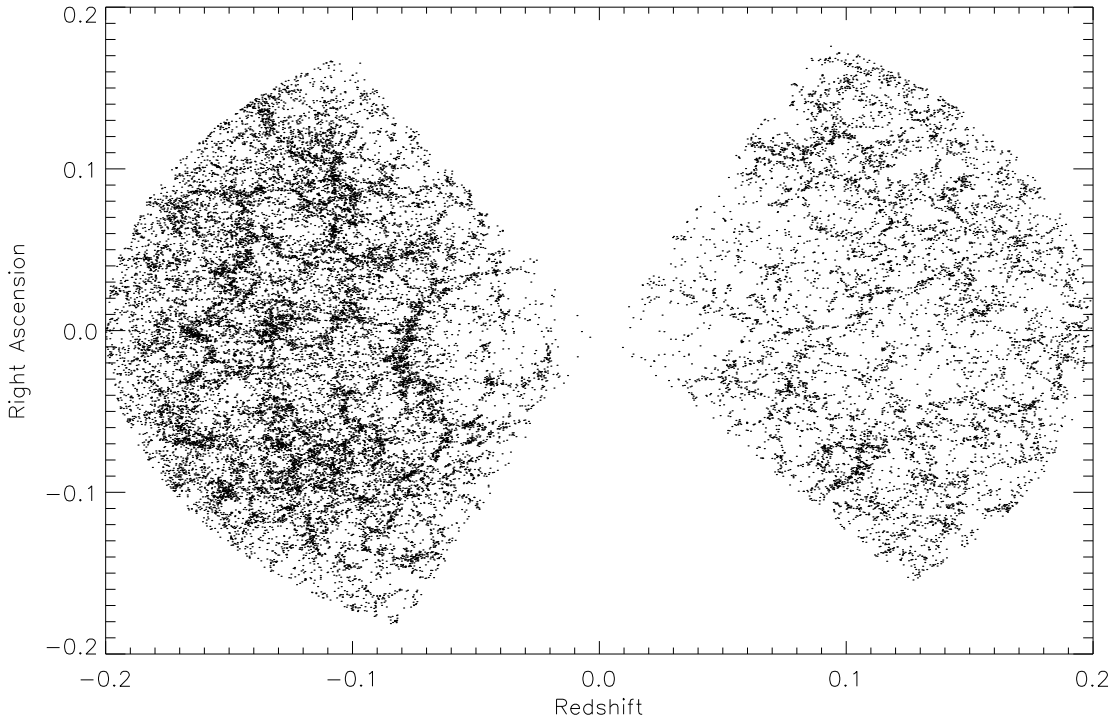

Figure 2.2: The galaxy distribution of a subset of the final sample from where the pair sample will be built. The galaxies in this plot are within the redshift interval mentioned in this section, however, for simplicity, only galaxies with stellar masses $\log(M_*/M_\odot) > 11$ and at an absolute declination below 10 degrees are plotted.

2.2 Sample Selection

It is possible to find several different pair criteria across the literature, as summarized in Table 2.2. From morphological signatures identified directly in the interacting system (e.g. van Dokkum 2005; Bell et al. 2006) to measurements of proximity between the galaxies that are potentially interacting, the methods vary considerably. Concerning the galaxies separation in the plane of the sky, i.e. projected separation, the norm has been to define $20\,h^{-1}$kpc as the maximum distance for a close pair. According to theoretical studies, these pairs are expected to merge within 0.5 Gyr (e.g. Barnes 1988; Patton et al. 1997, 2000).

In this work, taking advantage of the SDSS DR6 main spectroscopic sample of galaxies, two or more galaxies are considered a potential merger if they met a set of proximity conditions. A pair, or group, of galaxies is considered to be a merger candidate if the following conditions are met:

- Projected separation in the plane of the sky - each neighbour galaxy has to be within a co-moving separation defined by a circle of radius $r_p \leq 30\,h^{-1}$kpc, consistent with other works.

- Velocity offset along line of sight - the difference between the radial velocity of the neighbour galaxy and the searched galaxy should not be more than $v_{sep} \leq$ 800 km/s, equivalent to a difference in redshift of $\Delta z \approx 0.00267$.

The velocity offset limit is larger what is than commonly used in the literature and will possibly include some non-merging pairs. The average velocity offset of the members of each group is illustrated in the lower panel of Figure 2.3. Above a velocity separation of 600 km/s the number of groups remains approximately the same, without significant changes up to a velocity difference of approximately 1200 km/s. Following the same conservative approach, when compared with what is used in the literature, we opted to set the limit of the velocity offset at 800 km/s.

The distribution of the galaxies potentially undergoing a merger according to our criteria, as a function of projected separation and velocity offset, is shown in Figure 2.3.

Table 2.1: Representative sample of studies in the literature

Reference	Projected Separation (kpc)	Velocity Offset	Survey
Carlberg et al. (2000)	$r_p \leq 30\,h^{-1}$, $100\,h^{-1}$	$\Delta(v) \leq 1000 km/s$	CFGRS & CNOC2
Patton et al. (2000)	$5\,h^{-1} \leq r_p \leq 20\,h^{-1}$	$\Delta(v) \leq 500 km/s$	SSRS2
Patton et al. (2002)	$5\,h^{-1} \leq r_p \leq 20\,h^{-1}$	$\Delta(v) \leq 500 km/s$	CNOC2
Petrosian et al. (2002)	$r < 50$, 100	$\Delta(v) \leq 600, 900 km/s$	SBS
Lin et al. (2004)	$10\,h^{-1} \leq \Delta r \leq 30\,h^{-1}$, $50\,h^{-1}$, $100\,h^{-1}$	$\Delta(v) \leq 500 km/s$	DEEP2
Tran et al. (2005)	$R_s \leq 30\,h^{-1}$	$\Delta(v) \leq 300 km/s$	Galaxy cluster MS 1054-03 (z=0.83)
Bell et al. (2006)	$r < 20$	$\Delta(z)_{photometric} < 0.1$	GEMS
Patton & Atfield (2008)	$5\,h^{-1} \leq r_p \leq 20\,h^{-1}$	$\Delta(v) < 500 km/s$	SDSS & Millennium Simulation
de Ravel et al. (2009)	$\Delta r_p < 20\ h^{-1}$	$\Delta(v) \leq 500 km/s$	VIMOS VLT Deep Survey
Domingue et al. (2009)	$5\,h^{-1} \leq r_p \leq 20\,h^{-1}$	$\Delta(v) \leq 1000 km/s$	2MASS & SDSS DR5
De Propris et al. (2010)	$r < 20\ h^{-1}$	$\Delta(v) < 500 km/s$	2dF-SDSS LRG and QSO Redshift Survey

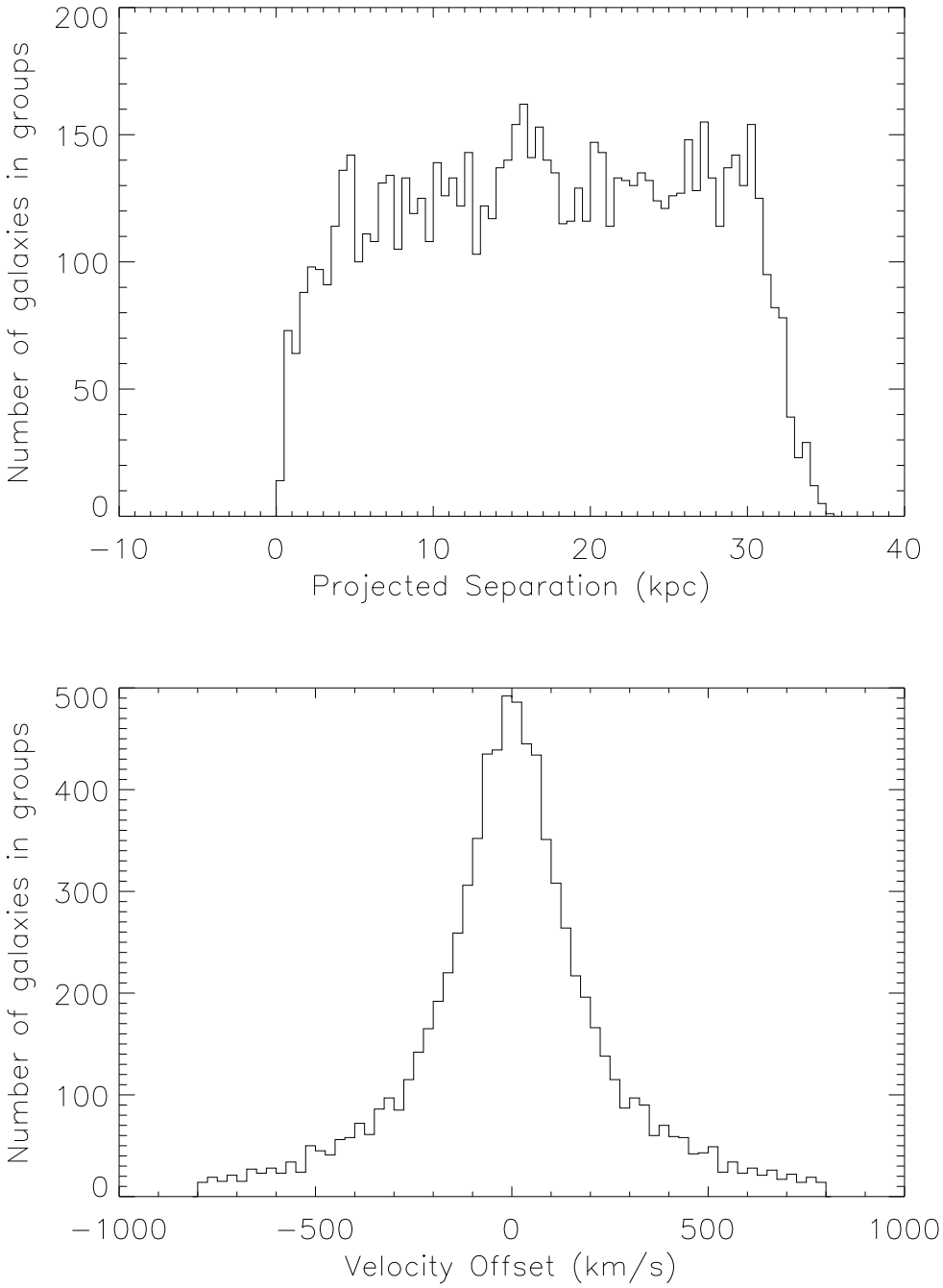

Figure 2.3: The distribution of the number of galaxies in groups as a function of the average projected distance, upper panel, and of velocity offset, lower panel.

2.2.1 The grid method for pair search

The search for pairs using the parent sample of galaxies is, conceptually, a simple process. Each galaxy in the sample is scanned for neighbour galaxies, within the same parent sample, that fulfill a set of pre-established conditions. This process, albeit straightforward, can easily become very time consuming and demanding in computational resources due to the sheer amount of galaxies to analyse, assuming each object would have to be compared with every other object in the sample and check if the conditions were met. For a sample of N elements, N×(N-1) operations would be necessary to compute. To avoid this problem, the first step of the pair search was to divide the parent sample of galaxies into several redshift bins in order to later apply the search for pairs. In fact, initially the redshift interval was divided into ten smaller intervals, or *slices*, each slice with a width of 0.0195 in redshift. However this method would introduce a boundary problem and to correct for galaxies located near the slice limits would be a challenging task. When we had converged on our selection criteria we found that removing the redshift slicing did not dramatically increase the execution time so we made away with the slices in the subsequent work. However, the slices were a useful tool to quickly test new selection criteria. The search for pairs started by placing the galaxies in an adaptive grid. In this work, the `grid2d` IDL package was used. This particular grid method is two dimensional and is based on rectangular bins and hierarchical sub-divisions of the individual bins, as seen in Figure 2.4. Because it is, as mentioned, an adaptive technique, the grid could be adjusted either for the refinement of the grid, *i.e.* total number of bins, or recursively for the number of objects per bin.

As stated before, the adaptive grid is two dimensional which means that it can only be applied to the first condition for the pair search, the projected distance. The galaxies are distributed throughout the grid according to, in this particular case, their right ascension and declination, but the search is carried out exclusively between galaxies inside the same bin, thus drastically reducing the number of calculations per galaxy.

2.2.2 Searching for neighbour galaxies

With the galaxies distributed in the grid, the sequence for the pair search starts with the projected separation - for each galaxy, hereafter *host* galaxy, defined by a unique set of right ascension and declination values, neighbours are within a circle of radius

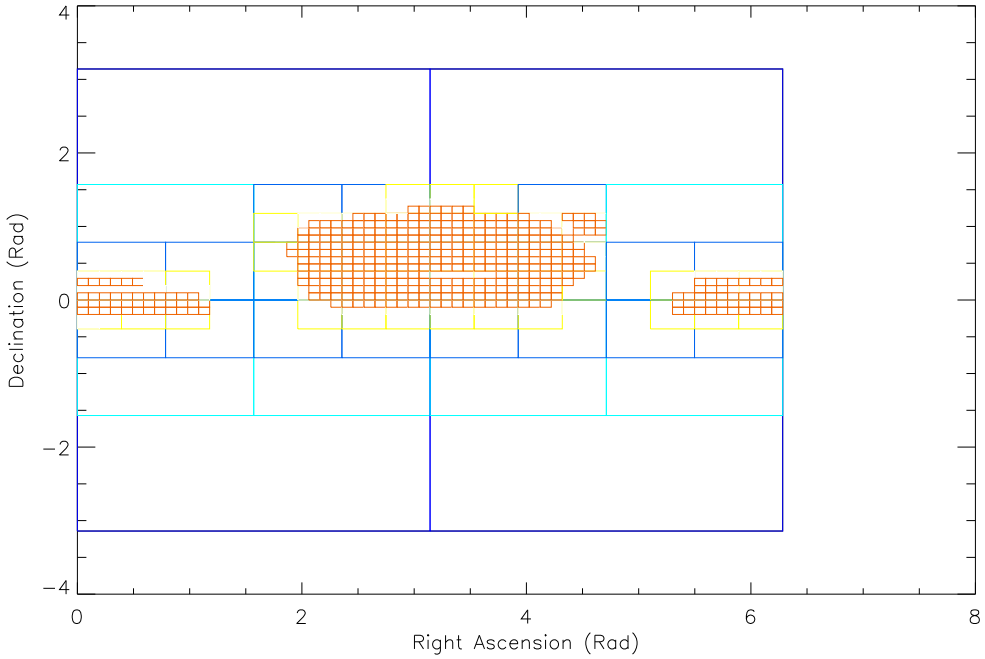

Figure 2.4: An example of the SDSS DR6 galaxies' coverage divided in the grid showing the first 6 levels of subdivision. The different colors represent the different levels.

$30h^{-1}$ kpc. The number of neighbours within that circle, as well as the distance to each neighbour, is stored and the next step, that consists on applying the velocity offset criterion, is carried out. We compare the redshifts of the neighbour galaxies with the host galaxy and keep only those that satisfy our velocity separation criterion $v_{sep} \leq 800$ km/s.

The next stage for building the merger sample is to account for the duplication that such a method naturally produces in the sense that a host galaxy becomes the neighbour of another galaxy. This duplication and the problem of strings of galaxies had to be accounted for, see Figure 2.5 . This issue of strings of galaxies arises when, for instance as illustrated in Figure 2.5, galaxy A is a neighbour of galaxy B but not of galaxy C although galaxy B is neighbours of galaxy C. In these type of situations, the galaxies are considered to be connected and they represent only one potentially merging system. Consequently, by applying the same principle to duplicate systems, only one potential merging system is accounted for.

The final sample of merger candidates is then constituted by the galaxies from the

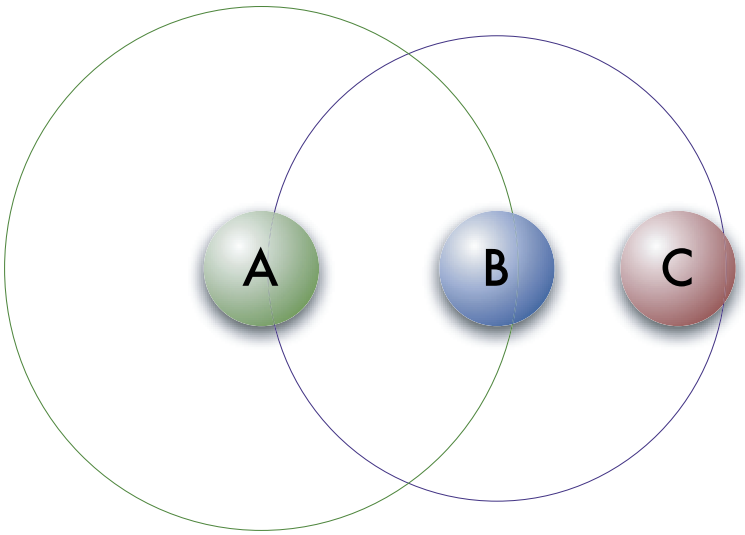

Figure 2.5: An illustration of the string of galaxies issue and the duplication problem. As shown, galaxy C is not in the neighbourhood of galaxy A, although to solve the string issue both will belong to the same group, since they are connected by galaxy B. The duplication problem, here demonstrated in galaxies A and B, is solved by, again, considering they are part of the same group.

SDSS DR6 potentially undergoing a merger, according to the defined criteria.

2.2.3 The merger sample

The merger sample is the sample containing the galaxies potentially undergoing a merger, fulfilling the proximity criteria defined in Section 2.2.2. The merger sample drawn from the spectroscopic SDSS DR6 is composed of 8028 galaxies, in a total of 3962 groups. As expected, the vast majority of the groups is composed of two members: 3869 are groups of two elements, 82 of three elements and 11 groups have more than three elements. It should be mentioned, however, that these numbers represent in reality the number of spectroscopic observations and not galaxies *per se*. We remove repeated observations of the same object before identifying close pairs using `sciencePrimary`, but in the procedure discussed above, we have assumed that there is only one spectroscopic observation within each galaxy. Although, some objects have multiple spectroscopic observations, as it can be seen in Figure 2.6 where the galaxy M101 has several spectroscopic targets. However, it is not a major concern and to verify if indeed that would constitute a problem and quantify its significance, a visual inspection was carried out, using the images available in the SDSS website, and it

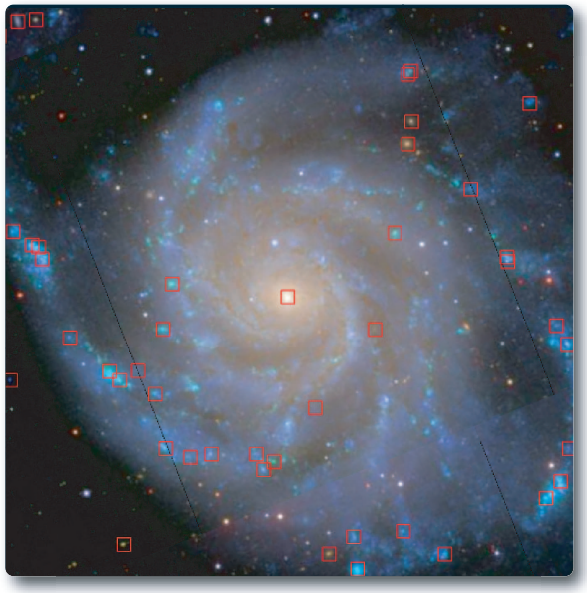

Figure 2.6: The M101 galaxy, also known as Pinwheel Galaxy, as imaged in SDSS, at a redshift of $z = 0.001$ as measured by spectroscopy. The image is 12' wide.

was not significant. Moreover, one should also consider the possibility of some cases being apparent, and not actual, duplicate observations of the same galaxy, specially at higher redshifts. In fact, some of the very close-by entries in the catalogue may appear as possibly being duplicate observations of different regions of a same galaxy but refer, in fact, to different real close-by objects. In addition, very late-stage mergers would indeed look like a single object with two nuclei and in this case it is reasonable to count that as a close pair. Given the marginal influence this problem has in the sample, we consider the full merger sample.

This selection resulted in a heterogeneous sample because it does include a wide range of mass ratios and merger stages. Because fibers cannot overlap, as mentioned in Section 2.1, and each fiber has a 3" diameter, galaxies involved in a late-stage merger may already be too close to allow placing a fiber on each object separately. At low redshifts this is not a significant problem, but at the upper end of the redshift interval galaxies lying at projected distances $\lesssim 9.90h^{-1}$ kpc might not be simultaneously observed in spectroscopy since that would lead to fiber collision and this would prevent us from identifying a possible merger and having a sample as complete as possible. To solve this problem, the search for groups of galaxies is later complemented with the photometric sample of the SDSS as described in Section 2.3.

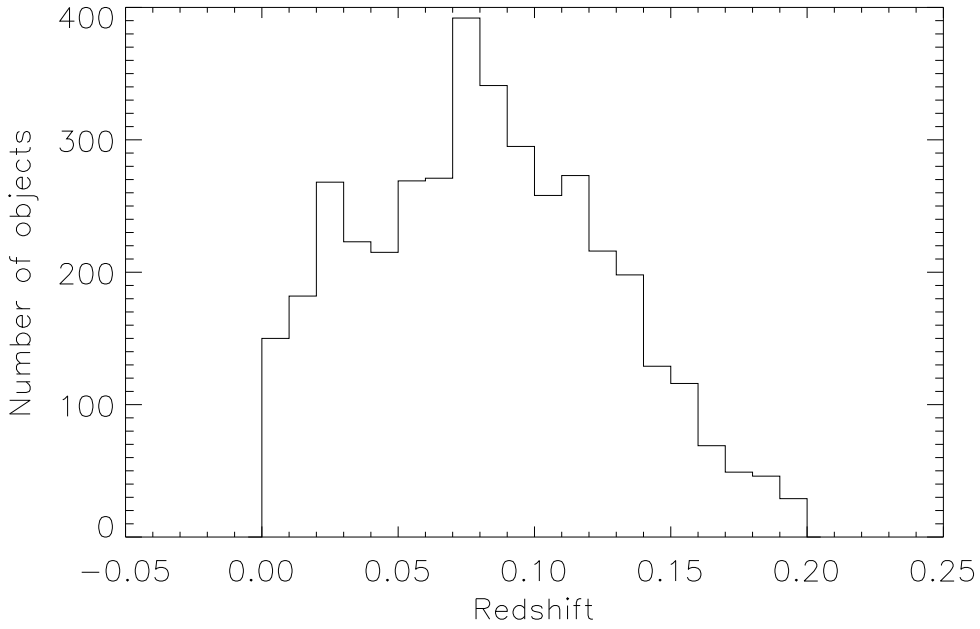

Figure 2.7: Spectroscopic redshift distribution of the galaxies from the merger sample involved in major mergers.

The redshift distribution of the merger sample is shown in Figure 2.7. The lowest redshift in the merger sample is 0.005014, the highest is 0.199080 and the median redshift is 0.066.

In the following chapter we will focus our attention on gas-poor, i.e., dry, mergers. Here we will study the full population of merging galaxies, both to study the increase in their star formation activity and AGN content, and to give a context for the rest of the thesis.

The focus for characterizing the merger sample is, at this point, two folded:

- Classifying the different types of mergers in the sample. In particular regarding:
  - Gas content, and/or star formation activity, of the galaxies in the merger
  - Number of galaxies involved in each merger
  - Stellar mass ratio between galaxies involved in the merger
- Examining the merger sample with respect to photometric features only. By

analysing only the photometric properties, that information can later be used when adding the galaxies from the SDSS that do not have any spectroscopic data.

It should be stressed at this stage that even though the aim of this study is to investigate the overall properties of mergers between gas-poor galaxies, one should emphasise the continuous nature of the possible different types of mergers and indeed the subjectivity inherent in designating a merger "dry" or "wet". Moreover, we make use of the complete sample, *i.e.* dry and non-dry mergers, to study AGN and star formation activities, as presented in Section 2.5, the last section of this Chapter.

2.2.3.1 Photometric properties

Classifying galaxies on the basis of their photometric properties is a challenging problem. In fact, even the simple Hubble classification scheme for galaxies presents some complexity to identify a galaxy. Due to our focus on dry mergers we are particularly interested in classification techniques that can be used to separate early-type galaxies from other galaxies and do not put emphasis on how the classification works on late-type galaxies. A straightforward approach is to select galaxies by their color-morphology relation, since early-type galaxies tend to be red and bulge-dominated, translating into photometric properties like color and concentration. Next, these parameters will be presented and the results of applying them to our sample will be analysed.

Concentration index A standard way to define early-type galaxies according to their morphology is the concentration index, C, which distinguishes ellipticals from spirals based on their radially averaged light distributions. Following Strateva et al. (2001) and Shimasaku et al. (2001), the concentration index is defined to be the ratio of the radii containing 90% and 50% of the Petrosian flux in the r-band, as stated in equation 2.1.

$$C_r = \frac{R_{90_r}}{R_{50_r}}, \tag{2.1}$$

where C_r is the concentration index calculated for the r-band and R_{90_r} and R_{50_r} are the r-band Petrosian magnitudes for R_{90} and R_{50}, respectively.

The SDSS determines the magnitudes in a modified Petrosian system, measuring galaxy fluxes within a circular aperture which radius is defined by the shape of the azimuthally averaged light profile (e.g. Stoughton et al. 2002). The photometric pipeline calculates the (circularised) radii containing, respectively, 50% (R_{50}) and 90% (R_{90}) of the light for the five *ugriz* bands.

Strateva et al. (2001) show that the concentration index correlates with galaxy type, specially to separate early- from late-types. Centrally concentrated ellipticals are expected to have larger concentration indices than spirals. Moreover, they estimate a cut-off index of $C_r = 2.63$ to separate early-type galaxies, with $C_r > 2.63$, and late-type galaxies for $C_r < 2.63$.

Initially we conservatively considered setting the limit for the concentration index to $C_r > 2.8$. This would appear to be a good criterion to separate early- and late-type isolated galaxies. However we wished to check whether it was reliable also for close pairs of galaxies. When dealing with potentially merging systems, depending on the separation between the elements of an interacting group, the concentration index proved not to be reliable since the radii, in particular R_{90}, can be strongly affected by the presence of a neighbour, it can be seen in Figure 2.8.

The concentration index for the galaxies in the merger sample artificially drops to lower values for galaxies that have a neighbour closer than $10h^{-1}$ kpc, unreasonably indicating these galaxies would preferentially have less concentrated light profiles and demonstrating that the light concentration of galaxies is only a suitable quantitative measure of morphology when the objects are isolated. This feature can be further analysed in Figure 2.9 where it is illustrated the difference between R_{90} and R_{50} for host galaxies when compared with a set of isolated galaxies with similar mass and redshift ($\Delta(z) \leq 0.01$ and $\Delta(Log(M_*/M_\odot) \leq 0.1)$. The difference in both R_{90} and R_{50} shows an increase of these quantities with decreasing projected separation, indicating that the Petrosian flux measured in the two regions is altered for galaxies in mergers, with hosts galaxies presenting somewhat higher values. The outer radius, R_{90}, is more affected than the inner R_{50} radius, indicating that the outskirts of galaxies become affected sooner than the more central regions. This greater difference for R_{90} when compared to R_{50} results in the decrease of the concentration index seen in Figure 2.8, make this criterion particularly weak when applied to galaxies in mergers.

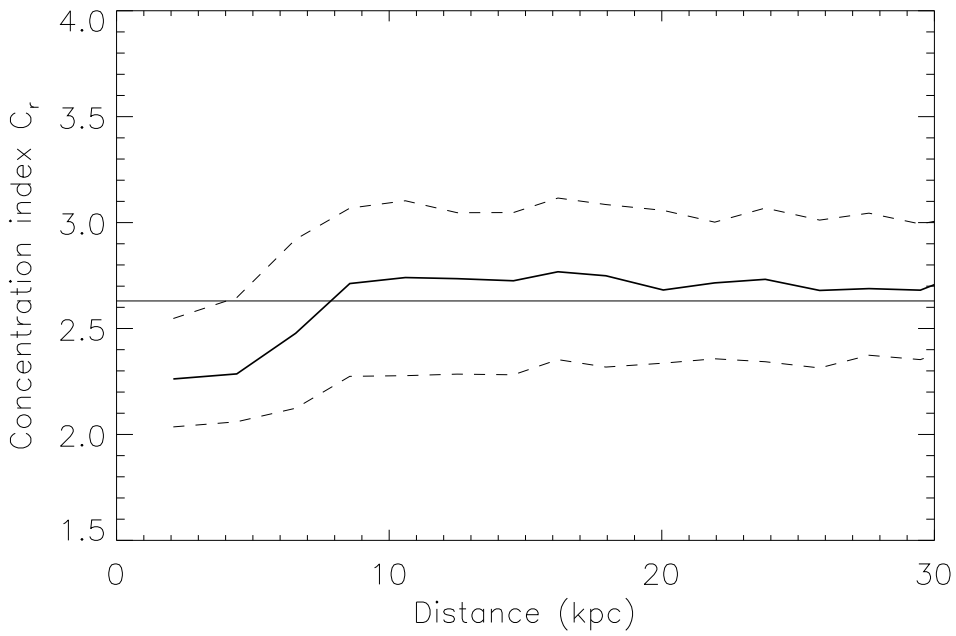

Figure 2.8: Median value of the concentration index parameter as a function of projected separation, for the galaxies in the merger sample. The upper and lower dashed lines are the 75^{th} and 25^{th} percentiles, respectively. The horizontal line indicates the C_r =2.63 limit.

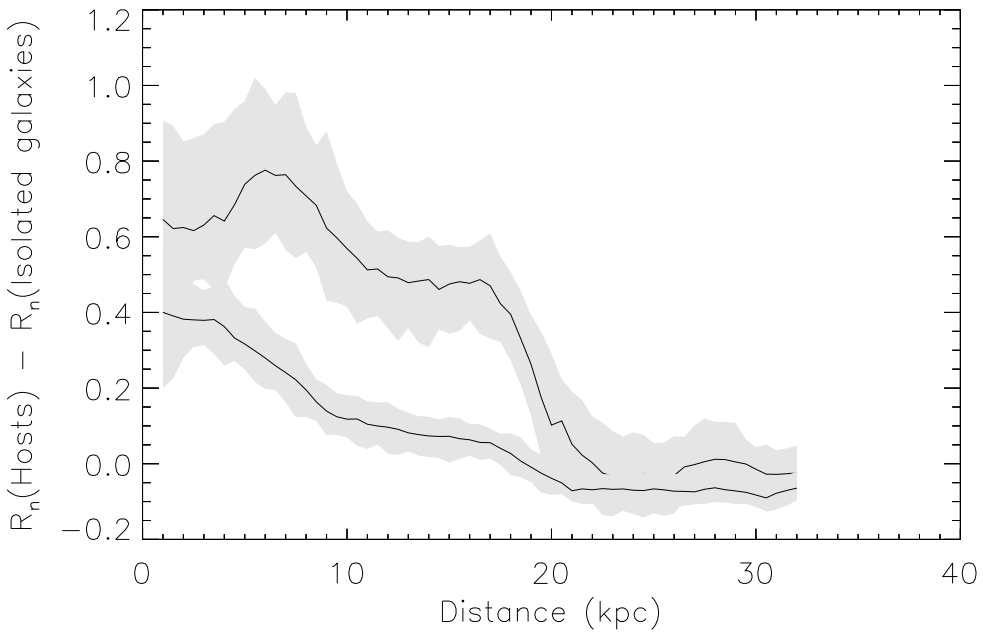

Figure 2.9: The median of the variation of the difference in R_{90} and R_{50} for galaxies in mergers and isolated galaxies. The shaded regions indicate the 68% confidence interval obtained with bootstrapping techniques. The subscript n indicates the 90, i.e. R_{90} represented in light grey, or 50, i.e. R_{50}, represented in dark grey.

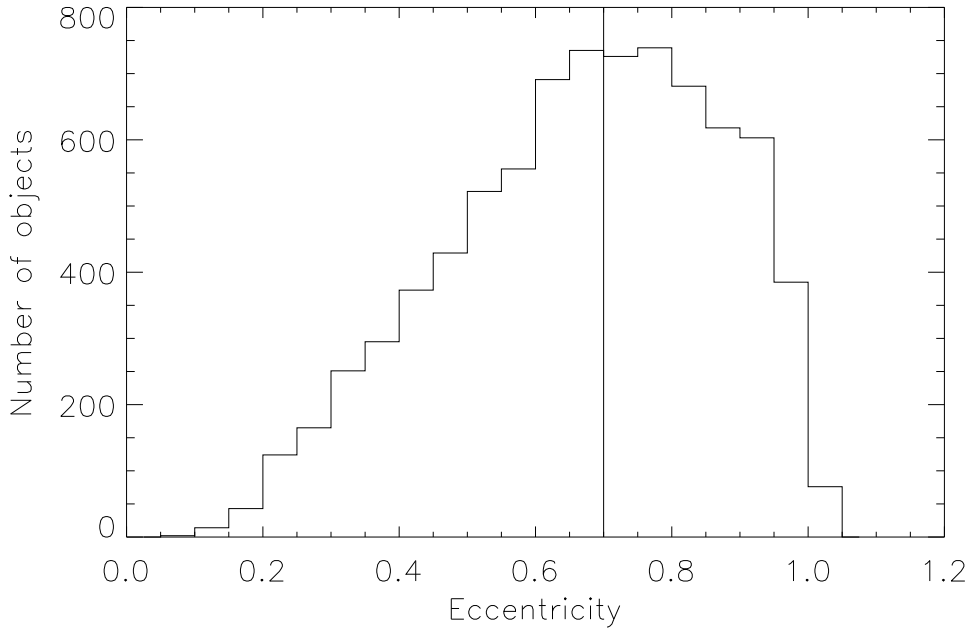

Figure 2.10: Eccentricity histogram for the galaxies in the merger sample. Overplotted, for reference, the vertical line at $E_r = 0.7$ indicates the tentative limit initially tried to establish a separation between different morphological classes (spheroids' eccentricities would lie above this limit).

Eccentricity Another possible photometric property that could, to a first approximation, successfully separate spheroidal from edge-on disk galaxies, to be applied to where edge-on spiral are often contaminants like color-selected samples of early-types, is the eccentricity, as defined in equation 2.2.

$$E_r = \frac{b_r}{a_r} \tag{2.2}$$

In this equation, a_r and b_r represent the isophotal major and minor axis, respectively, in the r-band. The first attempt to a separation between the two types was set at E_r= 0.7. Objects with $E_r > 0.7$ would be considered spheroidal and would represent a good selection of early-type candidates. However, a study of the distribution of the eccentricity, shown in Figure 2.10, for the galaxies in the merger sample, revealed that the eccentricity did not significantly improve our ability to distinguish spheroidals, since there was no separation between the two types of objects. This happens probably for the same reason as in the concentration index results: the photometry of each

galaxy in a pair, or group, is strongly affected and classifying individual galaxies using photometrically derived structural parameters is hindered by their interacting status.

Color At low redshift, using color as a defining parameter for early-type identification might naively viewed as straightforward, since these galaxies are expected to have old stellar populations easily characterised by their red colors (di Serego Alighieri et al. 2006; Renzini 2006). However, using solely color to detect these galaxies would likely contaminate our sample with objects reddened by dust thus introducing false positives: along with spheroidal morphologies with old stellar populations, the sample would contain dust reddened galaxies. However it turns out that this is a more useful technique and we will discuss this in more detail in section 2.2.4.3 below.

Given the analysis presented above, and to assess the contamination induced by color selection and construct a reference sample of mergers, a visual classification of the 3962 potential mergers was carried out, ensuring the coherence of the several criteria used to distinguish between different types of mergers and other events across the sample.

2.2.4 Visual classification of the merger sample

The visual classification of the merger sample was performed in order to ascertain the best possible quality of our merger classification method since, as shown in Section 2.2.3, a secure classification would not be possible if using solely a set of selected photometric parameters.

To recap, we identified pairs of galaxies using a spatial separation criterion of $30\,h^{-1}$kpc and 800 km/s. From this parent sample we now want to identify the early-type galaxies.The classification was done for each group of the merger sample considering the group as a whole and not just the individual galaxies making up the merger. The adopted criteria consisted in looking for the following features in each of the galaxies of the merger:

1. the presence of a disk
2. any blue colors
3. a spiral or clumpy pattern

4. the clear presence of a dust lane

5. a radially asymmetric distribution of light

The categorization of the groups was made in the following manner:

- if *all* galaxies in the merger did not show *any* of these features, the group would be classified as a *dry* merger.

- if *any* galaxy in the merger displayed *any* of these features, the group would be considered a *non-dry* merger.

This system implicitly considers mergers between early- and late-type galaxies, the so called *damp* or *moist* mergers, as being non-dry mergers.

The visual classification was carried out using the `jpeg` images from the SDSS DR6 website [5] and no other parameter or tool was used. In particular, we did not make use of the spectroscopic data for the galaxies in making the classification.

In practice, to carry out the classification we first created an HTML file with access to the JPG image of each galaxy centered on that galaxy, but grouped in the groups/pairs we had previously identified. Thus during the classification we could make reference to entire group. The retrieved images are centered at a given pair of right ascension (RA) and declination (DEC), have a size of 70×70 pixels and are scaled to 0.2"/pix, producing an image centered on a unique object. The linked images for each object in a group allowed an analysis of the individual galaxies in each group separately but the classification was carried out as a group, as described above. An important advantage of this visual classification is the possibility to use it to investigate the rate of contamination in color-selected dry merger samples.

The visual classification resulted in a sample of 890 dry mergers and 3072 non-dry mergers, translating into 1801 galaxies in dry mergers, hereafter dry galaxies, and 6227 in non-dry mergers, hereafter non-dry galaxies. To note that these terms, of "dry" and "non-dry" galaxies, are solely used because they belong to dry and non-dry mergers, respectively, and they do not refer to their particular nature.

[5] http://www.sdss.org/dr6

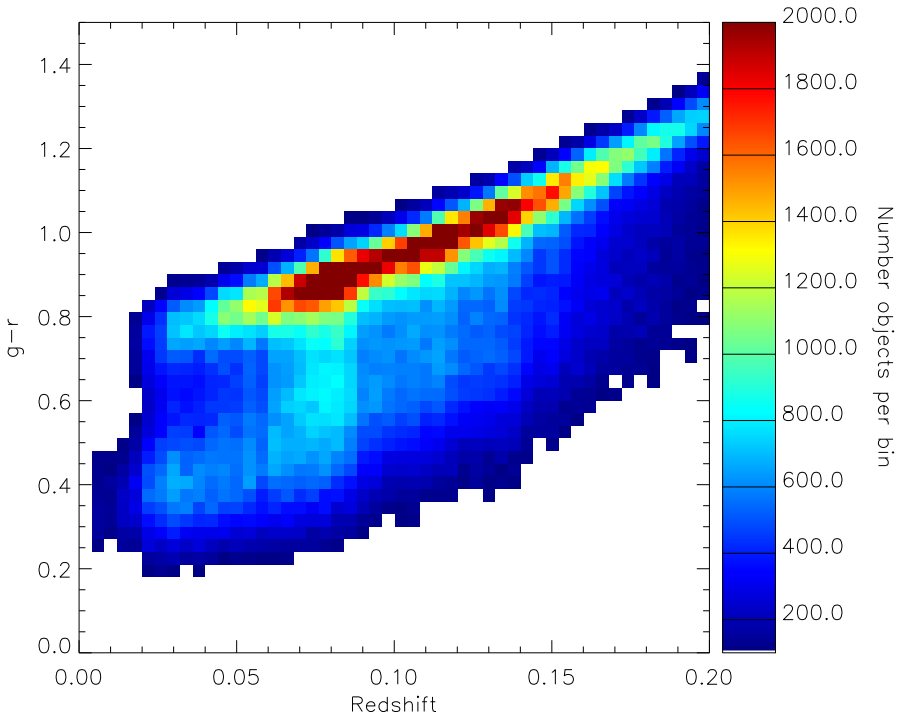

Figure 2.11: *g-r* color - redshift diagram for the galaxies in the parent sample of spectroscopic galaxies of the SDSS DR6. The bimodality of the galaxy population is clearly evident at low redshift but towards higher redshift the characteristic luminosity shifts towards more massive, and redder, galaxies and the blue sequence fades away.

2.2.4.1 Characteristics of the visually classified mergers

Armed with the visually classified sample of potential mergers, we can now study how our visual classification differs from other techniques for merger identification.

The color-redshift diagram for the galaxies in the main SDSS DR6 sample is shown in Figure 2.11 for reference and in Figure 2.12 the classified galaxies are over plotted. As can be seen in Figure 2.12, the position of dry galaxies is well constrained in the color-redshift diagram, placed, as expected, in the red-sequence, whereas the non-dry galaxies show a much wider scatter and even some overlapping towards the red-dotted region of the dry galaxies (recall that we do not make use of an explicit colour-cut when carrying out the visual classification).

The same behaviour can be noticed in the color-magnitude diagram in Figure 2.14, where *u-r* color is plotted against the r-band absolute magnitude. The distribution of

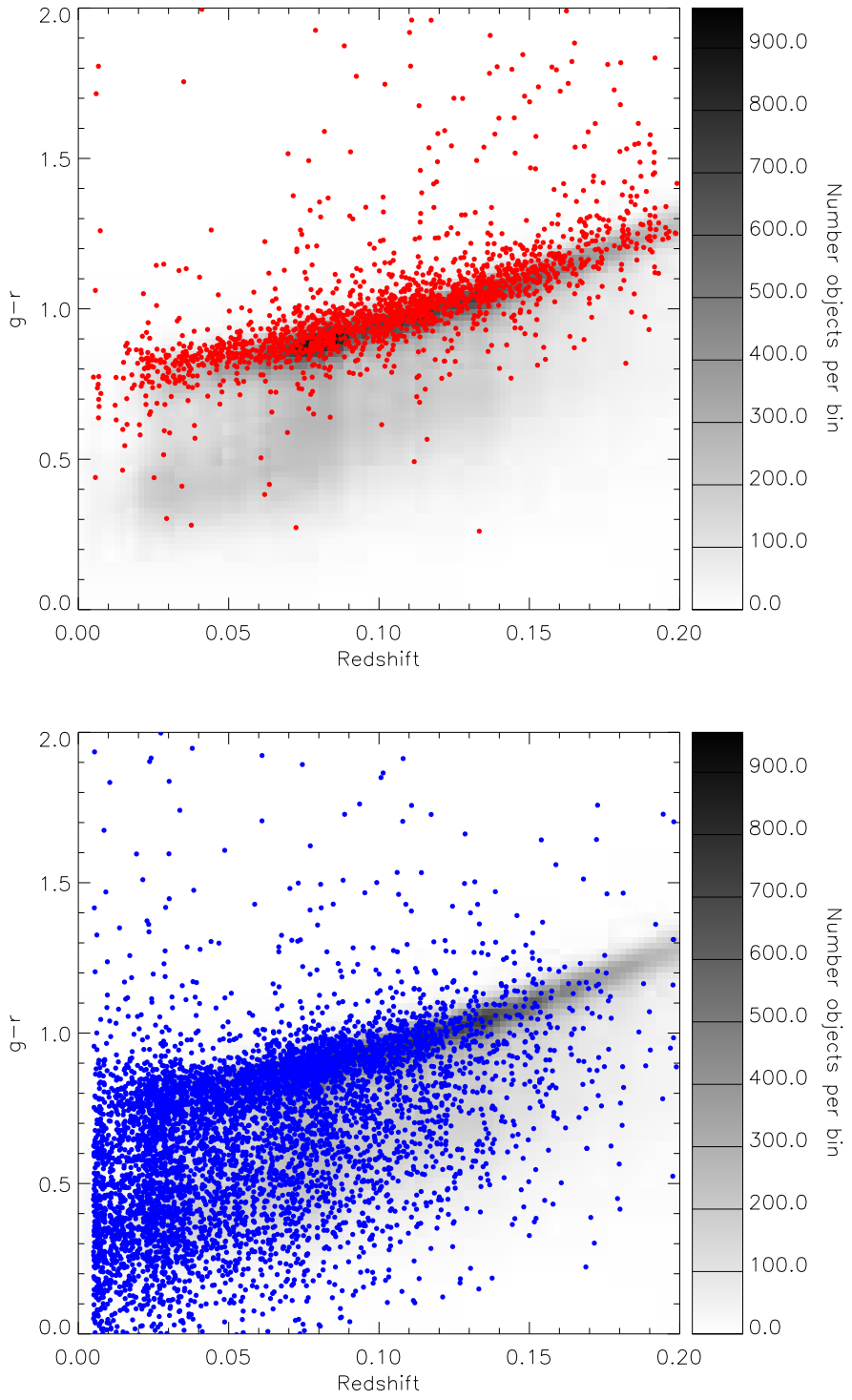

Figure 2.12: *g-r* color - redshift diagram for the galaxies in the merger sample (circles) plotted over the parent sample of spectroscopic galaxies of the SDSS DR6 (in gray scale). The red filled circles (upper panel) represent the galaxies in dry mergers and the blue filled circles (lower panel) the galaxies in non-dry mergers.

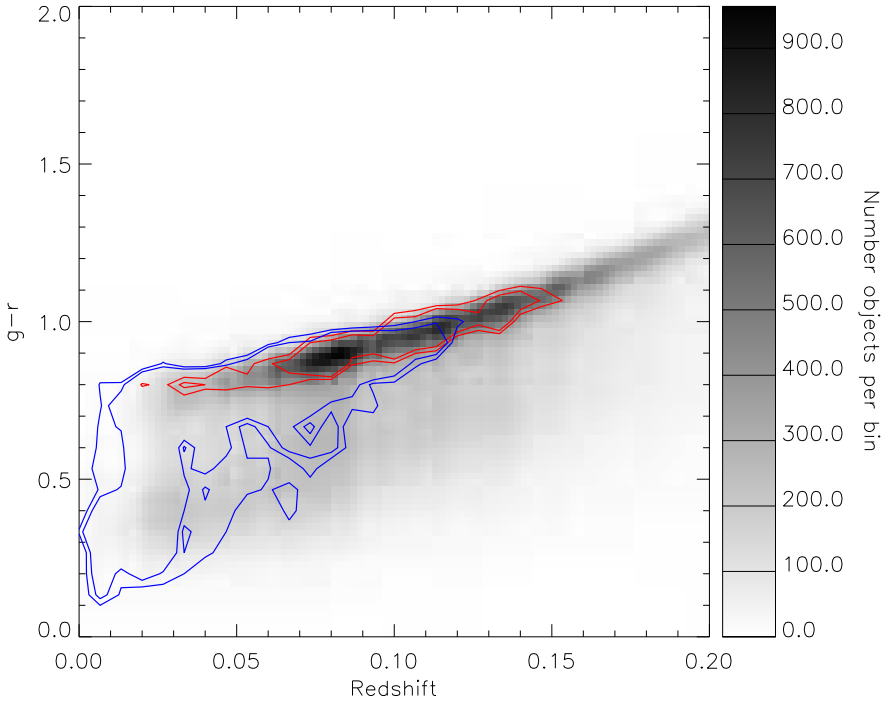

Figure 2.13: *g-r* color - redshift plane for the galaxies in the merger sample (contours) plotted over the parent sample of spectroscopic galaxies of the SDSS DR6 (in gray scale). The red contours represent the galaxies in dry mergers and the blue contours the galaxies in non-dry mergers.

non-dry galaxies is seen overlapping with respect to the distribution of dry galaxies.

There are two reasons for the abundance of non-dry pairs within the region defined by the dry pairs, as it is illustrated in Figures 2.12, 2.13 and 2.14:

- The non-dry classification was applied for the pairs/groups as a whole, thus, mergers between red spheroids and blue galaxies would be considered non-dry mergers. If one of the members were classified as dry (according to the definition adopted in Section 2.2.4) it is likely to reside on the red sequence, but we would classify the merger as a whole as non-dry. In other others, all the members in that merger would be assumed as non-dry.

- The high number of galaxies from non-dry mergers inside the region of dry galaxies also has a contribution from dust-reddened galaxies. During the visual classification, it became clear that a number of red galaxies were really edge-on

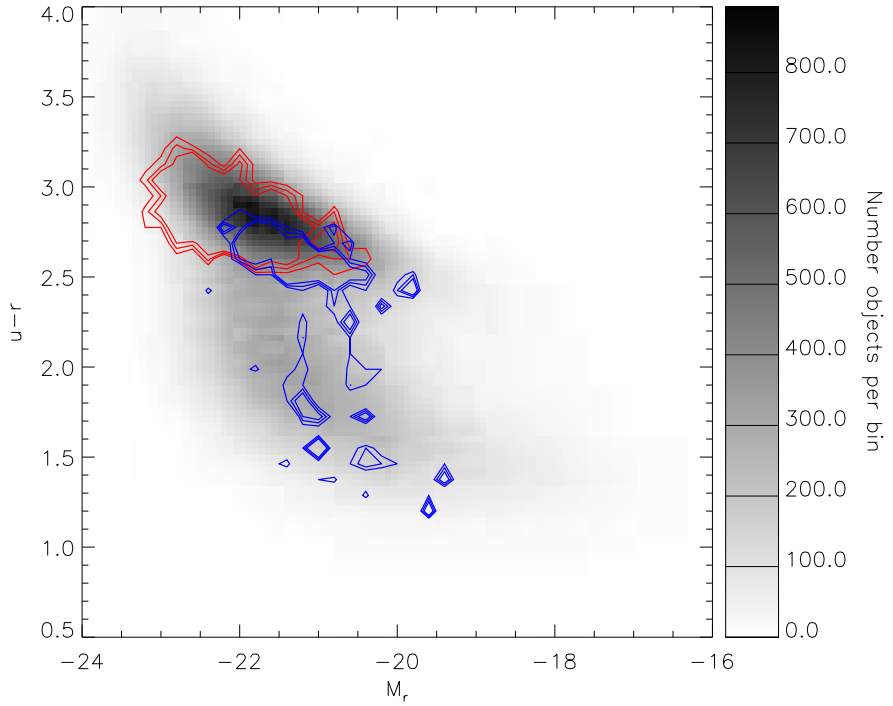

Figure 2.14: u-r color versus absolute r-band magnitude for all spectrosopic SDSS DR6 galaxies (in gray-scale). The solid red contours indicate the distribution in this color-magnitude diagram for the galaxies in dry mergers. The turquoise contours represent the same for the bluest galaxies in the non-dry mergers.

dusty disks. These, again, being intrinsically red, normally populate the red region of the color-z plane.

The advantage of having the visual classification for the galaxies in the merger sample is that now, using this information, it is possible to quantify the contamination and completeness of a color-based selection, while maintaining such a criterion. It will be of great help when enlarging the sample to include the galaxies having only photometric information, since this initial cut will minimize an otherwise too large a sample to be visually classified. Furthermore, because the region of dry galaxies is so well defined in Figure 2.13, we use it to explore how well we can identify a dry merger just by using a (redshift-depedent) colour cut.

2.2.4.2 Defining a color-redshift region for dry mergers

We would like to design a colour-cut that we can use to efficiently identify potential dry mergers using only photometric data. This will be very useful when we later turn to expand the same using photometric data. We now focus our attention on constraining the red region as thoroughly as possible.

To identify the region primarily populated by dry mergers, we focused our attention on galaxies with $\log M_* > 10.5$. This mass cut is somewhat arbitrary, as is any mass cut in a sample with such diverse types of galaxies, and was implemented so that the red region would be sensitive to early-type galaxies. The decrease in the relative number of red galaxies with stellar mass is illustrated in Figure 2.15 where the g-r color distribution of the SDSS DR6 above a fraction of 0.68 in each mass bin is plotted. It is clear the predominance of red galaxies in higher mass bins.

We note that the red region of the color-redshift plot where the galaxies comprising the dry mergers would fall is, hereafter, referred to as "lane", due to its shape in the diagram and, in order to constrain it, an upper and lower color limits would be needed to restrict the region. This would separate the galaxies that would be considered in dry mergers, i.e. red galaxies, from the bulk of galaxies in non-dry mergers, or blue galaxies. Both upper and lower limits of that region, hereafter lane, were adjusted by second degree polynomials that were defined iteratively by optimization of two variables:

- f: the ratio between the number of blue galaxies and the number of red galaxies

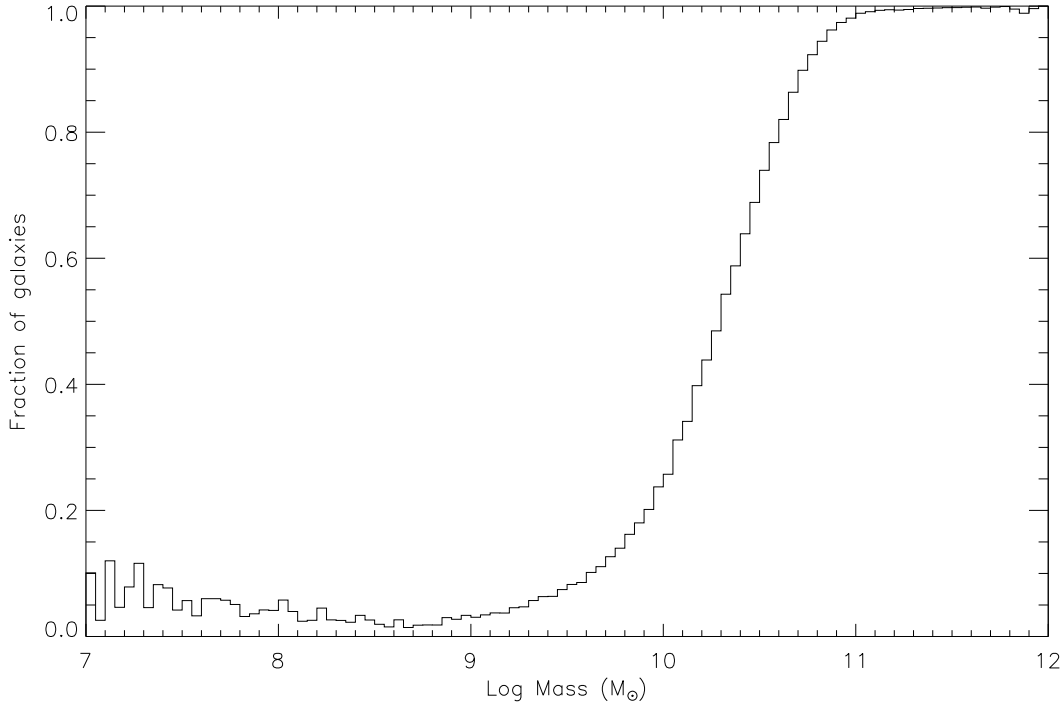

Figure 2.15: The *g*-*r* color distribution of SDSS DR6 galaxies above a fraction of 0.68 as a function of stellar mass.

inside the lane

- f_{in}: the ratio between the number of red galaxies inside the lane and the total number of red galaxies overall.

With this procedure, we aim at constraining these two parameters so that f assumes a value as small as possible and f_{in} as large as possible.

The starting points for the upper and lower polynomials were such that almost all red galaxies had to be inside the lane defined by those limits. Specifically, the lane region was set, before the iterations, so that it enclosed 98% of all the dry mergers. The values for f and f_{in} were stored and the new set of limits were established by letting the upper limit fixed at 0.99 % and increasing the lower limit by 0.5 %, for 1.5 %. The new set of f and f_{in} values was calculated, stored and a new increase of 0.005 in the lower limit was applied. This process was repeated until the lower limit reached 26 % and at that point the upper limit was decreased by 0.005, to 98.5 %, and the lower limit was reset to 1 %. The same method was imposed and in each step the values of f and f_{in} were stored. The iteration was stopped when the upper limit reached a minimum value of 74 % and the lower limit a maximum of 26 %.

An important remark should be made - for the merger to be considered dry, all of its members had to be inside the lane at the same iteration. When the upper or lower limits cut off a given galaxy, the other galaxies in the same merger were also discarded, even if they were still inside the lane. This way it is possible to guarantee that every dry merger is indeed made up of red galaxies.

The last step before defining the lane that could contain the galaxies in dry mergers was to analyse the output from f and f_{in} and investigate which combination of parameters gives an optimized result. In other words, what are the f and f_{in} so that the number of red galaxies inside the lane is as high as possible with as little as possible contamination from blue galaxies.

The results for the iterative search for the best lane are shown in Figure 2.16. This figure is color coded so that the lines with the same color represent the same lower limit with different upper limits. Ideally, a very good combination of limits would be represented by a (f, f_{in}) point in the quadrant indicated in Figure 2.16, where the number of red galaxies inside the lane would be greater than 90% and the fraction of

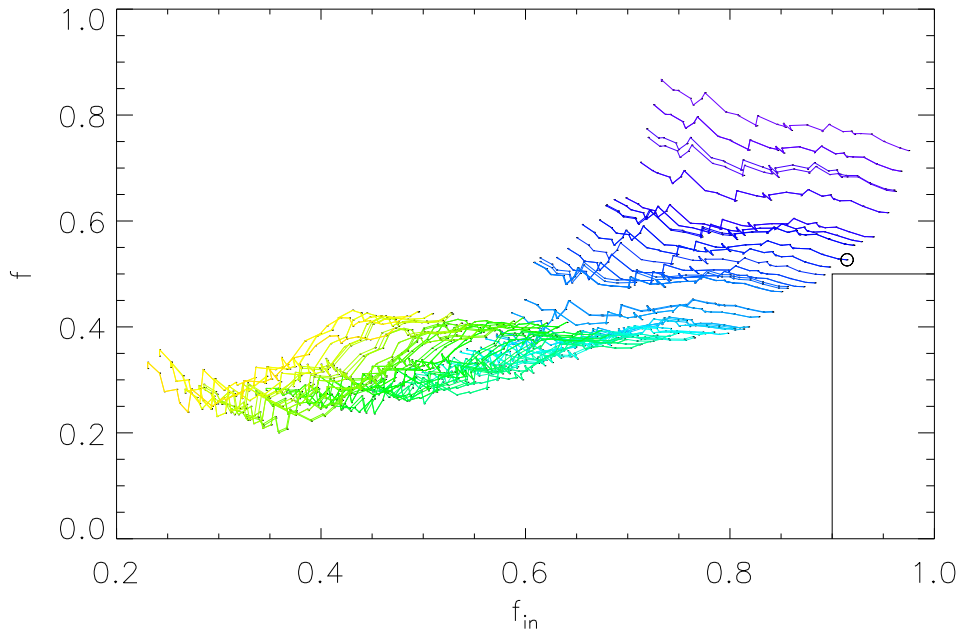

Figure 2.16: The parameter f as a function of f_{in} for the iterative search of a red region. The color coded lines represent the same lower limit for the different tested upper limits. The quadrant is for reference of the region where f_{in} is greater than 0.9 and f lower than 0.5. The small circle represents the optimized pair of (f, f_{in})

blue galaxies inside the lane would be less then 50%. The closest optimized solution is a compromise between having less contamination but less red galaxies or the exact opposite. Because the aim is to constrain a region of red galaxies, the latter solution was chosen. The set of (f, f_{in}) giving the optimized solution with these conditions is the pair of limits where the upper one contains 99 % of the galaxies and the lower limit encloses 7.5 %. In the region within these limits, the fraction of blue galaxies is 52.7 % whereas the number of red galaxies inside represent 91.5 % of the total number of red galaxies.

We then apply this selection cut to the entire sample of potential mergers with $\mathrm{Log}(\mathrm{M}_*/\mathrm{M}_\odot) \geqslant 9$. This lower limit in stellar mass was adopted since the completeness limit in mass for an old, unattenuated galaxy at the low redshift limit, z = 0.005, for the SDSS is $\mathrm{Log}(\mathrm{M}_*/\mathrm{M}_\odot) \approx 8.6$.

With these limits for the lane and the mass cut sample of galaxies, the equations defining the red region are given by equation 2.3 and equation 2.4 and the final lane is illustrated in Figure 2.17.

$$(g-r)_{upper} = (0.594z^2) + (1.622z) + 1.827 \tag{2.3}$$

$$(g-r)_{lower} = (-1.445z^2) + (3.024z) + 0.594 \tag{2.4}$$

Inside this lane, the number of dry mergers is 733 (instead of the previous 890) whereas the number of non-dry mergers drops to 703 (when compared with the initial 3072). This change in the merger numbers revealed the significance of establishing a limit when searching for dry mergers. Moreover, the special role of this red region is clear when adding the photometric sample of galaxies from the SDSS DR6. Below we will adopt these equations to identify potential dry mergers from the photometric sample. By taking this approach, complemented by a subsequent visual classification, we ensure that the selection of dry mergers is as consistent as possible in the spectroscopic and photometric samples.

2.2.4.3 Non-dry merger galaxies in the lane

The comparison done above between colors and the visual classification highlights the problems of using colour alone to select dry mergers, as mentioned previously in 2.2.3.1.

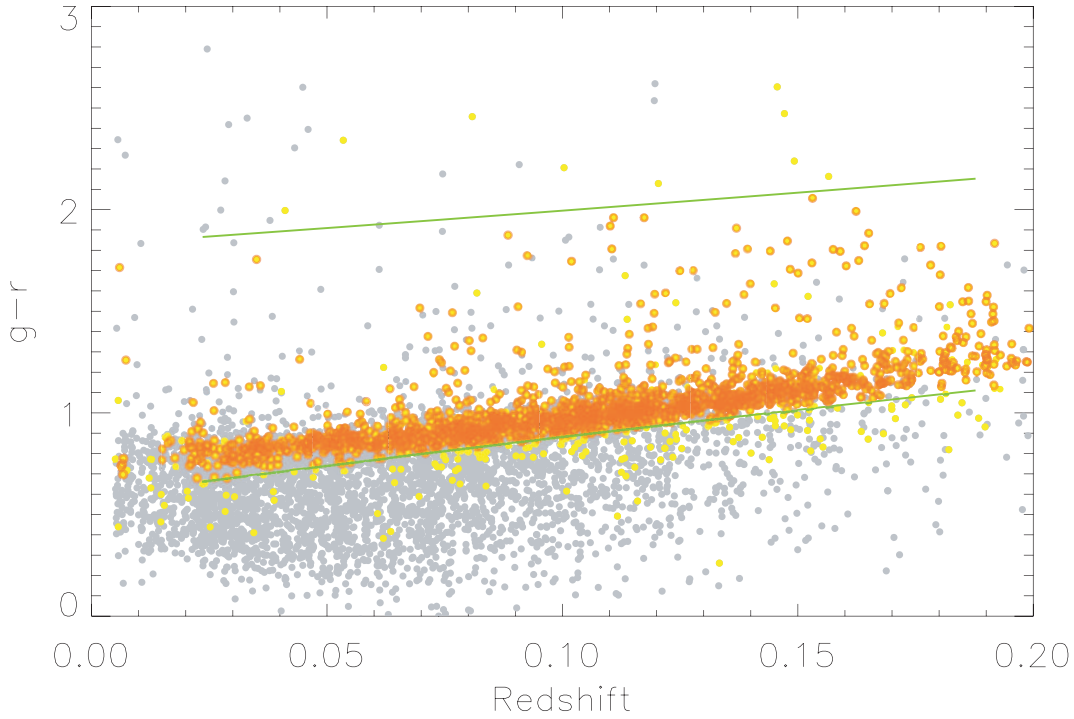

Figure 2.17: *g-r* color - redshift diagram showing the upper and lower limits (in green) of the lane defined according to equations 2.3 and 2.4. Grey points indicate all galaxies, after the mass cut, in the merger sample, yellow points represent the galaxies classified as being in dry mergers and circled yellow points are the galaxies in dry mergers and inside the lane.

We confirmed that such a choice, i.e. of using only color as a selection criterion, would lead to overestimating the number of dry mergers due to the presence of interlopers (that are not bona fide dry mergers) within our established colour limits. What is the reason for this strong contamination of the red sequence by what we deem non-dry galaxies? One possible reason might be reddening by dust - to test this we use the relative strengths between the Hα and Hβ emission line fluxes to provide an estimate of the dust attenuation within the region sampled by the fibre.

The ratio between the Hα and Hβ fluxes, as shown in equation 2.5, has been widely used as a proxy for dust estimations.

$$\left(\frac{f_{H_\alpha}}{f_{H_\beta}}\right)_{obs} = \left(\frac{f_{H_\alpha}}{f_{H_\beta}}\right)_0 e^{-[\tau(\lambda_{H_\alpha})-\tau(\lambda_{H_\beta})]} \tag{2.5}$$

Assuming a simple attenuation law (e.g. Charlot & Fall 2000) to account for the effects of dust in the ISM of the galaxies for each line,

$$\tau \propto \lambda^{-0.7} \tag{2.6}$$

where τ is the optical depth at λ wavelength, and a "reference" value for the intrinsic relation between Hα and Hβ, the Case B recombination (Brocklehurst 1971),

$$\left(\frac{f_{H_\alpha}}{f_{H_\beta}}\right)_0 = 2.86 \tag{2.7}$$

it is possible to estimate how much light has been attenuated by dust.

The visual evaluation of the merger sample carried out in section 2.2.4 classified as a non-dry group any system having at least one galaxy showing any of the five characteristics listed in that section. This leads to some of our non-dry groups having also red and dead galaxies, so, for a fair comparison with our dry merger galaxies, we only selected the dustiest galaxy of each non-dry merger (analogously to using only the bluest one for the comparisons performed in the previous section). The flux ratio of Hα to Hβ is plotted in Figure 2.18 and it shows a peak for the dry merger sample at 2.9, whereas the peak for the dustiest galaxies of the non-dry merger sample occurs for higher values, around 4, suggesting the extinction by dust is in fact strong for the

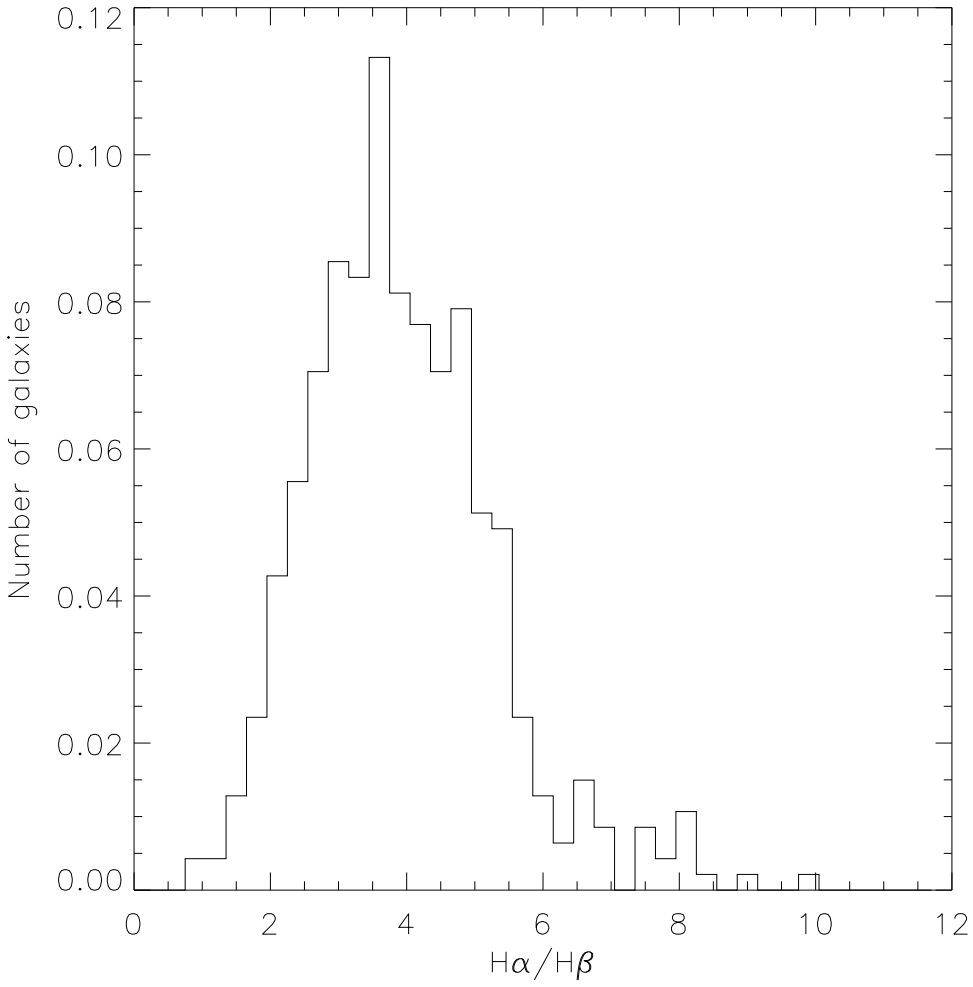

Figure 2.18: Normalized distribution of the Hα/Hβ flux ratio for the galaxies inside the color lane. The solid black histogram concerns all galaxies in dry mergers and the dashed histogram refers to the dustiest galaxies in non-dry mergers.

non-dry merger galaxies with red colors. That predominance is present for even higher values of Hα/Hβ, as revealed by a comparison between the trail of both distributions: only one fifth of the dry merger galaxies with Hα and Hβ emission lines fall above 3σ of the mean value of the respective distribution, while in the case of the dustiest galaxies in non-dry mergers, the corresponding fraction goes up to more than a half of the total sample. This confirms that the contamination by non-dry mergers in the red lane is in fact due to dust reddened galaxies.

2.3 Accounting for spectroscopic incompleteness - the photometric catalogue

In order to complete the sample of mergers drawn in section 2.2.3, the SDSS DR6 photometric catalog of galaxies was added. The first stage was to retrieve the complete photometric catalog of galaxies, classified as such from the `PhotoPrimary` through photometric parameters. Due to the way observations are carried out, the same object can be observed more than once and the `PhotoPrimary` guarantees that only the *main* observation of the object is being considered. Similarly to the spectroscopic catalog, the selected objects include all galaxies with Galactic extinction-corrected Petrosian r magnitude brighter than 17.77.

The total number of retrieved objects, from the SDSS DR6 photometric catalog of galaxies, was above 1.2 million. Note, however, that this set of objects also includes galaxies with spectroscopic observations, meaning the actual number of "new" galaxies to be analyzed, and later added for completeness, is roughly half.

2.3.1 New search for neighbour galaxies

The adopted procedure to find new potential mergers is, in essence, alike the search carried out before using only galaxies with spectroscopic measurements. In fact, to assure coherence and completeness, the search of new pairs or groups is made *exclusively* around galaxies with spectroscopic measurements (hereafter, spectroscopic galaxies). However, this time, the volume around each galaxy to be explored for neighbours comprises not only spectroscopic galaxies but also galaxies with merely photometric quantities (hereafter, photometric galaxies).

We recall that the redshift interval of the spectroscopic galaxies was set to be $0.005 < z < 0.2$. The lack of a spectroscopic redshifts for the photometric galaxies poses a problem since the photometric redshifts, although available, do not provide sufficient discrimination because the uncertainty is larger than the redshift separation adopted (e.g. Abazajian et al. 2009). To minimize the impact of this obstacle and take advantage of the new set of galaxies, the following method to search for neighbour galaxies was adapted.

In summary, a few intermediate steps were included in the previous method of building a volume with the projected separation and the spectroscopic redshift around each target galaxy, so that we now proceed as follows.

1. Apply projected distance criterion

2. Assign new redshift to neighbour photometric galaxies

3. Apply projected distance criterion and velocity offset

Step number 1. consisted in searching for neighbour galaxies using only the projected distance criterion. Identically to the procedure in section 2.2.2, a circle of radius $30h^{-1}$ kpc, at the redshift of the spectroscopic target galaxy, was defined and all neighbour galaxies were stored.

The following step was to assign a new redshift to the photometric galaxies according to the following:

- If the pair, or group, has more than one spectroscopic galaxy, the photometric galaxies will be assigned the spectroscopic redshift that is closest to the their photometric redshift.
- If the pair, or group, has only one spectroscopic galaxy, the photometric galaxies will acquire its redshift.

If the assigned redshift differs by more than 2σ from the photometric redshift estimate the photometric galaxy is excluded from belonging to the potential group. We chose 2σ since, in this case, the hypothesis that this object is at the same distance as the

nearby object appears unlikely. Here σ is the uncertainty estimate of the photometric redshift.

The last step consists in reproducing what was already done in section 2.2.2, this time using projected separation and velocity offset, since every galaxy now has a valid, and controlled, redshift. Note, that of course with the approach we cannot make general statements about the velocity separation of the members of the group because a number of them will have zero velocity separation. Note also that while photometric estimates are inaccurate for galaxies without clear features in their spectra, they are reasonably good for early-type galaxies which is what we need for our dry merger sample.

By construction, constraints on the projected distance were already ensured. In addition we require that the redshift of the spectroscopic galaxy and the photometric redshift agree within 2σ. In other words that $|z_{\rm spec} - z_{\rm photo}| \leq 2 * \sigma_z$, where σ_z is the estimated uncertainty on the photometric redshift. With this two criteria for projected distance and velocity offset, the total number of galaxies in the *new* sample of mergers is of the order of 3×10^4.

Having a sample of potential mergers with both photometric and spectroscopic redshift information, allowed us to explore the effectiveness of building a merger sample using only photometric redshifts. To that end, we tried to retrieve the merger sample mentioned in Section 2.2.3 using now the photometric redshifts of the galaxies. The projected distance between galaxies was already assured and, in addition, the velocity offset was calculated using the photometric redshifts of the galaxies within a 1σ interval for their photometric redshifts. Using this criterion, only 1891 groups were recovered, in a clear contrast with the 3962 groups previously found - less than 50% of the groups were retrieved. Even though photometric redshifts have been widely used to investigate potential merging systems, this difference shows the weakness behind this type of redshifts, mainly when dealing with galaxies that are so close together where the accuracy of the measurements can become crucial.

2.3.2 A complete merger sample

The new search for neighbours including galaxies with photometric data only, increased, as expected, the number of potential mergers. The number of galaxies in

mergers is now 36905 in a total of 15101 pairs or groups (to be contrasted with the numbers of Section 2.2.3, namely 8028 galaxies arranged in a total of 3962 groups). Note that this increase in the number of mergers is greater than the increase in the total number of galaxies, 3962 groups to 15101 from adding the galaxies without spectroscopic observations. This means that by not considering galaxies without spectroscopic measurements, a significant number of potential mergers was being neglected due to the problem of fiber placement.

As mentioned before, one of the main goals of having defined a lane in a color-redshift diagram where, according to our criteria, the galaxies constituting dry mergers should fall, is to make use of that region to find new potential dry mergers, this time using the SDSS DR6 photometric catalog. This color cut in the merger sample is aimed at identifying dry mergers and, as done before, each group is considered a candidate dry merger if *all* galaxies of that group are inside the lane, defined previously by equations 2.3 and 2.4. This color cut was preceded by a cut off in the r-band where objects with extinction corrected r-band magnitude $r < 14.5$ were discarded since they were probably stars and were assumed to have been misclassified as galaxies. It should be stressed at this point that using the color lane only selects *candidate* dry mergers. The final status as a dry merger depends, as it was the case for the spectroscopic merger sample, on a visual classification.

Applying the color cut resulted not only in a reduction on the number of mergers but also allowed to focus towards dry mergers alone. The number of groups where all galaxies are inside the lane is 3721, approximately 25 % of the total number of mergers.

In comparison to the merger sample with only spectroscopic galaxies (section 2.2.4.2), where the fraction of dry mergers over the total number of mergers is slightly over 18 %, this increase shows that even though the lane allowed to significantly focus on dry mergers, it is still not sufficient to define one. To that increase contribute:

- the contamination from non-dry mergers - at this stage, there is no separation between dry and non-dry mergers from a visual classification.

- the assigned redshifts - attributing a redshift may force the inclusion of galaxies in the lane, i.e. in the color-redshift diagram. A photometric galaxy initially lying outside the lane according to its photometric redshift, may be shifted along the

redshift axis, eventually falling within the lane once assigned the redshift of its spectroscopic neighbour.

- the lack of a mass cut - all objects are considered regardless of their stellar mass, since, at this stage, there is no information on the stellar mass of the photometric galaxies.

The following stage, visually classifying the mergers, is analogous to what was done with the spectroscopic merger sample and will allow to, once again, separate dry from non-dry mergers using the criteria described in section 2.2.4.

Due to the above mentioned problems of considering galaxies without spectroscopic information, it is not possible to reproduce entirely the method, and analysis, of the merger sample containing pure photometric galaxies. As we have seen, the use of photometric redshift can lead to unsatisfactory results for individual mergers. The main advantage of visual classifying the new sample of mergers is statistical, allowing us to derive a correction factor to apply to the spectroscopic sample.

2.3.3 Visual classification of the photometric merger sample

Visual classification was carried out for all the groups inside the lane, following the same methodology described in section 2.2.4. The number of new dry mergers is of 461, that will add to the 733 previously obtained with the spectroscopic sample alone. Therefore, a total 1194 groups which is an increase of 63% relative to the previous number of 733. This implies for instance that using the spectroscopic sample would recover only about half of the real number. This is clearly of importance when you want to calculate mass functions for instance. Note however that our analysis does suppress any likely dependence on local density. This could have some importance at the very most massive end of the mass function as the very most massive galaxies reside in very high density regions.

We should note that there are also some other concerns related to this - what exactly constitutes a *new* dry merger was also taken into consideration. By adding the photometric galaxies, it was expected that mergers already "found" when the spectroscopic merger sample was built, would have new neighbours. Indeed, during the visual inspection, that was verified to be case for over a hundred dry mergers. However, it was also noticed that some dry mergers were showing false new neighbours

- the photometric counterpart of an already existing spectroscopic neighbour was being treated as a new element of the group despite our minimum lower limit for projected separation mentioned in Section 2.3.1 . Using those mergers would introduce false positives in the mergers with $N > 2$ elements - *e.g.* a group with 2 galaxies would have 3 elements with one of the galaxies presenting two matches, one relative to the spectroscopic data and another one to the photometric data. Therefore, because this problem was found in a relatively small amount of the mergers when compared with the total number, and those mergers would be represented in the spectroscopic merger sample in any way, they were not considered as new.

2.4 Samples of isolated galaxies

The benefits of building an isolated sample from the same parent survey are many-fold - not only the photometric and spectroscopic techniques and algorithms are applied in the same manner, but it also addresses an aperture problem introduced by the different redshifts at which the galaxies are. The region of the galaxy that the 3" fibers sample is, naturally, a function of redshift.

Therefore, a major advantage of using a large survey such as the SDSS is the ability to build different sets of galaxies using the same parent sample (the SDSS DR6) and being able to, in this case, compare to the merger sample as defined in previous sections. During the course of this work, a sample of galaxies without nearby neighbours was created using the procedure described in Section 2.2.2. When the search for neighbours was carried out among the 549 572 galaxies (see Section 2.1.1), a "flag" was used to mark the galaxies *with* neighbours, which would make up the merger sample, and *without* neighbours, which have been named "isolated". Consequently, an isolated galaxy would be any galaxy without a companion galaxy within a radius $\mathrm{r}_p \leq 30\,h^{-1}$kpc *and* a velocity offset of $\mathrm{v}_{sep} \leq 800$ km/s.

The *matched* sample of isolated galaxies was assembled using galaxies flagged as having no neighbours, as previously mentioned, and with similar characteristics to the galaxies in the merger sample, namely, spectroscopic redshift and stellar mass. For each galaxy in the merger sample, a set of isolated galaxies was gathered satisfying the following conditions:

- The difference between the spectroscopic redshift of the galaxy in the merger sample and the isolated galaxies, $\Delta(z)$, is ≤ 0.01.
- The difference in stellar mass between the galaxy in the merger sample and the isolated galaxies is $\Delta(\log(M/M_{\odot})) \leq 0.1$.

Each galaxy in the merger sample was then matched to a set of isolated galaxies sharing similar attributes. The number of isolated galaxies "per" merger galaxy was, as expected, distinct - some merger galaxies had thousands of similar isolated galaxies whereas other galaxies would have few hundreds.

The isolated sample in itself is settled as a control sample depending on the quantity being compared - a representative isolated galaxy is defined *per* merger galaxy as the isolated galaxy showing the median of a certain quantity. For instance, if a comparison sample is needed to study the flux of a particular spectroscopic line between galaxies in a merger and those with no neighbours, the galaxy in the merger would be compared against the galaxy representing the median of that spectroscopic line among the set of isolated object for that merger galaxy. The flexibility of this procedure allows not one but several optimized comparison samples.

2.5 General properties of the merger sample

With an unabridged sample of mergers and the availability of spectroscopic information, we can carry out a simple assessment of changes in intrinsic properties of mergers as a function of separation. The following section covers the nature of the interacting galaxies regarding in particular their star formation and nuclear activity.

2.5.1 Star formation activity

As mentioned before, one of the most well studied phenomena in interacting galaxies is the star formation activity that shows a significant increase during the interaction. The strong tidal forces generated during the encounter create instabilities in the available gas eventually leading to episodes of violent star formation. From a spectroscopic vantage point, the measurement of this type of activity in a galaxy can be done using the information of a line, a set of lines, composite indices or even a ratio between them.

The Balmer Hα emission line is probably the most commonly applied in star formation studies since it is particular sensitive to young and massive stars and will dominate the spectrum of a galaxy that is currently forming stars(e.g. Kennicutt & Kent 1983; Ryder & Dopita 1993; Young et al. 1996; Charlot et al. 2002) . We use the equivalent width of Hα (EW(Hα)) as a tracer of star formation. For this we use measurements following the method of Brinchmann et al. (2004); Tremonti et al. (2004). Those authors measure the equivalent width from SDSS spectra while correcting for stellar absorption using the best-fit combination of Bruzual & Charlot (2003) models.

By comparing the $EWH\alpha$ of the galaxies in the merger sample with the $EWH\alpha$ for the sample of galaxies without nearby companions, the effects of the presence of a close neighbour are evident as seen in the upper panel of Figure 2.19. The difference between the $EWH\alpha$ of galaxies in mergers and the $EWH\alpha$ of the "isolated" similar galaxies (as defined in Section 2.4) is represented by $\Delta(EWH\alpha)$ and is plotted as a function of projected distance.

From Figure 2.19 it is possible to conclude that enhancement in star formation activity does not depend strongly on the stellar mass ratio between the elements of the merger. Galaxies in both major and minor mergers show an increase up to a factor of three for projected separations below $\sim$10 kpc. There seems to be nevertheless a slight difference for the distance at which the proximity to a neighbour galaxy starts to take effect - galaxies in minor mergers tend to enhance their star formation activity at slightly larger distances when compared with galaxies in minor mergers.

These results suggest that even though there is strong dependence of triggered star formation on the merger stellar mass ratio. However, they seem to indicate that the tidal forces responsible for the triggering of the star formation are experienced slightly sooner if the galaxies are enrolled in minor mergers. However, the effect of aperture may be playing a role since the $EWH\alpha$ is being measured in the central region of the galaxy, meaning that bigger, or more massive, galaxies could indeed be reacting to the presence of a neighbour as strongly as less massive galaxies but such activity outside the central region would not be detected.

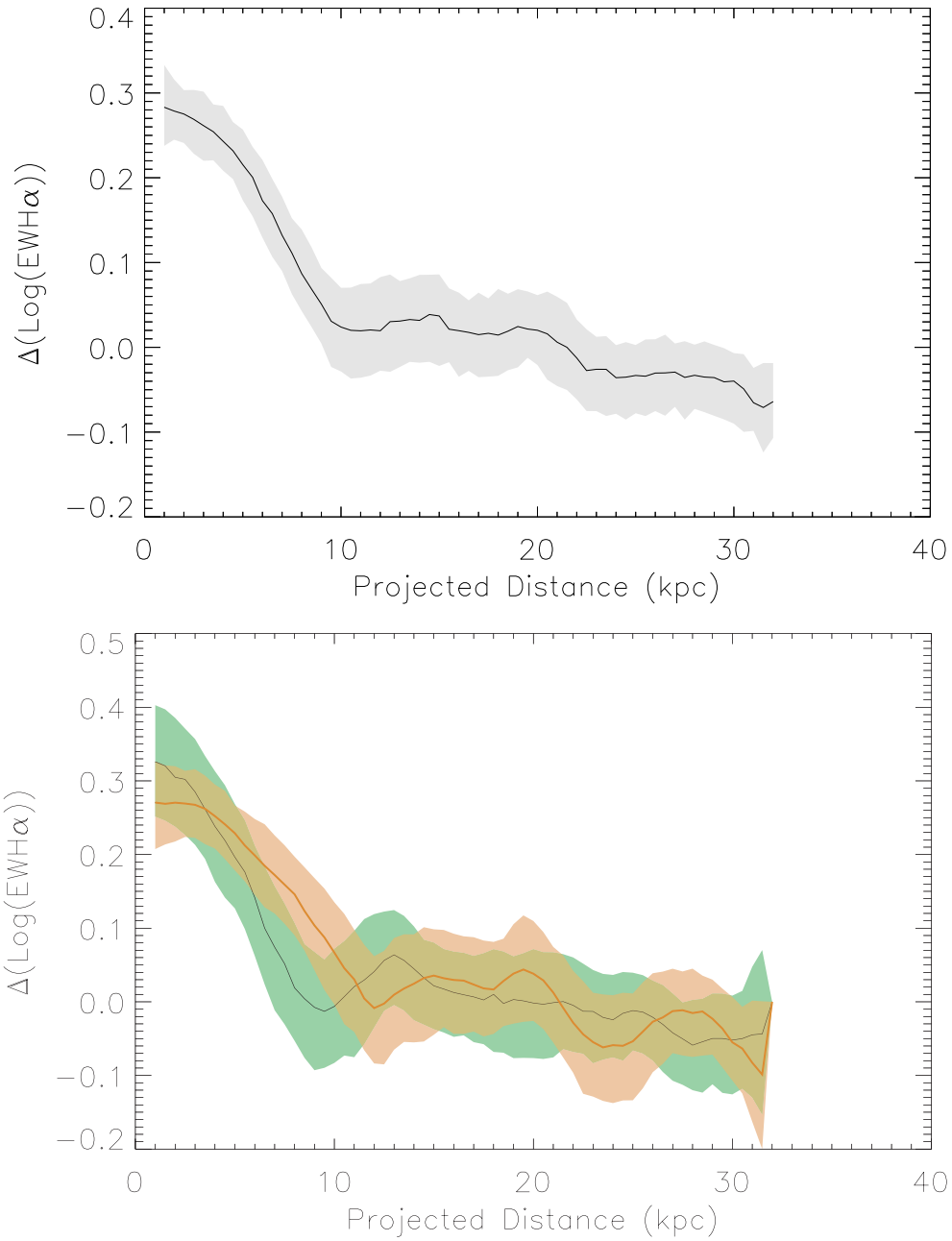

Figure 2.19: Enhancement in the Hα emission as a function of projected distance. In the upper panel, the solid line indicates the median trend for the galaxies in the merger sample. The lower panel, the solid line indicates the median for galaxies in major mergers (green) and minor mergers (orange). The shaded areas represents the 1σ deviation as obtained by bootstrap re-sampling techniques.

2.5.2 AGN activity

Simulations have in the last 5-7 years increasingly included AGN activity as a physical process influencing galaxy evolution. In an influential set of simulations Springel et al. (2005a) and Di Matteo et al. (2005) showed that if strong feedback from the AGN onto the host galaxy could be realised, then star formation could be efficiently quenched. This led to a much better agreement between observations of massive galaxies and theoretical models as was further elaborated in semi-analytic models (Bower et al. 2006; Croton et al. 2006; De Lucia et al. 2006). However, strong observational evidence is still lacking to completely verify theoretical predictions (e.g Silk & Rees 1998; Di Matteo et al. 2005; Springel et al. 2005b).

By analysing the fraction of AGN galaxies within the sample of merging galaxies, a relation with merger status can be therefore investigated. In this work we make use of the classification as AGN-host galaxy, based on spectroscopic data, as described in Kauffmann et al. (2003). This classification follows the classic classification scheme introduced by Baldwin et al. (1981) (hereafter BPT), where a set of spectroscopic indexes classify a galaxy in star-forming, AGN or composite, the latter displaying optical features from both HII, typical in star forming galaxies, and Seyfert, characteristic of AGN-host galaxies. An example of a classification scheme with a BPT diagram is illustrated in Figure 2.20, from Brinchmann et al. (2004). For reference, the BPT diagram for the galaxies in the merger sample is illustrated in 2.21. In fact, the branch where AGN-host galaxies are placed is often referred to as a mixing line (e.g. Kewley et al. 2006b) due to the nature of the galaxies filling the branch - the pure AGN would be on the top part of the branch, while with increasing star formation activity, the galaxies move downwards on the diagram, their emission line spectrum becomes mixed and in the bottom part is considered to be dominated by star formation activity.

For reference, Figure 2.21 shows the BPT diagram for the galaxies in the merger sample. According to this classification scheme, number of AGN-hosts in the merger sample is 1120, approximately 15% of the total number of galaxies undergoing a merger, consistent with an incidence of AGN-host galaxies of $\sim$ 15% found in the SDSS DR6 galaxy sample, for the redshift interval $0.005 < z < 0.2$.

The fraction of AGN galaxies within the merger sample is plotted in Figure 2.22 as a function of projected separation. Contrary to what may have been expected, the

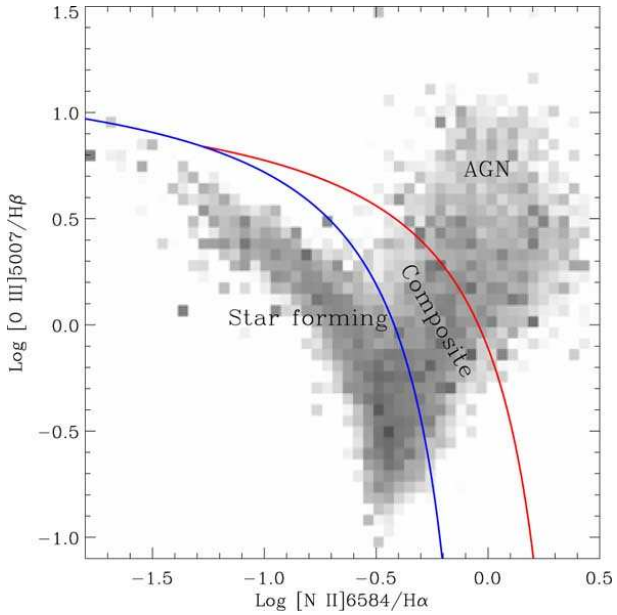

Figure 2.20: The distribution of the galaxies in Brinchmann et al. (2004) sample in the BPT line-ratio diagram. The lines show the division of their sample into the three categories of star forming, composite and AGN.

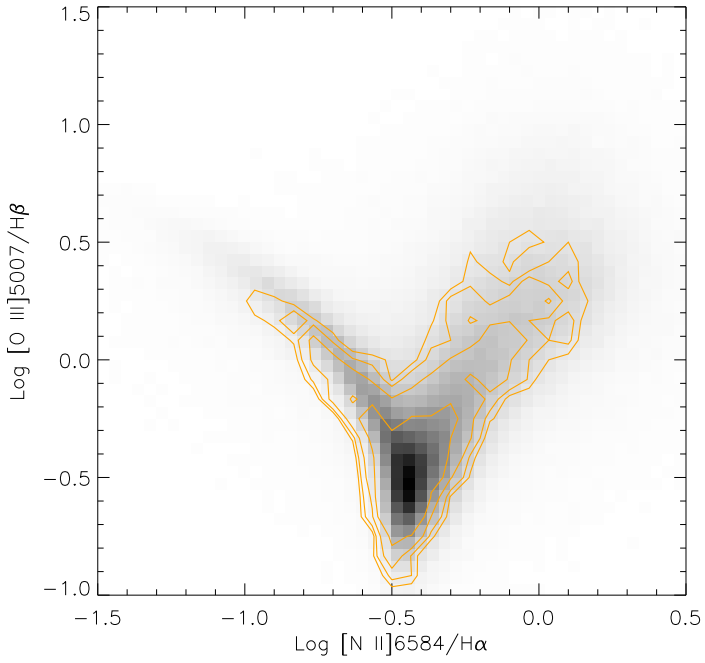

Figure 2.21: The distribution of the galaxies in the merger sample (contours) plotted over the sample of spectroscopic galaxies of the SDSS DR6 (in gray scale), in the same BPT line-ratio diagram described in Figure 2.20

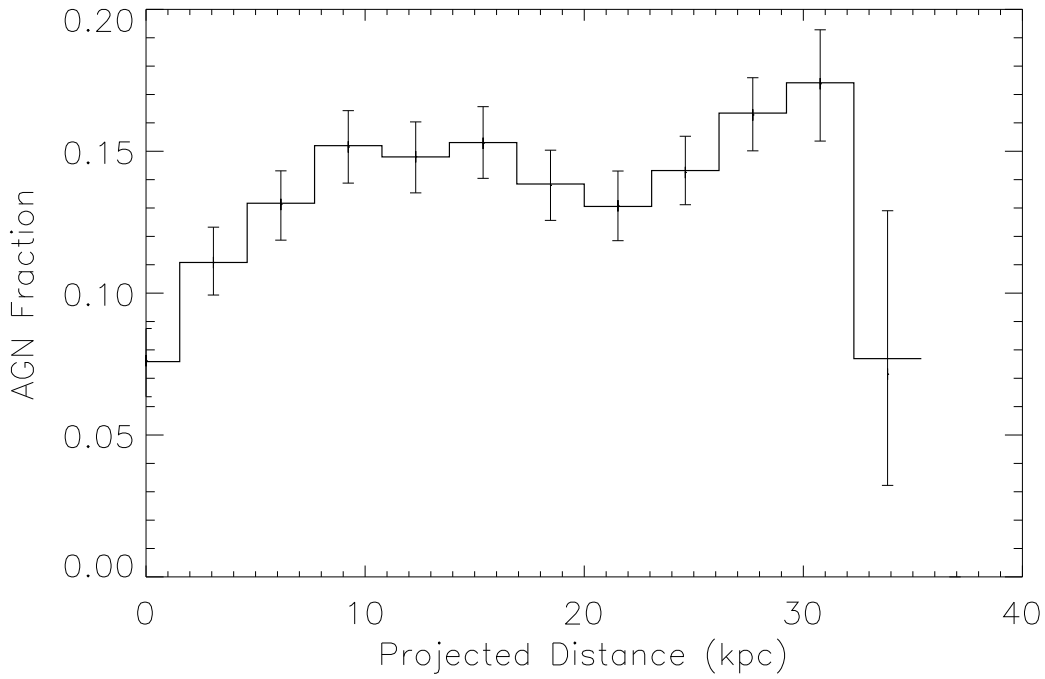

Figure 2.22: AGN fraction in mergers as a function of projected distance. The estimation of the error bars was carried out with bootstrap repetitions and correspond to the 16%-84% confidence interval, equivalent to a $\pm 1\sigma$ uncertainty bars for a Gaussian distribution.

AGN fraction does not increase for late stage mergers, i.e. small separations. In fact, the fraction of AGN in mergers shows a decrease below 10 kpc.

The decrease in the AGN fraction with projected separation within the merger sample could be explained by this mixing, if an increase in composites and star forming galaxies could be reproduced. In Figure 2.23 are represented the fractions of both composite and star forming galaxies as a function of projected separation between the group members.

The slight increase in the fraction of composite galaxies accompanied by the strong increase in star forming galaxies in fact points towards the mentioned mixing process. The star formation activity triggered by the merger process starts dominating the spectrum and the AGN becomes hidden and, therefore, not detectable.

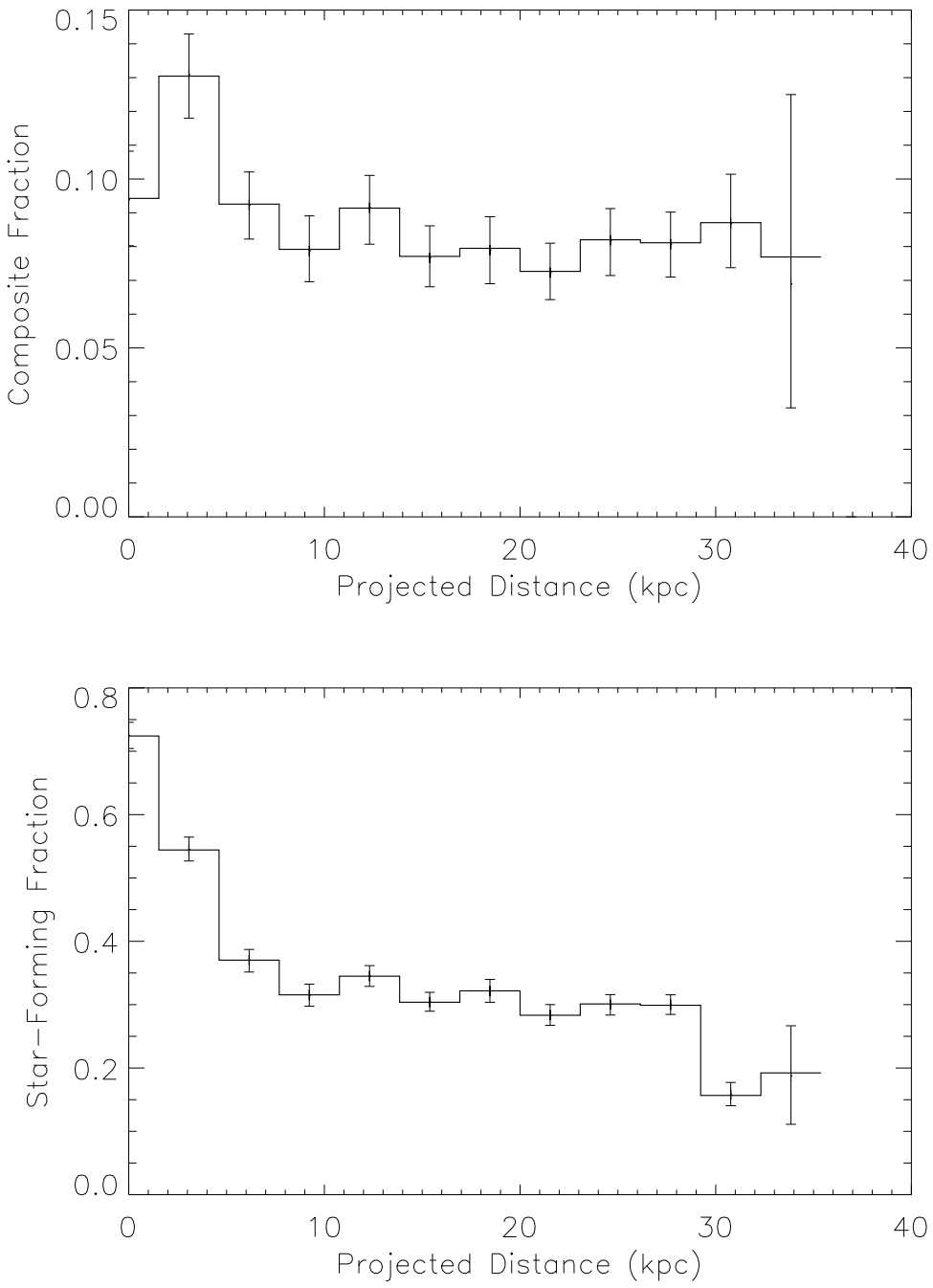

Figure 2.23: Composite (top) and star forming (bottom) fraction in mergers as a function of projected distance. The error bars are determined using bootstrapping re-sampling techniques.

Chapter 3

Properties of Dry Mergers

Ever since mergers between gas-poor galaxies have been observed, in particular at z <2, a new path of massive galaxy assembly has been uncovered. However, the exact role of these mergers in building massive galaxies is still under great debate and even though some open questions have been settled - there is now evidence that galaxies evolving passively since z=2 is not the only path to build the massive ellipticals seen in present-day - other questions have been raised: how do dry mergers differ from non-dry mergers in building up new galaxies? Do end-products of low redshift dry mergers show compatible properties with the local population of elliptical galaxies? How many massive galaxies in the local Universe have been assembled via dry merging?

This Chapter contains the results of the analysis of the merger sample built from the SDSS DR6 described in Chapter 2, introducing a very large sample of mergers between gas-poor galaxies. We study the properties of this type of mergers and discuss its relevance to the build-up of the high-mass end of the galaxy mass function.

Throughout we assume standard cosmology Ω_M=0.3, Ω_Λ=0.7, h=0.7.

3.1 Evolution of the stellar population with redshift

Being the building blocks of the structure of the universe, galaxies are however primarily defined by their stellar content. Therefore, the distribution of galaxies with stellar mass is a fundamental constraint on models for galaxy formation and evolution. This was already emphasised in a classic paper by Cowie et al. (1996) who studied the properties of galaxies as a function of K-band luminosity and coined the concept of *downsizing* - stars in more massive galaxies tend to have been formed earlier and over a shorter period of time. Subsequently a large number of studies have followed to explore the evolution of the stellar mass function with redshift (e.g. Marchesini et al. 2009) and established a significant growth in the stellar mass in galaxies with decreasing redshift, amounting to a factor of 2-4 from $z = 1.5 - 2$ to the present.

Going to slightly lower redshifts there is evidence that much of the stellar mass in massive galaxies was assembled by $z \sim 1$ (e.g. Bundy et al. 2007; Cimatti 2007; Cowie & Barger 2008; Cimatti 2009) and with a weak evolution until $z \sim 0$. This compares well with the evidence from stellar populations in local massive galaxies which indicate that the stellar content of local massive elliptical galaxies was predominantly formed before $z \sim 1$ (e.g. Thomas et al. 2005) although the process of *assembly* of the stellar mass and *formation* of the stars might not occur at the same time.

In general the majority of stellar mass is locked up in red and old galaxies (Brinchmann & Ellis 2000; Hogg et al. 2002) also pointing to an early formation epoch for their stars. This has led some to conclude that the massive end of the mass function was in place already at $z \sim 1$ as argued for instance by Scarlata et al. (2007) in their study of the mass functions in the COSMOS survey. While the evidence certainly point to a majority of the massive end of the mass function being in place by $z \sim 1$, the exact percentage is open to discussion, with Abraham et al. (2007) arguing for about 80% based on the Gemini Deep Deep Survey (GDDS, Abraham et al.) while Pozzetti et al. (2007) finding about 60% for the VIMOS Very Deep Survey (VVDS; Le Fevre et al. 2003). Thus there certainly appears to be a need to identify channels for the assembly of massive galaxies at relatively late epochs.

Evidence seems to indicate an increase in the total stellar mass enclosed in massive

galaxies since $z = 1$ (e.g. Renzini 2006). This has frequently been taken as a sign of a transformation of blue star forming galaxies at z=1 into the old objects observed at the present epoch (e.g. Brinchmann & Ellis 2000; Bundy et al. 2007, 2009) although Faber et al. (2007) have argued that the number density of blue galaxies has remained nearly constant since $z = 1$, whereas the number density of massive red galaxies has increased indicating that some fraction of early-type galaxies could have been assembled at late times.

While the common understanding has for some time been that early-type galaxies form through massive mergers, more recent work has painted a more nuanced picture. For instance Naab et al. (2006) argued that a scenario where all early-type galaxies originate from major mergers of gas-rich spiral galaxies is unable to reproduce the observed properties of very massive elliptical galaxies. Similarly Bell et al. (2005) argued that the properties of high luminosity ellipticals are not compatible with an assembly via a process of merging of spirals with significant associated star formation, since the stellar populations of these progenitor galaxies would have the wrong age and abundance characteristics.

A possible way to reconcile these results is to postulate that some of these massive galaxies have been assembled through gas-poor mergers where few new stars are formed. This process of galaxy merging with no significant associated star formation, dubbed *dry* merging (e.g. van Dokkum 2005; Bell et al. 2005), is also consistent with the lack of very massive star-forming galaxies at low redshifts to build the massive non-star-forming early-type galaxies (Bell et al. 2004; Naab & Ostriker 2009).

A previous study by Khochfar & Silk (2009) suggested the existence of a shut-off mass scale (Figure 3.1) where dry mergers would be predominant for the build up of massive galaxies. Using semi-analytic models, they found that the overall number of dry mergers is enhanced in relation to the number density of non-dry mergers at a mass scale of $\mathrm{M}_{*,c} \sim 6.3 \times 10^{10} \mathrm{M}_{\odot}$, and argue that dry mergers are favoured in building up massive galaxies since galaxies at $M_{*,c}$ are no longer forming stars and will only grow through mergers. The existence of such a mass cut-off is still under debate and only surveys with a significant number of galaxies, such as the one presented in this thesis, can shed some light to this theory.

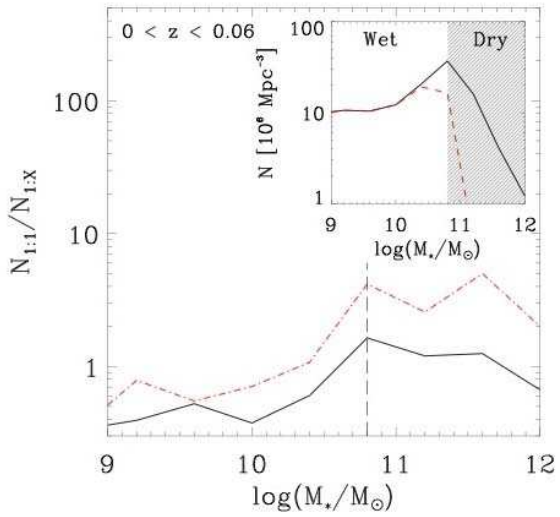

Figure 3.1: Fraction of 1:1 to 1:2 (solid line) and 1:1 to 1:3 (dot–dashed line) mergers as a function of remnant stellar mass within the redshift interval $0 < z < 0.06$. Inset graph: number density of all mergers (solid line) and of only wet mergers as a function of remnant mass within the same redshift interval. The black vertical dashed line indicates $M_{*,c}$ (Khochfar & Silk 2009)

3.2 Mergers between gas-poor galaxies

Dissipationless mergers were thought to be of little importance, in part because massive galaxies normally reside in dense regions where relative velocities typically are too high to make mergers a likely occurrence. In fact the first examples of dry mergers were found in clusters (e.g. van Dokkum et al. 2001). It was subsequently realised that while rare, the dissipationless merger of massive galaxies might help explain part of the assembly of the most massive galaxies.

Despite being an appealing channel for the formation of very massive galaxies, the observational evidence for dry mergers is a bit conflicting with some authors arguing for dry mergers as a significant process for the assembly of massive galaxies (Naab et al. 2006; Bell et al. 2006; Hopkins et al. 2009a; Liu et al. 2009; Eliche-Moral et al. 2010), while others find it to be of marginal importance, such as Masjedi et al. (2006) based on their study of the correlation function of SDSS luminous red galaxies (LRGs). Some recent studies have tried to disentangle the importance of dry and wet mergers - often implemented as "red" versus "blue" mergers - as a function of look-back time. For

instance Bundy et al. (2009) find that the relative importance of dry major mergers increases relative to that of wet mergers at more recent times. A similar result is revealed by Chou et al. (2011) where the number fraction of dry mergers increases with decreasing redshift. This points to dry mergers being an important process in the build-up of massive galaxies at the present epoch.

Nonetheless there are significant discrepancies between the different merger estimates in the literature and the techniques used also differ rather significantly between different authors. Furthermore the efforts mentioned above are mostly focused on major mergers, where the definition of major does vary but is typically something like mergers with mass-ratios of 1:4 or larger, and these might present only part of the picture. This was recently highlighted by López-Sanjuan et al. (2010) who emphasised the need to include minor mergers to explain the growth of ellipticals at low redshift. This is also consistent with the work of Bundy et al. (2009) who found that the observed major mergers do not explain the mass growth of spheroids at $z < 1$, although both results do, to some extent, depend on the uncertain time-scale of galaxy mergers. In fact there is much work to be done in disentangling the time-scales of the mergers themselves to determine the place of dry mergers (e.g. Bundy et al. 2009; De Propris et al. 2010; Chou et al. 2011; Tojeiro & Percival 2011)

A fundamental difficulty for studies of the formation and evolution of massive galaxies is however that they are strongly clustered. This means that large volumes must be sampled to reduce the importance of cosmic variance. Another reason for discrepancies among different studies is that the classification of galaxies as dry mergers differs significantly between authors with limited checks on the sensitivity to the results.

3.3 Merger properties

As mentioned previously, having spectroscopic information is a major advantage to investigate the role of mergers in the build up of galaxies. The spectroscopic information allows not only to more accurately establish a merging status for the galaxies through their spectroscopic redshift, but it also allows estimation of masses of the stellar and gas components, chemical composition, star formation and nuclear activity, among others.

The primary objective of this work is to understand how galaxies are assembled via merging of early-type galaxies and its importance in the build up of the high-mass end of the galaxy mass function. To that end, and with the availability of a large sample of mergers, we can explore how different merger properties may influence the mass function of galaxies.

3.3.1 Major and minor mergers

In the process of assembling galaxies via dry merging, galaxies of comparable stellar mass play a bigger role than mergers of satellite galaxies into a larger one. To analyse the impact of these different types of mergers, we divide our sample into *minor* and *major* mergers referring to the ratio between the stellar mass of the galaxies in the group. A group is considered *minor* if the stellar mass ratio of the galaxies is $< \frac{1}{3}$ and *major* if the stellar mass ratio is $\geq \frac{1}{3}$. In the case of groups with more than two galaxies, we consider the masses for the most massive and second most massive galaxy. We should note, however, that major mergers may not necessarily be between galaxies with a substantial stellar mass component. A group with low mass galaxies will be a major merger as long as their stellar masses obey the ratio mentioned above.

The spectroscopic merger sample is, as a result, composed of 1941 major mergers and 2021 minor mergers. The distribution of masses plotted in Figure 3.2 show the total mass for the merger sample. The stellar masses for each group were summed to estimate the final mass of the assumed end-product of the merger. Even though the major and minor merger classification did not take into account any stellar mass cut-off, it is clear from Figure 3.2 that major mergers are more significant for the build-up of massive galaxies than minor mergers, specially for galaxies above $M_* \sim 10^{11}$ $M_\odot$.

We note that the mass functions shown throughout this Section are already corrected for the 0.63 completeness factor, as mentioned in Section 2.3.3 of Chapter 2, unless stated otherwise. The effect of this correction factor can actually be seen in Figure 3.3, where mass functions for different sets of galaxies are plotted. Using mergers based solely on galaxies with spectroscopic information would in fact be underestimating the number of galaxies in mergers.

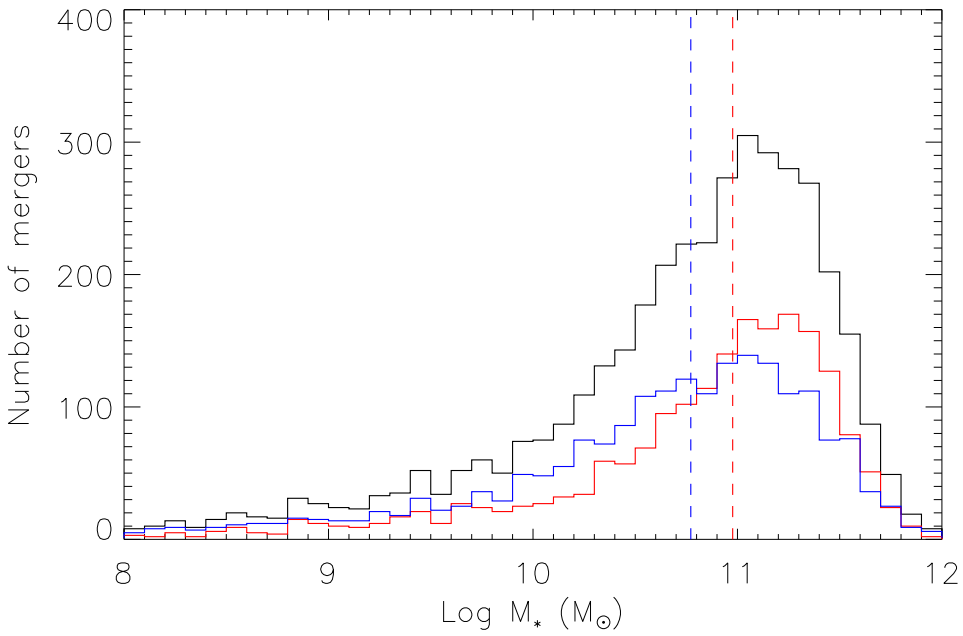

Figure 3.2: Total stellar mass distribution for minor and major mergers. The histograms illustrate the distribution of the total mass of the mergers. The black histogram is for all the merger sample, the yellow and red histograms are for minor and major mergers, respectively. Indicated in a dashed line are also the medians for minor mergers in yellow, and for major mergers, in red.

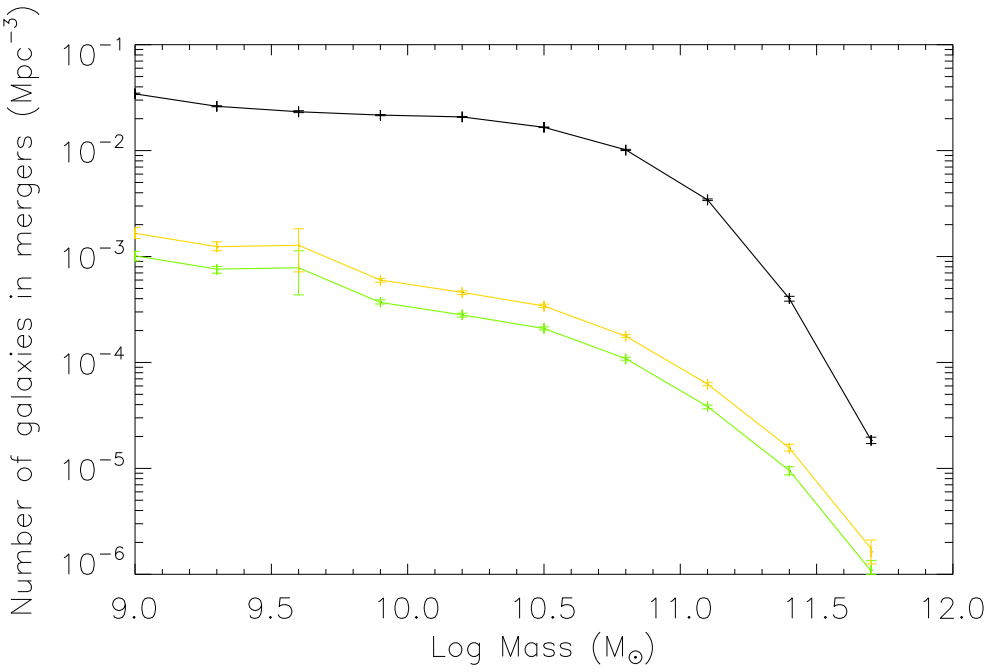

Figure 3.3: Mass distribution for galaxies in mergers with error bars derived by bootstrapping methods. For reference, the solid black line illustrates the mass function for all galaxies in the SDSS DR6 spectroscopic sample within the redshift interval $0.005 < z < 0.2$. The green line corresponds to the mass function of galaxies in the merger sample without the correction factor of 0.63. The yellow line represents the mass function of galaxies in mergers corrected of 0.63 as mentioned in Section 2.3.3

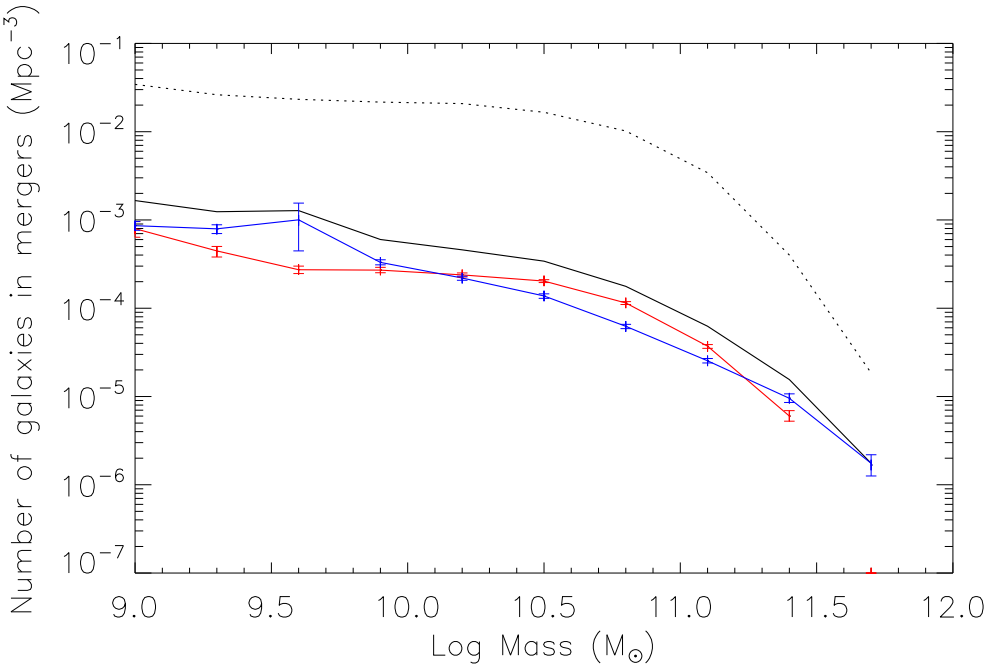

Figure 3.4: Mass distribution for galaxies in mergers. The solid black line including all galaxies in mergers and, for reference, the dotted line is the mass function for the galaxies in the SDSS DR6. The red line is the mass distribution of galaxies in major mergers and the blue line is the same for galaxies in minor mergers. The error bars are calculated using bootstrapping methods.

The mass functions for galaxies in major and minor mergers is shown in Figure 3.4. Galaxies in major mergers sample the higher-mass bins of the mass distribution, specially at masses above $\log M_*/M_\odot = 11.4$, in accordance with Maller et al. (2006) who predict a higher incidence of major mergers for high-mass galaxies.

As previously mentioned, one major advantage of having spectroscopic information on the galaxies is to study in detail their star formation activity usually indicated by the presence of emission lines. Applying star formation criteria could be, at a first approximation, a useful tool to separate between galaxies involved in gas-poor and gas-rich mergers - galaxies in dry mergers would show virtually no star formation and galaxies in non-dry mergers would, on the other hand, reveal star formation activity taking place as a result of the interaction. Figure 3.5 shows the mass function for the SDSS DR6 spectroscopic galaxies within the redshift interval used to build the merger sample, i.e. $0.005 < z < 0.2$, and the distribution for the galaxies in the mergers sample in three different bins of star formation rate per unit stellar mass, or specific

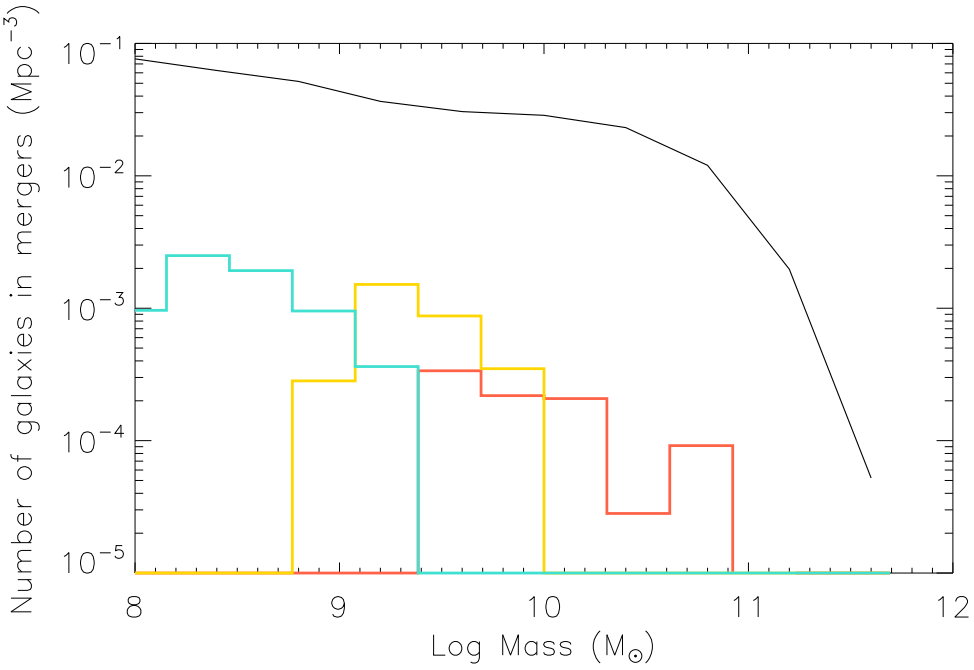

Figure 3.5: The mass function of the SDSS DR6. The solid black line represents the overall mass function for the spectroscopic sample of galaxies of the SDSS DR6 for the redshift interval $0.005 < z < 0.2$. The coloured histograms show galaxies in the major merger sample in bins of specific star formation rate (SSFR). The blue histogram shows the distribution for galaxies with higher SSFR ($10^{-10} < SSFR < 10^{-1}$), the yellow histogram is for $10^{-11} < SSFR < 10^{-10}$ and the red histogram for galaxies with $0 < SSFR < 10^{-11}$

star formation rate (SSFR). This quantity is particularly useful, since SFR has been shown to be correlated to stellar mass and a normalization by stellar mass would solve that dependency (Brinchmann et al. 2004).

The red histogram of Figure 3.5 places dry mergers into context and reveals their importance in the assembly of massive galaxies. We opted to consider only galaxies in major mergers given that their contribution would clearly be more significant to build up new massive galaxies and we should note not all galaxies in the major merger sample were plotted due to errors in their SFR estimates. As expected, galaxies with virtually reduced star formation activity, i.e. $0 < \mathrm{SSFR} < 10^{-11}$, are positioned in the higher mass bins and dominate the high mass end. There is, however, a noticeable continuum of SSFR with high mass mergers varying in their star formation properties. Thus, isolating dry mergers having star formation criteria as a basis alone would lead

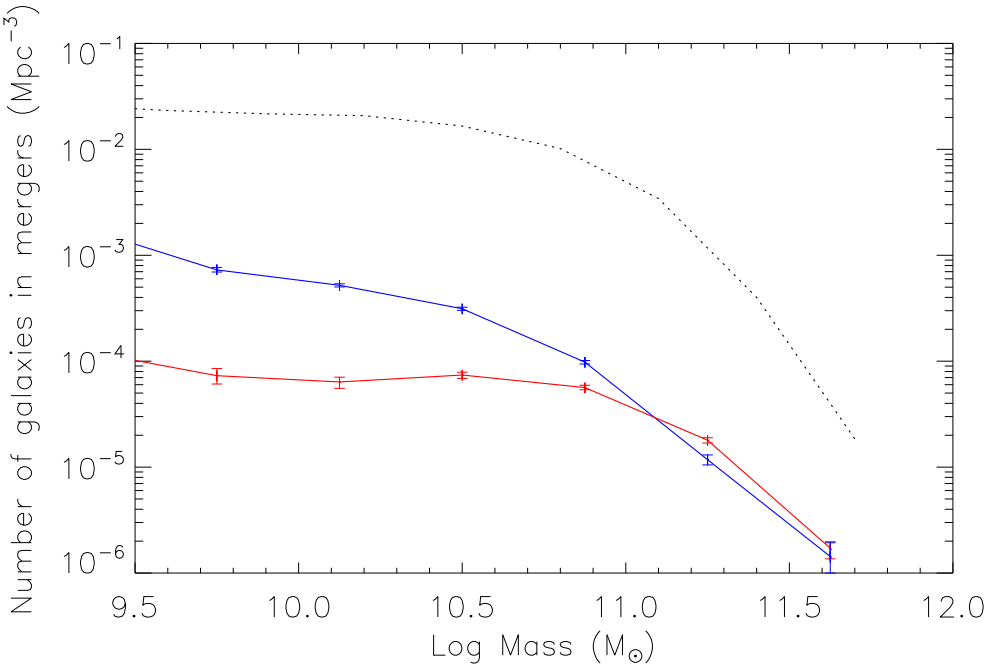

Figure 3.6: Mass distribution for galaxies in dry and non-dry mergers. The red line represents the distribution for galaxies in dry mergers and the blue line illustrates the same for galaxies in non-dry mergers. The dotted line represents the mass function for all spectroscopic galaxies in SDSS DR6 inside our redshift interval. The error bars are calculated using bootstrapping methods.

to arbitrary cuts.

3.3.2 Dry and non-dry mergers

With the visual classification described in Section 2.2.4, we analyze to what extent the galaxy mass function depends on dry and non-dry mergers. In Figure 3.6 are plotted the mass functions for galaxies in dry mergers and for galaxies in non-dry mergers. At low and intermediate masses, up to $\log M_*/M_\odot = 11$, galaxies in dry mergers do not contribute significantly and the lower mass bins are dominated by galaxies in non-dry mergers. This feature is even more pronounced when considering only galaxies in major dry and non-dry mergers, as shown in Figure 3.7.

The contribution of galaxies in dry mergers remains close to constant up to galaxy

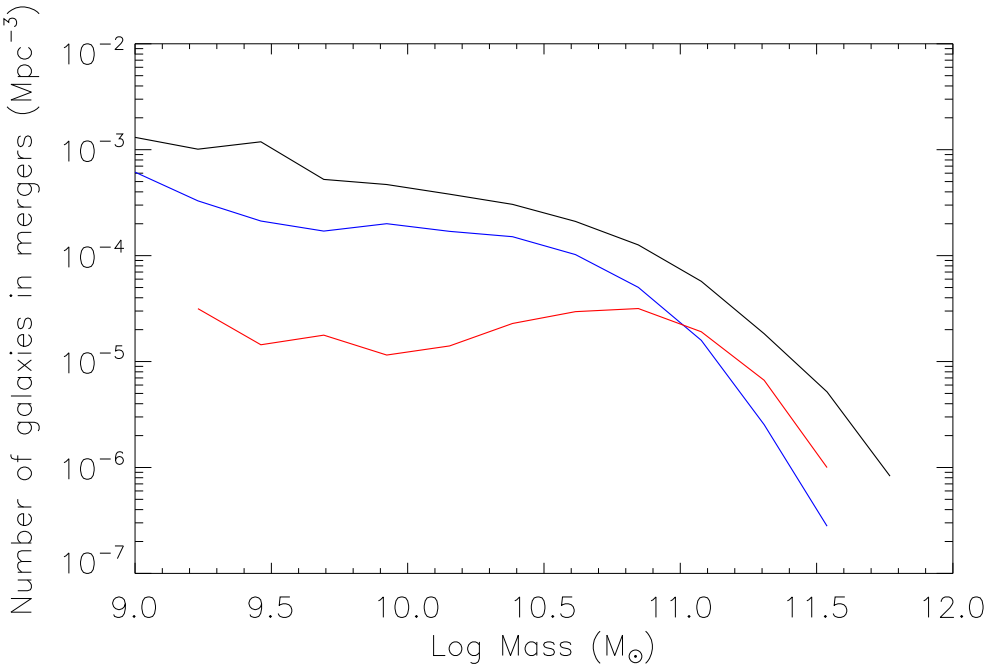

Figure 3.7: Mass distribution for galaxies in dry and non-dry major mergers. As in Figure 3.6, the red line represents the distribution for galaxies in dry mergers and the blue line illustrates the same for galaxies in non-dry mergers. For reference, the solid black line includes all galaxies in dry and non-dry major mergers.

stellar masses of $\log M_*/M_\odot \sim 11$. Even though this contribution is significantly lower than the galaxies in non-dry mergers for the low and intermediate mass parts of the mass function, the number density of galaxies in non-dry mergers is overcome by galaxies in dry mergers at $\log M_*/M_\odot \sim 11$. When looking to the number of dry and non-dry mergers, and assuming the mass of the end galaxy as the sum of the progenitor's stellar masses, it is possible to directly assess the impact of each type of merger - dry and non-dry, major and minor. In Figure 3.8 are illustrated the mass functions for the mergers' remnants. Once more, dry mergers probe the most massive end of the galaxy mass function, with their putative remnants sampling high stellar masses, specially at $M_* \sim 11.5$ $M_\odot$, where the contribution of galaxies resulting from non-dry mergers drops significantly.

3.3.2.1 Is there a mass cut-off?

As previously mentioned, a recent study by Khochfar & Silk (2009), using semi-analytical models of galaxy formation, have suggested a mass cut-off at $M_{*,c} \sim 6.3 \times 10^{10} M_\odot$, or $\log(M_*/M_\odot) \sim 10.8$, as a boundary for transition of galaxies being formed predominantly in gaseous mergers, i.e. non-dry mergers, to being formed through dry mergers. As a consequence, a new way to detect dry mergers would be by establishing a mass limit below which the contribution of non-dry mergers to the number density of all mergers would be dominant as compared with dry mergers.

To assess the existence of such a cut-off mass, we have estimated a sample of remnants of dry and non-dry mergers, assuming the stellar mass of the end-product of these mergers would be the sum of the galaxies involved in the merger. Figure 3.9 illustrated the number of remnants in each type of merger. Even though there is a stellar mass where the role of dry mergers to build up galaxies overcomes the contribution of the non-dry mergers, that mass is much higher than the suggested $M_{*,c}$, possibly as high as $\log(M_*/M_\odot) \sim 11.2$. The repercussion of using the $M_{*,c}$ indicated by Khochfar & Silk (2009) to separate dry mergers would severely contaminate such selection with non-dry mergers.

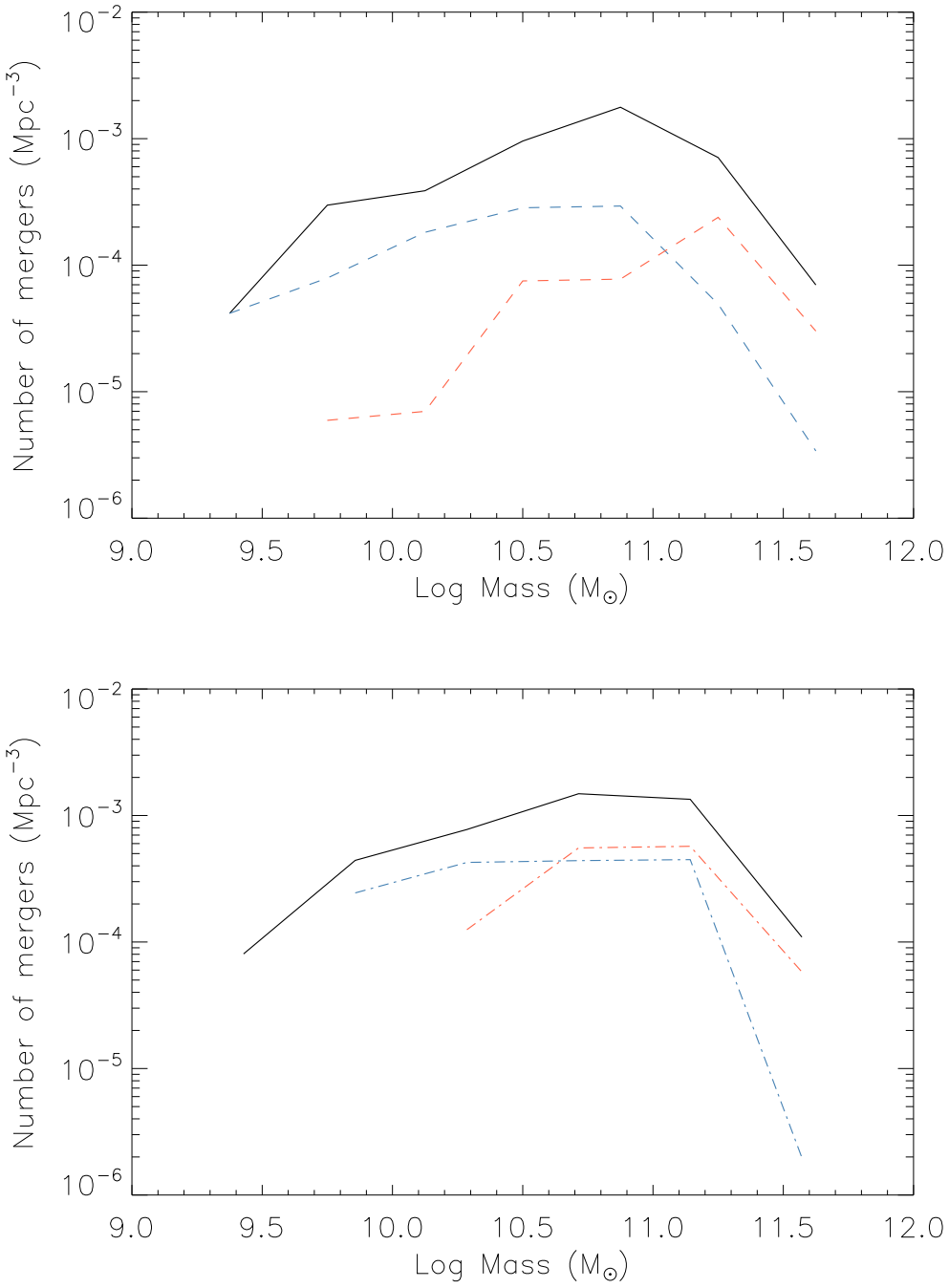

Figure 3.8: Mass distribution for major mergers(upper panel) and minor mergers (lower panel). The solid black line represents the estimation for the mass function considering all the putative end-products of the systems in the merger sample. The blue and red lines are in turn the mass functions for the remnants of non-dry and dry mergers, respectively.

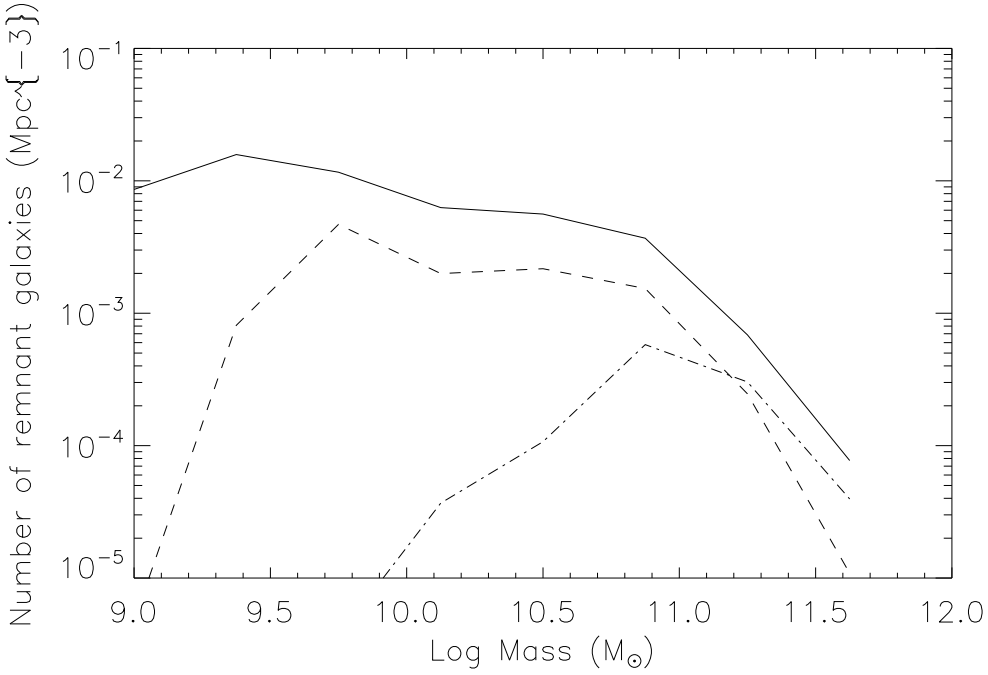

Figure 3.9: Number density of all mergers (solid line), of non-dry mergers (dashed lined) and dry mergers (dash-dotted line).

3.3.3 Merger fractions

To understand the importance of dry merging it is necessary to grasp some key quantities that hold information on the properties of the mergers. Some definitions have been proposed for merger rate, pair fractions and merger fraction, however, the most commonly used is a) the pair fraction, or some variation of the pair fraction, that typically estimates the number of galaxies with close neighbours within a given sample and b) the merger rate, which is usually defined as the number of galaxies merging per unit volume and per unit time.

Here we define a volume corrected *merger fraction* as the ratio between the number of mergers and the total number of galaxies:

$$f_m = \frac{\rho_m}{\rho_g} \tag{3.1}$$

where,

$$\rho_m = \sum_{i=0}^{x} \frac{1}{V_{max}^i}$$
$$\rho_g = \sum_{j=0}^{y} \frac{1}{V_{max}^j} \tag{3.2}$$

with ρ_m representing the volume corrected distribution of mergers, with x being the total number of mergers. ρ_g is the volume corrected distribution of all considered galaxies, i.e., y represents the total number of SDSS DR6 spectroscopic sample of galaxies inside the redshift interval.

Another quantity can be derived from the previous one that is the volume corrected *galaxy merger fraction*, the ratio between number of galaxies merging and the total number of galaxies:

$$f_{gm} = \frac{\rho_{gm}}{\rho_g} \tag{3.3}$$

where ρ_{gm} is given by,

$$\rho_{gm} = \sum_{k=0}^{z} \frac{1}{V_{max}^k} \tag{3.4}$$

and ρ_{gm} is the volume corrected distribution of galaxies in mergers, with z the total number of galaxies merging.

We find a total merger fraction for SDSS DR6, in the redshift interval $0.005 < z < 0.2$ of $f_m = 0.093$. However, since we have the information for the stellar masses of the galaxies, we investigate the merger fraction for different stellar mass ratios, in particular for major and minor mergers. We estimate a merger fraction for major mergers of $f(_m)^{major} = 0.012$ and for minor mergers of $f(_m)^{minor} = 0.080$, in agreement with a higher frequency of mergers among galaxies with very different masses with relation to mergers of galaxies of approximately the same stellar mass (e.g. Lotz et al. 2010).

The galaxy merger fraction, i.e. the total fraction of galaxies undergoing a merger,

f_{gm} is 0.031.

We note that in our sample of spectroscopic mergers, the presence of systems having N galaxies is completely dominated for groups with N=2, with more than 97% of the systems having two elements.

3.3.4 Merger rate

To establish a merger rate is not an easy task since one can only estimate a timescale for the mergers, assuming (a) the systems *will* merge and (b) they will merge at a average timescale. Assuming a T_m as an average timescale for the merger to take place, we can simply define a merger rate as

$$R_{mg} = \frac{f_m}{T_{mg}} \tag{3.5}$$

Several studies (e.g. Lin et al. 2004, Mateus 2008), use $\mathrm{T}_{mg} \sim 0.5$ Gyr obtained from N-body simulations. Here, we adopt the method of Patton et al. (2000) and we establish a merger timescale for our sample, following (Binney & Tremaine 1987). We estimate T_{mg} through the dynamical friction timescale T_{fric} given by

$$T_{fric} = \frac{2.64 \times 10^5 r^2 v_c}{M \ln \Lambda} \tag{3.6}$$

where r is the initial physical separation between galaxies in kpc, v_c is the circular velocity in km/s, M is the mass in $M_\odot$ and T_{fric} is in Gyr. We take the assumptions of Patton et al. (2000) and assume circular orbits and a dark mater density profile given by $\rho \propto r^{-2}$. The $\ln \Lambda$ is the Coulomb logarithm and is estimated to be $\ln \Lambda \sim 2$. We take advantage of the availability of stellar masses and we estimate the merger rates for different mass bins, determining a mean physical separation $\bar{r}_p$, a mean velocity offset $\bar{v}_c$ and a mean stellar mass $\bar{M}_*$, for each merger and for each mass bin.

In accordance to the behavior of the merger fraction, the merger rate shows an increase towards minor mergers, or mergers between galaxies with very different stellar masses. The average merger rate for the merger sample is 0.025 Gyr^{-1} for an average T_{fric}, that we take to be the merger timescale T_{mg}, of 0.36 Gyr. We note, however, this calculation

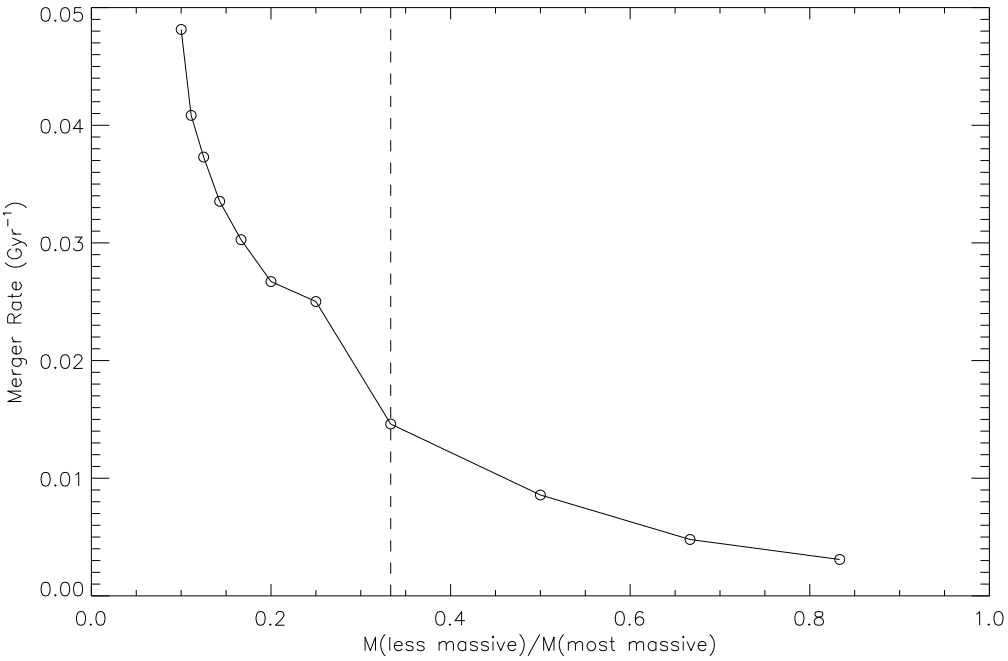

Figure 3.10: Merger rates for different mass ratios of the merger sample. The mass ratio considers the ratio between the most massive and the second most massive galaxies, in the case of mergers with N>2.

is an approximate value taking into account the characteristics of the sample and it spans over a wide range of values for T_{fric}, even when considering different mass bins.

3.3.5 Environment

Even though the set of conditions mentioned in Section 2.2 have been used to find close pairs or groups, and thus a potential merger, the effects of environment in which these potential mergers are immersed cannot be neglected. During the visual inspection, some of these systems were found in crowded environments and therefore may not merge.

To address this issue, we adopt the criteria outlined by Barton et al. (2007) to estimate the number of dry mergers that are truly isolated and, therefore, will most likely merge. In order to study triggered star formation in close pairs, Barton et al. (2007) have used N-body simulations and semi-analytic models to demonstrate that the majority of galaxies in close pairs reside within cluster- or group-sized halos. They showed that close pairs in low density environments, i.e. with only one neighbor within 700 h^{-1} kpc, represents the ideal scenario to isolate the effects of the interaction.

Applying this criterion to our dry merger sample, combined with the velocity separation criterion already used of 800 km/s, we find that 18% of these systems are truly isolated. The results on the number of neighbours of the potential dry mergers within this limit is illustrated in Figure 3.11.

Most of these systems are in fact isolated or have only one neighbour galaxy inside the volume defined by the above mentioned projected distance and velocity offset.

3.3.6 Dry merger spectral properties

To understand the role of dry mergers in the galaxy assembly at low redshift, it is critical to study how the dry mergers systems compare to the galaxies that are not in close pairs or groups. Through spectral indicators we contrast the properties of the stellar populations of dry merging systems to the galaxies without the presence of

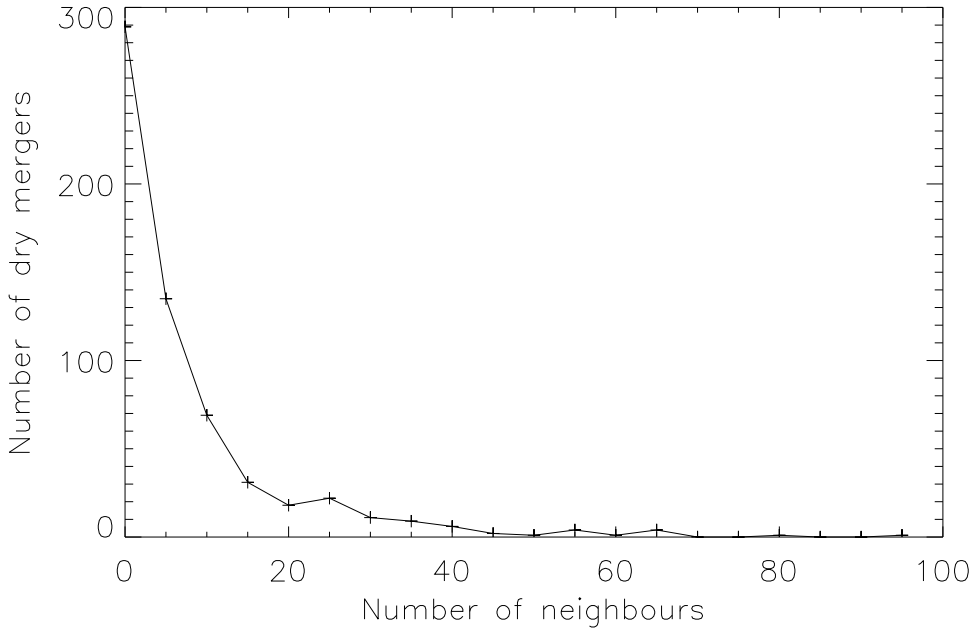

Figure 3.11: Distribution of the number of neighbours of the dry merger systems.

another nearby galaxy. We make use of a selection of six spectral absorption indices to analyse the two samples of galaxies: the age sensitive H-Balmer indices Hδ_A and Hγ_A, and some metallicity sensitive indices, Mg, Mg_2, Fe4531 and Fe5015. Some studies have shown that composite indices, such as [Mg+Fe], are better fitted to probe metallicity and that the sum of Hδ_A and Hγ_A is more robust to probe age than the two indices separately (Gallazzi et al. (2006) and references therein). Our final set of spectral indices then includes: [Hδ_A+Hγ_A], [Mg_2Fe], Mg_2, Mg and D4000, where [Mg_2Fe] is defined by equation 3.7 from Gallazzi et al. (2006):

$$[\mathrm{Mg_2Fe}] = 0.6\,\mathrm{Mg_2} + 0.4\,\log\,(\mathrm{Fe4351} + \mathrm{Fe5015}) \tag{3.7}$$

From the sample of dry mergers we estimated a sample of dry merger assumed end products, or *remnants*, where the stellar mass of the end product galaxy is the sum of the stellar masses of the galaxies in the group and the amount of elements in the remnant is the weighed sum, according to stellar mass, of the elements of their parent galaxies. We note that our conclusions are not altered when co-adding the spectra. Then, from the sample of isolated galaxies was drawn a set of galaxies with similar stellar mass (where $\Delta \log(M_*/M_\odot) \leq 0.10$) for each merger remnant. Naturally, several isolated similar galaxies were matched to every single remnant and each set of

similar galaxies (one per remnant) contained a different number of objects. To build a sample of representative isolated and similar objects the galaxy with the median stellar mass in its set was defined to be the typical isolated galaxy similar to its remnant. Thus, the set of isolated and similar galaxies contained as much elements as the sample of merger remnants.

The variation of the different spectral indices with stellar mass for the different samples of galaxies is shown in Figure 3.12.

The sample of galaxies in mergers is in agreement with the parent SDSS sample of galaxies, however the isolated sample shows a sustained difference, for all indices, towards higher values, or lower values in the case of $H\delta_A$ and $[H\delta_A+H\gamma_A]$, indicating a non negligible role of the environment in the galaxies' stellar populations. The dry merger remnant sample follows this trend, showing a very good agreement with the isolated sample, hence revealing that the early-type galaxies assembled via dry merging share the same spectral characteristics of early-type galaxies already in place.

3.4 Galaxy assembly through dry mergers

With a classified sample of galaxies in mergers and an average merger timescale, we can now estimate the contribution of dry mergers to the assembly of galaxies. To that end, we assume that the remnant resulting from the merger of two, or more, galaxies in each group, has a stellar mass equal do the sum of its progenitor's stellar masses. This is a reasonable assumption for dry mergers because the low gas content in these systems means that little additional star formation will take place.

For a given mass interval, we can then (1) estimate a remnant mass function for the dry merger sample, assuming the remnant's mass is approximately the same as the total mass of the elements in merger, and (2) estimate how much of the galaxy mass function is built via dry merging, since z=0.2, using both the SDSS DR6 stellar mass function and the dry merger sample stellar mass function.

The mass function for the dry merger remnants is shown in the upper panel of Figure

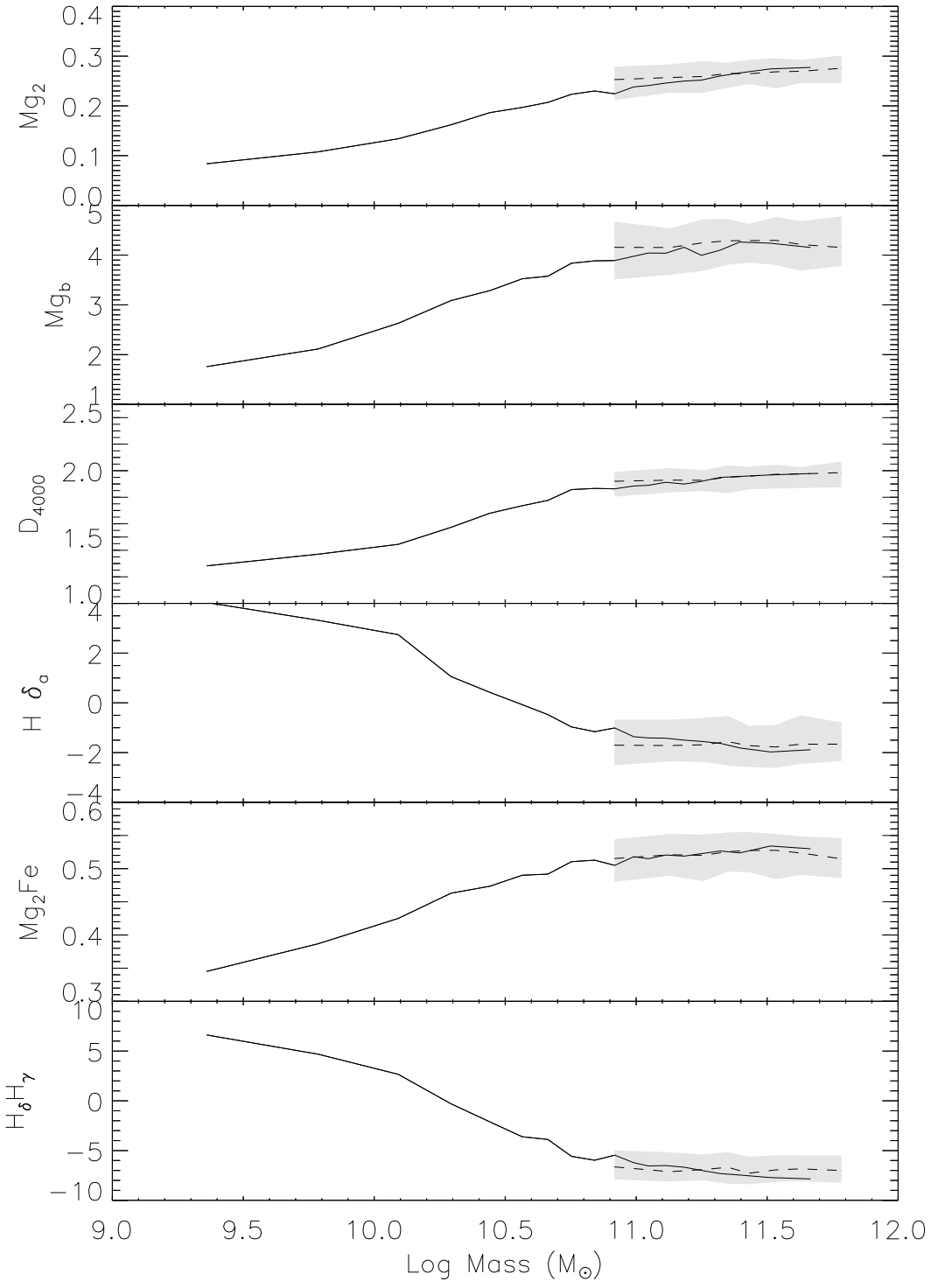

Figure 3.12: Spectral indices abundance as a function of stellar mass. Solid black line represents the sample of isolated galaxies from SDSS DR6, as mentioned in Section 2.4. Dashed line is the sample of end product galaxies from dry mergers and the shaded region shows the 1σ confidence interval.

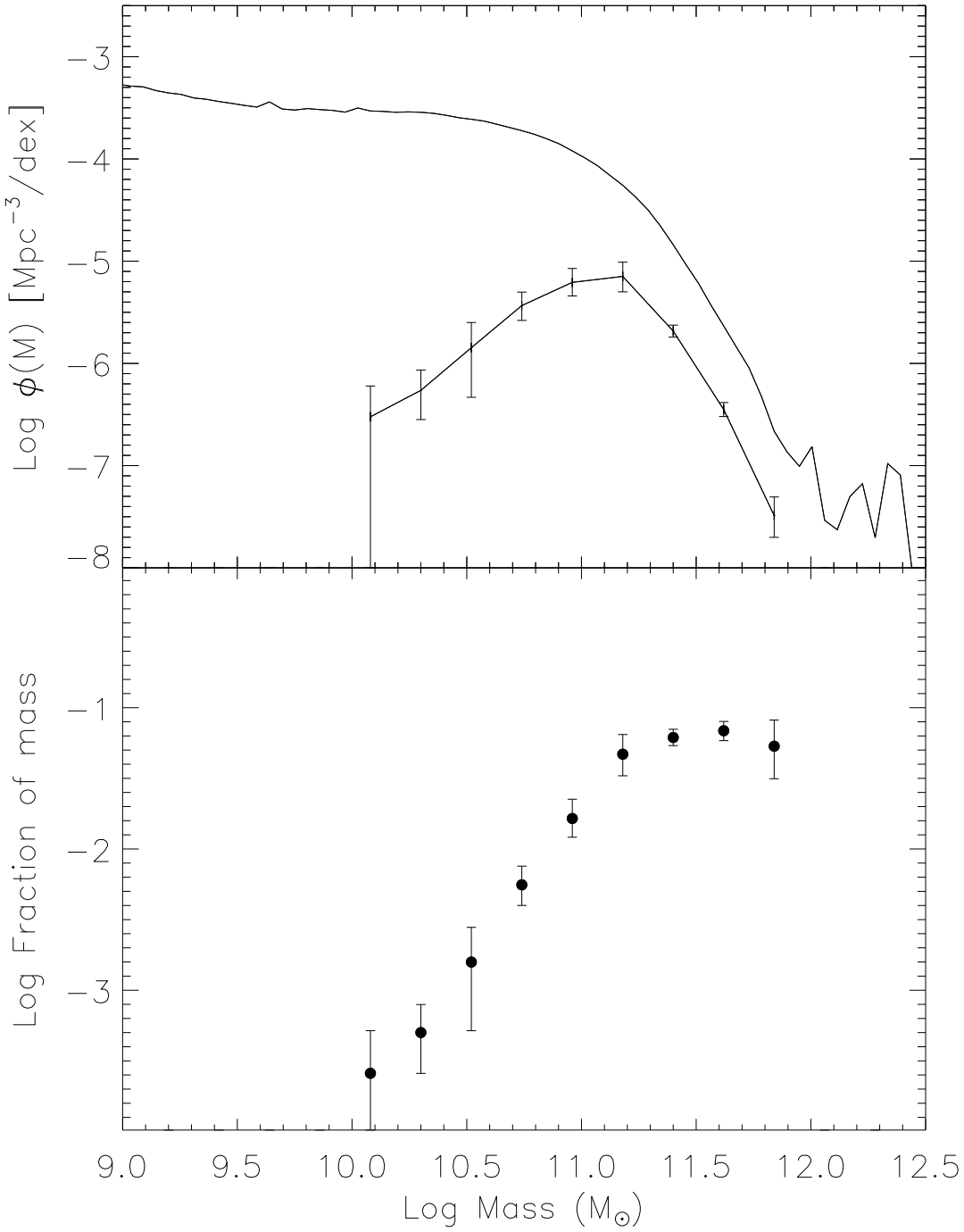

Figure 3.13: Top: The solid line shows the SDSS stellar mass function, with the dry merger remnant mass function estimate being the solid line with error bars. Bottom: The ratio of the dry merger remnant function to the total stellar mass function. This shows the region of the stellar mass function where dry mergers are important.

3.13 with the overall mass function for the galaxies in the SDSS DR6, as referred to in Section 2.1.1 of Chapter 2. The remnants are in fact more frequent towards higher mass bins with the median for the stellar mass distribution of these systems at $\log M_*/M_\odot = 11.36$. Galaxies with stellar masses above this median value in the SDSS DR6 galaxy sample, limited to the redshift interval $0.005 < z < 0.2$ (Figure 3.13), represent 3% of the objects, revealing the relevance of dry merging in assembling very massive galaxies.

The number density of dry mergers, i.e. the number density of remnants per Mpc^3, per mass interval, is given through Equation 3.8:

$$\Phi(M_1 \leq M \leq M_2) = \sum_{i=0}^{x} \frac{1}{V^i_{max}(M_1 \leq M \leq M_2)} \tag{3.8}$$

where Φ represents the number density of galaxies with stellar mass M within the mass interval $[M_1, M_2]$ and x the total number of remnants, i.e. the total number of dry mergers. By finding the ratio between the stellar mass functions shown in the upper papel of Figure 3.13, in each mass bin, it is possible to retrieve the fraction of galaxies product of a merger between gas-poor galaxies. The fraction in each mass bin is listed in table 3.1. For comparison we include in the table an estimate of the dry merger fraction from the simple model of galaxy evolution proposed by Peng et al. (2010), on the basis of SDSS and zCOSMOS data. In their study, Peng et al. developed a purely empirical model to identify key features of galaxy evolution and found that even though the effects of dry merging are on average small for the population of passive galaxies, their importance increases with the observed final mass – as we have shown in Figure 3.13 as well. To compare their numbers to ours we have scaled their dry merger rates to our redshift interval assuming that the rate of dry mergers is constant with time, which likely leads to an overestimate.

While the differences in methodology between studies are too large to warrant a detailed comparison of the numbers, we note that the trend with mass is very similar and there is a fairly good agreement overall. That the Peng et al. numbers are higher is reasonable as one would expect merger rates to be somewhat higher at earlier times while we have assumed constancy.

In conclusion, the average fraction of galaxies assembled through mergers of gas-poor galaxies for $10.1 < \log(M_*/M_\odot) < 11.8$ is 0.028. We conclude that for present day

$\log M(M_\odot)$	Fraction	Peng et al.
[10.0, 10.2]	0.000258	0.0115
[10.4, 10.6]	0.00158	0.0159
[10.9, 11.1]	0.0164	0.0332
[11.3, 11.5]	0.0615	0.0762
[11.5, 11.7]	0.0686	0.114
[11.7, 11.8]	0.0533	0.161

Table 3.1: Fraction of dry merger remnants in different mass bins

galaxies with $\log(M_*/M_\odot) > 10$ up to $\sim 7\%$ of their stellar mass is involved in dry mergers, since $z = 0.2$, with galaxies of stellar mass $11.5 < \log(M_*/M_\odot) < 11.7$ being more predominantly assembled through this type of mergers.

Given that the median redshift of the galaxies in dry mergers is 0.1, which translates into $1.3Gyr$, these fractions are then an estimation of the upper limit for the contribution of dry mergers to the local mass function. Assuming that, typically, the merger time-scale is situated at $\sim 0.4Gyr$, these galaxies would have merged by redshift zero.

Chapter 4

Metals and Gas in Mergers

One of the main parameters in the galaxy merger process is the gas of the progenitor galaxies. The classification of wet, dry or moist mergers is a direct allusion to the amount of gas available to form new stars in merging galaxies. However, despite the gas-dependent merger classification used exhaustively throughout the literature for the past decades, particularly for the case of gas rich galaxies, obtaining reliable gas measurements is still a complex task and star formation activity or blue colors are often used as a proxy for the existence of gas.

This Chapter focuses on the analysis of metallicity and gas content in the merger sample outlined in Chapter 2. The question we want to ask in this Chapter is whether or not mergers lead to a significant channeling of low metallicity gas from the outskirts of the galaxies into the center. It starts by putting the metallicity of mergers into context, it continues to explore the content in metals and in gas in the central regions of merging galaxies, leading up to the analysis of the gas content of mergers when compared with isolated galaxies.

4.1 Metallicity in Mergers

Gas and metals are closely linked through the process of star formation. They therefore offer important constraints on the process of galaxy evolution. As new stars are formed from pristine gas, they reprocess this gas by enriching the inter-stellar medium (ISM), through stellar winds and supernovae, with metals. The metallicity is therefore strongly connected to the evolution of a galaxy - for instance, considering a massive galaxy with several episodes of star formation, such a galaxy is expected to be more metal rich than low mass galaxies, since their stars have been supplying the ISM as they died and their deeper potential wells are able to retain those metals expelled by the stars. However, as mentioned before, galaxy interactions can not only strongly affect the ISM of a galaxy and remove some of it through tidal effects, hence lowering the total amount of metals in the galaxy, but also redistribute gas and metals within a galaxy.

4.1.1 Mass-Metallicity Relation

The metal content of galaxies and its relation with luminosity has been studied for the last three decades (e.g Lequeux et al. 1979; Garnett & Shields 1987) and the mass-metallicity relation (hereafter, M-Z relation) in particular, has been having more focus for the last decade (Garnett 2002; Tremonti et al. 2004). There is general agreement that lower mass galaxies are shown to have low metal content, whereas massive galaxies are more metal rich. In a landmark study using spectroscopically confirmed star-forming galaxies in the SDSS DR2, at z $\sim$ 0.1, Tremonti et al. (2004) found a tight correlation between stellar mass and metallicity, with a steep relation for galaxies with stellar masses up to $10^{10.5}$ $M_{\odot}$ and a flatter relation for galaxies with stellar masses above this value. Recently this has been extended to a so-called mass-metallicity-star formation rate fundamental plane (MZR-plane Mannucci et al. 2010).

Following Tremonti et al. (2004), we make use of the oxygen abundance as a proxy for metallicity, to explore the properties of the ionized gas in the merger sample. Even though *metallicity* correctly refers to the mass fraction of all elements heavier than helium, what is more common in applications is to infer the metallicity from the abundance of certain tracer elements. In stellar astrophysics this is often the iron

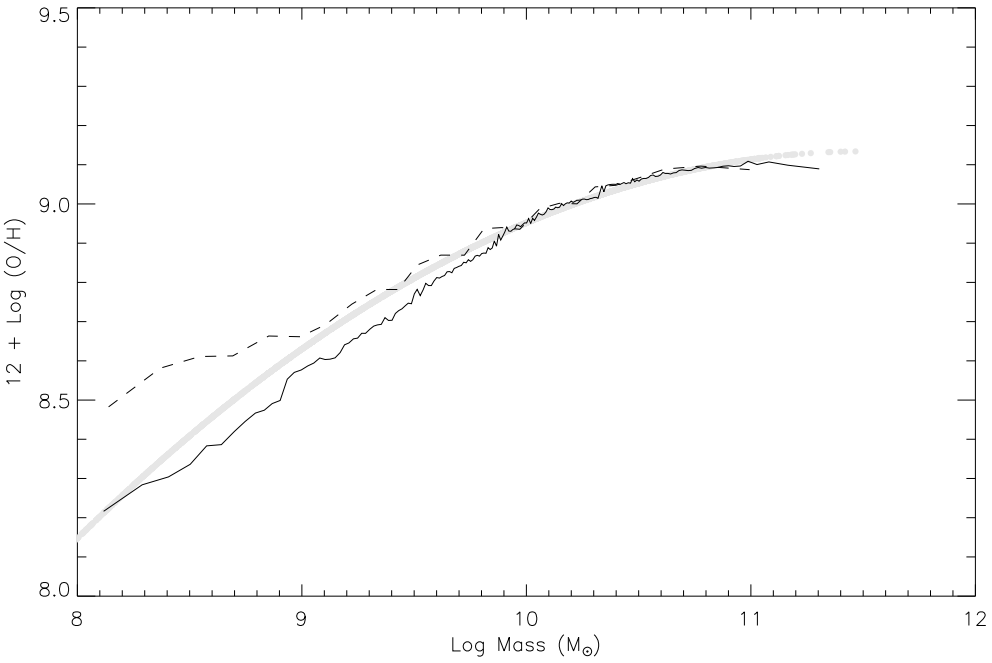

Figure 4.1: The median of the M-Z relation for galaxies in the SDSS DR6 within the redshift interval $0.005 < z < 0.2$ (solid line) and for the galaxies in the merger sample (dashed line). The grey line denotes the M-Z relation as given by Equation 4.1

abundances, while for optical spectroscopy the obvious element is oxygen as this shows strong lines in the optical (e.g. [OIII]4959, [OII]3727) and it is the most abundant heavy element. Here, the O/H ratio denotes the abundance by number of oxygen relative to hydrogen. The mean mass-metallicity relation determined by Tremonti et al. (2004) is given by Equation 4.1, where the stellar mass is given in solar masses.

$$12 + \log(\mathrm{O/H}) = -1.492 + 1.847 \log \mathrm{M_*} - 0.08026 \log \mathrm{M_*^2} \tag{4.1}$$

To calculate a M-Z relation for our sample, we followed the same approach as Tremonti et al. (2004), but using the SDSS DR6 galaxy sample. We calculated the median oxygen abundance in bins of stellar mass for all star forming galaxies and all star-forming galaxies in mergers. This M-Z distribution for SDSS DR6 and for the merger sample is illustrated in Figure 4.1. Both distributions agree with the M-Z relation given by Tremonti et al. (2004), although we do see some deviation from the fit below 10^9 $\mathrm{M_\odot}$ and above 10^{11} $\mathrm{M_\odot}$ that might be due to the sample being different - since they use the 2^{nd} Data Release from the SDSS - and that the quadratic function is no longer a good fit.

Some studies hint to a decrease in the metallicity for close pairs of galaxies (Kewley et al. 2006a), resulting from the gas inflow to the central regions of the galaxy *diluting* the metal content in that region. Other studies (Ellison et al. 2008; Michel-Dansac et al. 2008) point towards the opposite direction and find a slight increase in the metallicity for galaxies with close companions. Since close pairs are associated to a slight increase in star formation rate, the fundamental MZR relation would suggest that we should see a decrease in metallicity, further confusing the issue. The complex interplay of galaxy interaction and its effect on metallicity is indeed far from understood and investigating the metallicity of galaxies in mergers can give valuable information about the gas dynamics during the merger process. Our goal is to study whether interactions lead to noticeable changes in the gas and metal content of the central regions of galaxies, and whether inflow of gas into the centers of galaxies is an important process in galaxy mergers.

4.1.2 Measures of gas content in galaxies

The gas and stellar content of galaxies varies strongly both within the galaxies, and between galaxies. It is therefore very useful to take out some of this variation by considering relative quantities, i.e. ratios. Here we first outline which quantities we use and why which predominantly deals with variation between galaxies, and further below we explain how we proceed to further minimize aperture effects within galaxies.

In order to investigate the gas content of the galaxies in the merger sample, we define r_{gas}:

- **Ratio of Gas to Stars**: Measures the amount of gas of a galaxy when relative to the amount of stars. In other words, it is a ratio between gas and stars content:

$$r_{gas} = \frac{\Sigma_{gas}}{\Sigma_{stars}} \sim \frac{M_{gas}}{M_{stars}}$$

Here, Σ is used to denote surface average properties(e.g. surface densities, surface SFR). In this case M_{gas} and Σ_{gas} are, respectively, the mass and gas column surface density - potentially available to form new stars - and the M_{stars} and Σ_{stars} are, respectively, mass and the surface mass density of stars in the galaxy. The two ratios are considered approximately similar here even though the Σ quantities refer to a

surface density within a given aperture. Assuming Σ is representative for all the gas, or stars, in the galaxy, the ratio between the quantities are approximately equal. Of course if the radial profile of stars and gas is dramatically different the two ratios can be significantly different, but we will minimize this potential problem here by always doing relative comparisons between galaxies at similar redshift.

In this work, a new technique to estimate the gas content recently developed by Brinchmann et al (in prep) was used. In general, for sufficiently large regions, one can assume that gas and dust are closely associated and, as an alternative to the direct, and difficult, measurement of the gas content of galaxies, dust is instead used as a tracer. This procedure has been used in several studies (e.g. Boulanger et al. 1985; Dame et al. 2001; Leroy et al. 2009) and it is usually based on *emission* measures - dust radiates in the infrared region of the spectrum when heated up by nearby stars. However, this new technique mentioned above is sensitive to the dust *absorption*.

The estimates for the gas masses were obtained from dust attenuation, τ_ν, (Charlot & Fall 2000) using the Balmer decrement, paired with metallicity estimates to deduce the gas column density probed by the spectrum. The metallicity can be written as a function of the gas surface density, through $Z = \Sigma_Z/\Sigma_{gas}$, and assuming the dust-to-metal ratio to be $\xi = \Sigma_d/\Sigma_Z$, the gas estimates can be determined by:

$$\Sigma_{gas} \approx 0.2\frac{\tau_\nu}{\xi Z}\mathrm{M}_\odot\mathrm{pc}^{-2} \tag{4.2}$$

The factor 0.2 includes the characteristics of the grains such as the optical cross section, mass density and radius. This approach has been shown to be relatively insensitive to the detailed properties of dust grains while being sensitive to surface mass density of gas in the region sampled by the spectrum in the galaxy. A major advantage of this technique is the possibility of being easily applied to large surveys.

A detailed discussion of the merits of this estimator is not appropriate here, but it appears to give good relative gas column mass densities. Figure 4.2 shows a comparison of the column density of gas measured in various regions of M101 using a combination of HI and CO maps on the x-axis, and using this new spectroscopic method on the y-axis. As can be seen, the correlation is good with a spread of a factor of $\sim$2 or so. Other tests of the method give similar results but the method does break down in very gas rich regions, thus we will not attempt to apply it to very late merger stages where

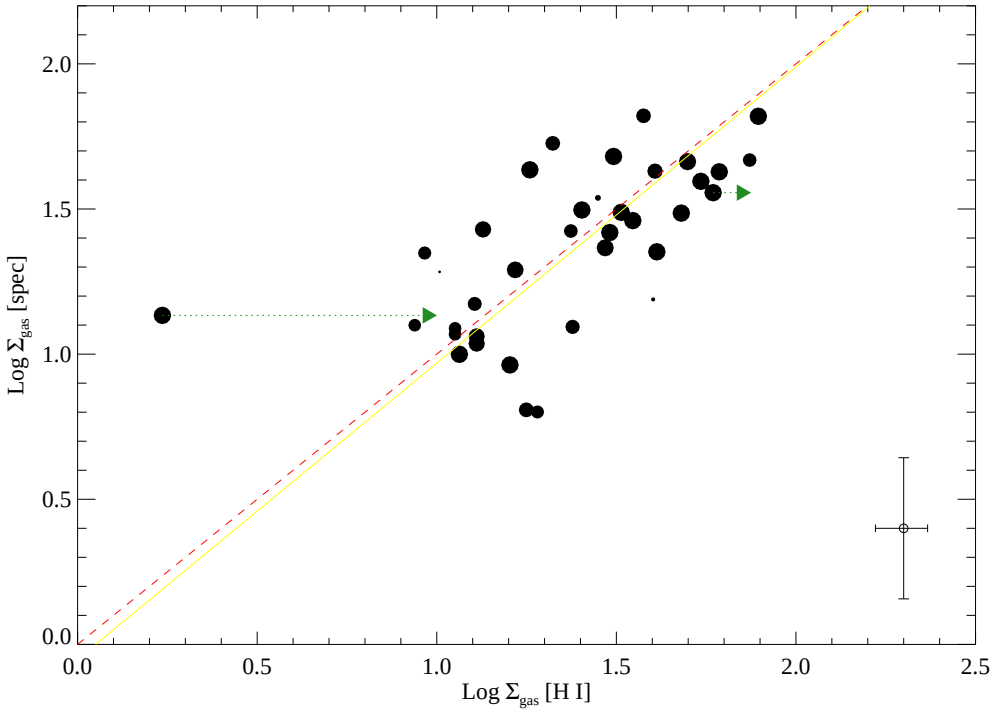

Figure 4.2: A comparison of Σ_{gas} measured from H_I (x-axis) versus the Σ_{gas} measured using the spectroscopic method for 37 regions in M101 (taken from Brinchmann et al in prep). The points have been scaled according to the uncertainty estimate so that the largest circles correspond to objects with 1σ uncertainty on log Σ_{gas} less than 0.2 dex. The smalles circles correspond to uncertainties larger than 0.8 dex. The median uncertainties are indicated by the error bars in the lower right. The dashed red line shows the 1-1 relation, while the solid line shows the best unweighted, linear fit to the data which has a slope of 1.02. The green arrows show the contribution of M_{H2} to the total gas where it is$>$ 25%.

that might be the case.

As mentioned above and as we will discuss further below, we will do all of our studies relative. So even if this method has some undiscovered systematic uncertainty inherent to it, we will not be affected by this as long as similar galaxies have similar offsets as they will cancel out. Thus we expect this method to give useful gas content estimates for our sample.

- **Star Formation Rate & Specific Star Formation Rate**: The star formation

rate (SFR) is the rate at which the gas is being transformed into new stars, whereas the specific star formation rate (SSFR) is the rate at which the galaxy is forming new stars *per unit stellar mass*.

- **Roberts Time**: This time-scale(Roberts 1963; Kennicutt et al. 1994) measures the amount of time that will take for the gas of a given galaxy to form new stars, assuming a given star formation rate. Therefore, T_R can be written like:

$$T_R = \frac{M_{gas}}{SFR}$$

This quantity is particularly useful, since it makes use of the information from both the star formation rate *and* the amount of gas still available to form new stars. This time-scale can also be thought as a depletion time-scale: how long does the available gas take to be transformed into stars, however, as stated by Kennicutt et al. (1994) it constitutes a lower limit since it does not account for gas recycling. This quantity is also useful because it is likely to have a different dependence on aperture size than either r_{gas} or SFR on their own.

4.1.3 Using a control sample

The mass-metallicity relation shown in Figure 4.1, reveals a clear trend of higher stellar mass galaxies having a higher metal content. Clearly a blind comparison of galaxies would not be a good idea and one needs to take this variation with stellar mass into account when doing the comparisons.

This behaviour is noticed when comparing r_{gas} with the stellar mass of galaxies, as illustrated in Figure 4.3. On the x-axis we plot the stellar mass and on the y-axis r_{gas} — and each position in this diagram is coloured according to the median redshift of the galaxies ending up there. This figure shows the complex interplay of two effects: the immediate effect is that more massive galaxies have relatively less gas — a well-known trend seen in all HI surveys (e.g. Catinella et al. 2010). But coupled to this general decline in r_{gas} with stellar mass, there is also a dependence on the amount of gas to the amount of stars with redshift, which is a sign of an aperture effect - galaxies at lower redshifts have only their central regions sampled by the fiber, whereas at higher redshifts the fiber covers a larger radii, if not all galaxy. Moreover, gas discs are more extended than stellar discs. This naturally leads to a underestimation of the

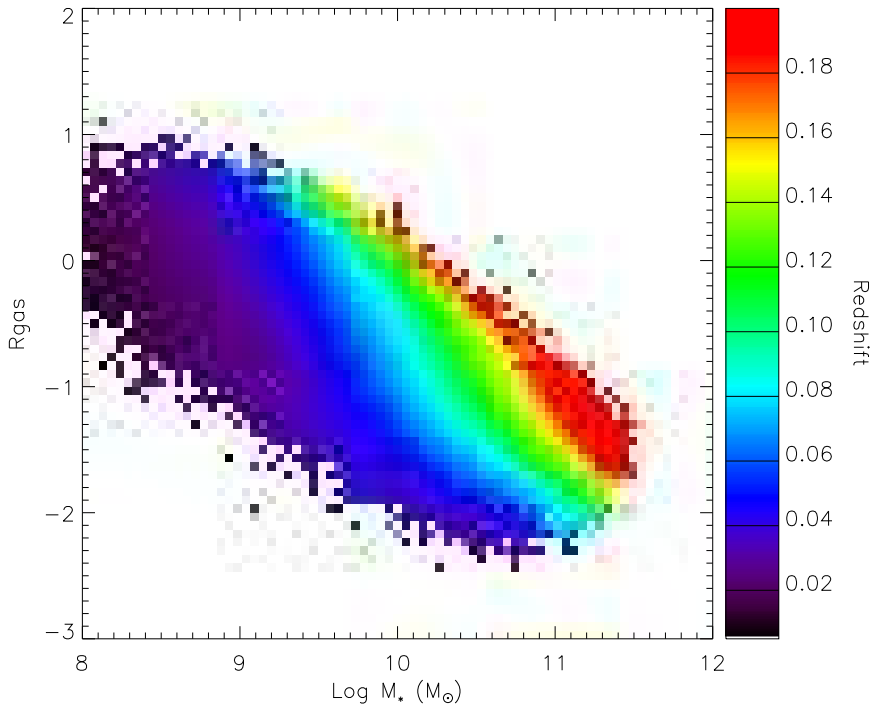

Figure 4.3: Distribution of r_{gas} as a function of stellar mass for the redshift interval $0.005 < z < 0.2$. The dependence of r_{gas} in redshift in each mass bin is clearly seen, in particular for galaxies with stellar mass $\gtrsim 10$ $M_{\odot}$ where r_{gas} covers a wide range in redshift, with lower redshift galaxies presenting lower values of r_{gas}.

gas content of galaxies at lower redshifts and an aperture correction would be needed. However, by comparing the merger sample with the control sample, and since they are both obtained at similar redshifts, we expect that we will mostly be able to remove this effect.

As mentioned before, there are major advantages in using a sample of isolated galaxies drawn from the same survey as the merger sample. In this case, the isolated sample was built based on the parameters of the sample of galaxies making up the merger sample and, as described in section 2.2.3, only galaxies similar in stellar mass and redshift were selected, for each merger galaxy. The most important benefit of this method is that the relative measurements, between a given galaxy in a merger and the set of its similar galaxies, allows us to directly compare identical galaxies and obtaining robust results when analysing the effects of a neighbour galaxy.

4.2 Investigating the metals and gas in mergers

4.2.1 The low-metallicity gas content of mergers

In order to investigate whether the interaction between galaxies influences their gas dynamics, here we explore whether the metal abundance in the inner regions for galaxies in the merger sample changes with the separation of the galaxies. Earlier studies (e.g. Zaritsky 1993) generally seemed to find that spiral galaxies have relatively steep metallicity gradients. However more recently Moran et al. (2010) have found that gas-phase metallicities show a relatively flat profile with increasing radius, with a drop in the metallicity for the outer regions. While some galaxies have strong metallicity gradients, it appears that as a population they tend to have relatively flat metallicity profiles. Observations indicate that, regardless of their inner profiles, galaxies have low-metallicity gas in the outer regions, thus that reservoir of metal poor gas far out in the galaxies can be mixed up during mergers.

By comparing our merger sample to isolated galaxies, we can investigate in particular the gas inflow towards central regions — is the low-metallicity gas from the outskirts of the galaxy being channelled to the center during a merger? To answer this question we limit the redshift interval to galaxies in the range $0.02 < z < 0.08$ in order to sample the central region of the galaxies — higher redshift galaxies, as previously mentioned, would have larger regions sampled while the low redshift cut-off is to reduce the severity of aperture effects. For this analysis there were a total of 1687 galaxies from the merger sample. Across this redshift range the aperture of the SDSS fibre subtends from ~ 1.2 kpc to ~ 4.5 kpc

The result obtained by comparing the metallicity abundance of the galaxies in the merger sample with the sample of isolated galaxies, i.e. $\Delta \log(O/H)$, is shown in Figure 4.4. In the Figure we plot the difference between the metallicity of galaxies in mergers and the metallicity of their respective isolated counterparts.

For merging galaxies, an increase in the metallicity is clearly seen for projected separations below 10 kpc - as the galaxies get closer during the merger event, the central regions of these galaxies are more metal enriched when compared with their isolated counterparts. This result points in the direction of no significant inflow of low-

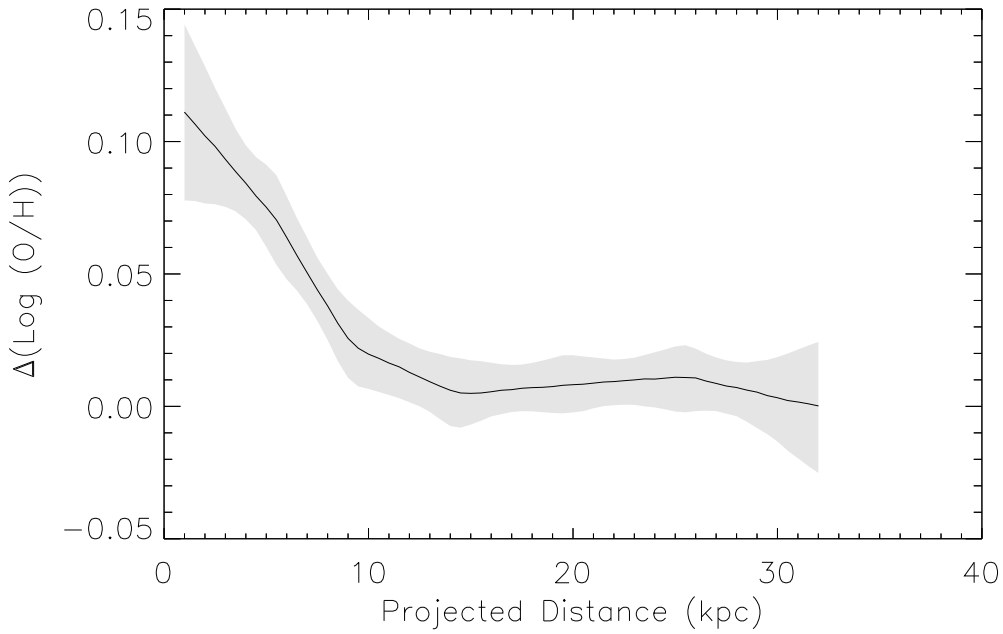

Figure 4.4: The median distribution of the difference in metallicity as a function of projected separation. The lower and upper shaded areas represent the 68% and 84% percentiles, respectively, as obtained by bootstrap re-sampling, with n=999.

metallicity gas to the center. If that was the case, there would be a *dilution* of the metal content and the metallicity would show a decrease. Instead, the observed increase in metallicity could be attributed to the increased star formation rate triggered by the merger event, that would lead to metal injection and, therefore enriching the ISM in the central regions of the galaxies. This picture would be consistent with the enhanced star formation activity shown in Section 2.5.1 of Chapter 2, but to fully understand this increase in metals in the central regions, one should also analyse how their gas content changes with separation.

4.2.2 The gas content of mergers

As mentioned, the analysis of the gas content of the central regions of galaxies in mergers can shed invaluable light on the gas dynamics during the encounter. By focusing on star-forming gas-rich galaxies and inspecting how the gas content behaves during a merger event, we can start to constrain the role of inflow of gas to inner regions and contrast this with the triggered star formation to paint a picture on the metallicity content of central parts of merging galaxies.

Using the same approach, we compare the galaxies in the merger sample with the set of isolated galaxies to investigate whether merging galaxies are more gas rich in their central regions than the galaxies without any neighbour nearby. Moreover, for robustness, only galaxies classified as star forming (according to the prescription of Brinchmann et al. (2004)) are used, in a total of 1658 galaxies. This relative measurement, of the difference between r_{gas} of galaxies in mergers and their relative isolated counterparts, is shown in Figure 4.5.

For separations above 10 kpc, there is virtually no difference in the median r_{gas} – galaxies in mergers present the same ratio as isolated galaxies. On the other hand, a trend is seen for projected separations below 10 kpc towards negative values of $\Delta \log r_{gas}$ meaning that, in the central region, merging galaxies are gas depleted relative to isolated galaxies. This decrease appears consistent with the increase in metals found for galaxies in mergers (see Section 4.2.1) and also with the increase in star formation observed for merging galaxies when compared with isolated galaxies (see Section 2.5.1), considering a simple scenario where the metal enrichment caused by the increase in star formation is not significantly affected by the inflow of low-metallicity gas. Nonetheless,

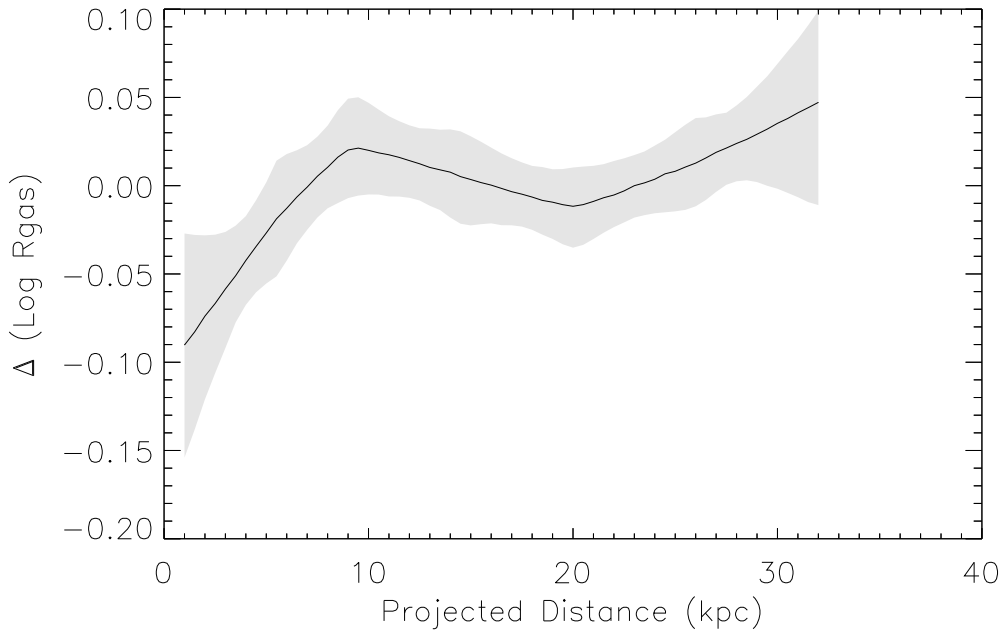

Figure 4.5: The median for the variation of $\Delta \log r_{gas}$ as a function of projected distance. The lower and upper shaded areas represent the 68% and 84% percentiles, respectively, as obtained by bootstrap re-sampling, with n=999.

an increased star formation capable of using up the gas and ejecting metals back into the galaxy's ISM would have to be consistent with lower gas depletion time, i.e., the available gas to form new stars would have to be consumed more rapidly, increasing both the rate of star formation and the amount of metals.

4.2.3 The gas consumption time-scale in mergers

As mentioned earlier, the Roberts time can be interpreted as a gas consumption time-scale, which gives information on the time it would take to convert all the available gas into stars, with constant star formation rate at the present value, assuming there is no recycling of the gas and that no gas is being added to the region studied. Given the previous results of a decrease in r_{gas} coupled with an increase in star formation for galaxies with projected distances below 10 kpc, analysing the time-scale for gas to convert into stars should give a clear picture of the process behind gas depletion in mergers. Once again, we use a relative measure by comparing T_R of galaxies in mergers with the T_R of isolated galaxies - do mergers and isolated galaxies show similar depletion times for their gas?

The results in Figure 4.6 reveal a pronounced decrease in T_R, which is the result of a shorter gas consumption time-scale for galaxies in mergers when compared with isolated galaxies: galaxies in the merger sample are running out of gas faster than their isolated similar galaxies. Because T_R depends on the mass in gas M_{gas} and on the star formation rate (SFR), we could predict a decrease in T_R given the previous results. The fact that such behaviour is observed in T_R is then consistent with a scenario where the central region of the galaxy during a merger process is somehow blocked to exchanges with the outer regions of the galaxy.

One noticeable difference between the different trends seen before, is that this does not reach a value of zero at large separations. Although it is not clear why this is the case, it might indicate that there is still some enhancement of star formation activity to separations above 30 kpc. Even a small effect of this enhancement would become important when measuring T_R since it depends on both the SFR and the gas mass. A special sample of isolated galaxies that would make a good comparison sample in this case would be constituted of galaxies with no neighbours within a radii of >100 kpc. As the trend in Figure 4.6 seems to indicate, for separations larger than 30 kpc

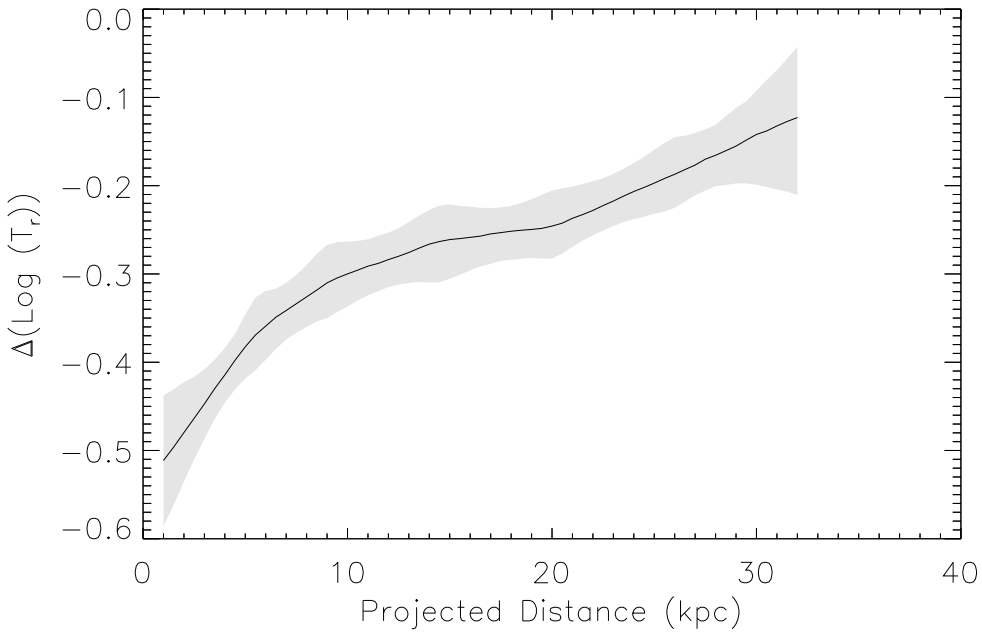

Figure 4.6: The variation in Roberts time, or gas consumption time-scale, as a function of projected separation. The lower and upper shaded areas represent the 68% and 84% percentiles, respectively, as obtained by bootstrap re-sampling, with n=999.

it would eventually reach zero.

4.3 Discussion

Concerning the metallicity and gas content of the central regions of galaxies in mergers, the results can be summarized as follows:

- An increase in metallicity of $\sim$ a factor of 1.5 for projected distances below 10 kpc.
- A decrease in r_{gas} of $\sim$ a factor of 1.5 for projected distances below 10 kpc.
- A decrease in T_R, more pronounced for projected separations below 10 kpc, of a factor of 4.
- Additionally, from Chapter 2, an enhancement of star formation activity for projected distances below 10 kpc up to a factor of 3.

As mentioned in Chapter 1, several mechanisms can be prompted by the merger event which contribute significantly for the evolution of a galaxy - e.g. feedback from triggered AGN activity - however, these results for the metal and gas content of central regions of galaxies are not expected to be affected by such processes, since they are probing the particular time on the merger event *before* those processes take place.

We have a measurement of the increase in star formation activity as a function of separation of the galaxies and coupled to that we find a decrease in the gas content, an increase in the metallicity and a decrease in T_R. Considered together these results seem to suggest a scenario where no in-falling, or negligible in-falling, of low-metallicity gas takes place. In other words, these results seem to be pointing towards a simple scenario for gas depletion during the late stages of a merger event - a *closed box model* for the central regions of galaxies. The closed box model, a formalism first introduced by Tinsley (1980) for the chemical evolution of galaxies, can be interpreted as **a)** a closed region where **b)** there is some "initial" gas to form new stars and **c)** no inflow or outflows of gas mass, leading to a metal enrichment of the region as stars keep being formed from the available gas assuming that **d)** the initial mass function (IMF) does

not change.

A qualitative assessment of the possibility of using a closed box model, where the enhanced star formation activity that result from the tidal forces perturbing the gas into stars is the solely responsible for the gas dynamics, explains simply all the observed features regarding metallicity and gas content of the central regions of galaxies. In a closed system, where no inflows or outflows of material take place, the increased star formation rate gives rise to a decrease in r_{gas} since the gas is being consumed into stars and the ratio of gas mass to stellar mass decreases. The decrease in gas fraction combined with a increase in SFR, is translated into lower values of T_R. Because there is no replacement of the gas, there is no dilution of the metal content and the final metallicity is higher than the initial metallicity due to the metal ejection that in the meantime is enriching the medium.

But even though this results are consistent between them and with a closed box model for the central regions of merging galaxies, another approach is needed: to verify if this simple model could predict these behaviours for the variations of r_{gas}, Z and T_R.

To note that changes in gas fraction and metal content will likely be mass dependent and likewise the increase in star formation rate. However even with these large samples we are limited in our ability to study the effect of mass on these trends. Thus average trends will be used throughout this analysis of exploring whether the observed relations are consistent with a closed box solution or not. For this we will here go through this calculation using an average mass galaxy, of 10^{10} solar masses as an illustrative case. We have also calculated all these trends as a function of mass and have verified that this illustrative case is a good representation of the average. There is a wealth of information in these data, but to extract this out further we need to do a considerably more sophisticated analysis, including a proper chemical evolution model and a more careful treatment of the time-evolution of these quantities, which is outside the scope of this first attempt here.

The closed box model

To investigate the closed box model for the central regions of merging galaxies we build a simple model where galaxies that were previously isolated, i.e. with projected distances r > 30 kpc, become galaxies in mergers after a timescale, Δt_m. We assume that the central regions of merging galaxies are consistent with the closed box model where exchanges of material during the merger time-scale, Δt_m, with the surrounding medium are, at most, negligible. It should be emphasized that this model does not consider very late stage mergers, where the central regions are already merged and, therefore, other types of activity (e.g. AGN heating and feedback) will certainly play a major role.

We establish a set of initial conditions for the quantities mentioned before - $\mathrm{r_{gas}}$, Z and T_R - that describes the galaxies at projected distances greater than 30 kpc, i.e., isolated.

$$\mathrm{r_{gas,0}} = \frac{\mathrm{M_{gas,0}}}{\mathrm{M_{*,0}}} \tag{4.3}$$

$$\mathrm{SFR_0} = \left.\frac{\mathrm{dM_*}}{\mathrm{dt}}\right|_0 \tag{4.4}$$

$$\mathrm{T_{R,0}} = \frac{\mathrm{M_{gas,0}}}{\mathrm{SFR_0}} \tag{4.5}$$

$$\mathrm{Z_0} = \mathrm{y}\ \ln \mathrm{r_{gas,0}^{-1}} \tag{4.6}$$

Where M_{gas} and M_* are the mass in gas and the mass in stars, respectively. The star formation rate is denoted by SFR and Z is the metallicity, that depends on the yield, y. The subscript 0 indicates the initial values for these quantities.

To let this closed system evolve for a time Δt_m, it is also necessary to estimate the following parameters:

- **A recycling fraction:** a fraction of enriched gas is returned to the ISM via stellar winds and supernova explosions and will be available to form new stars. Our typical gas recycling fraction is assumed to be 0.5.

- **A star formation rate, SFR:** the rate at which a galaxy forms stars is not straightforward to estimate since its determination is dependent of models for their star formation histories. While in 2.5.1, the increase in the star formation activity was measured by the $EWH\alpha$, because this quantity is proportional to the ratio between SFR and stellar mass, it is intrinsically related to the rate at which stars are being formed.

  To tackle this problem, we first calculate the median SFR for the star-forming galaxies in the SDSS DR6 sample and assume a *median* galaxy of mass $M_* = 10^{10} M_\odot$ as being representative of a star-forming galaxy. The SFR for a galaxy of $M_* = 10^{10} M_\odot$ is determined to be $\sim 0.49\ M_\odot/yr$ and the typical mass increase expected over a typical merger time-scale is modest. This can be shown by calculating the gain in mass for the star formation rate, $\psi(t)$, of each galaxy. If the galaxy forms stars at a rate $\psi(t)$, then over a time Δt the increase in stellar mass can be written as,

$$\Delta M_*(t) = \int_0^{\Delta t} (1 - R)\, \psi(t) dt \approx \Delta t (1 - R) \langle \psi(t) \rangle \tag{4.7}$$

  where, $\langle \psi(t) \rangle$ denotes some average SFR. In this case Δt is the time-scale of the merger, Δt_m and R is the above mentioned recycling fraction. If we assume that $\sim 50\%$ of this mass is recycled, over a period of 0.5 Gyr (a typical timescale for a merger), the increase in stellar mass is $\sim$1.3% of $10^{10} M_\odot$.

  The next step is to take into consideration how much is the star formation activity enhanced for galaxies in mergers. As previously mentioned, there is an increase on the star formation activity as given by the EWHα: when compared with a sample of isolated galaxies, galaxies in mergers show an increase by a factor of ~ 3. We assume that the $\Delta \log EWH\alpha \approx \Delta \log SSFR$, where the SSFR denotes the specific star formation rate.

  The specific star formation rate can be defined as the SFR per unit stellar mass,

$$\mathrm{SSFR} = \frac{\mathrm{SFR}}{\mathrm{M_*}}. \tag{4.8}$$

  Considering the difference between isolated and merging galaxies given by $\Delta \log \mathrm{SSFR}$, we have:

$$\Delta \log \mathrm{SSFR} = = \frac{\left(\frac{\mathrm{SFR}}{\mathrm{M}_*}\right)_{\mathrm{merger}}}{\left(\frac{\mathrm{SFR}}{\mathrm{M}_*}\right)_{\mathrm{isolated}}} = \left(\frac{\mathrm{SFR}_{\mathrm{merger}}}{\mathrm{SFR}_{\mathrm{isolated}}}\right)\left(\frac{\mathrm{M}_{*\mathrm{merger}}}{\mathrm{M}_{*\mathrm{isolated}}}\right)^{-1} \tag{4.9}$$

Considering that a) an increase in stellar mass for galaxies during the time Δt_m, i.e. that passively forms new stars without the triggered star formation of a e.g. merger, is ∼1.3% and that b) the enhancement in star formation activity resulting from the merger event is of a factor of 3, Equation 4.9 can then be written as:

$$\left(\frac{\mathrm{SFR}_{\mathrm{merger}}}{\mathrm{SFR}_{\mathrm{isolated}}}\right) \approx 3 \tag{4.10}$$

The variation in the SFR due to the merger is then $\Delta SFR = 3$.

Variation of r_{gas}

To investigate if the decrease in r_{gas} in the central regions of galaxies is consistent with the proposed closed box model, this variation in the r_{gas} fraction after the time Δt_m, i.e. from isolated to being in a merger, is calculated analytically. To that end we define that after a time Δt_m, the mass of gas available to form stars, $\mathrm{M_{gas,t}}$ and the stellar mass,$\mathrm{M_{*,t}}$, can be written as functions of the mass initially available and both the initial SFR and the SFR *affected* by the merger:

$$\mathrm{M_{gas,t}} \approx \mathrm{M_{gas,0}} - \mathrm{SFR_0} - \frac{\Delta \mathrm{SFR}}{2}\frac{1}{2}\Delta \mathrm{t_m} \tag{4.11}$$

$$\mathrm{M_{*,t}} \approx \mathrm{M_{*,0}} + \mathrm{SFR_0} - \frac{\Delta \mathrm{SFR}}{2}\frac{1}{2}\Delta \mathrm{t_m} \tag{4.12}$$

where

$$\mathrm{M_{*,t}} + \mathrm{M_{gas,t}} = \mathrm{const}$$

and $\frac{\Delta SFR}{2}$ is an estimate of what would be the enhanced star formation rate during the merger period from 30 kpc to ∼10 kpc.

From Equation 4.3 we then have the fraction of r_{gas} given by :

$$r_{gas,t} = \frac{M_{gas,0} - SFR_0 - \frac{\Delta SFR}{2}\frac{1}{2}\Delta t_m}{M_{*,0} + SFR_0 - \frac{\Delta SFR}{2}\frac{1}{2}\Delta t_m} \tag{4.13}$$

$$\approx r_{gas,0} - \frac{SFR_0}{M_{*,0}}\frac{\Delta SFR}{2}\frac{1}{2}\Delta t_m \tag{4.14}$$

The difference between r_{gas} for an isolated galaxy with respect to a galaxy in a merger, illustrated in Figure 4.5 as the $\Delta \log r_{gas}$, is therefore:

$$\frac{r_{gas,t}}{r_{gas,0}} = \frac{r_{gas,0} - \frac{SFR_0}{M_{*,0}}\frac{\Delta SFR}{2}\frac{1}{2}\Delta t_m}{r_{gas,0}} \tag{4.15}$$

Taking into consideration that the specific star formation rate for a typical galaxy of $M_* = 10^{10} M_\odot$ of the SDSS DR6 sample to be $1.11 \times 10^{-10} yr^{-1}$, the term holding the SFR, the Δt_m and the recycling factor, is calculated to be:

$$\frac{SFR_0}{M_{*,0}}\frac{\Delta SFR}{2}\frac{1}{2}\Delta t_m = (1.11 \times 10^{-10})\left(\frac{3}{2}\right)(0.5)(0.5 \times 10^{-9}) = 0.042 \tag{4.16}$$

For the typical galaxy mentioned above, the median gas fraction r_{gas} is determined to be 0.14 and combining with the estimate from Equation 4.16, Equation 4.15 then can be written as:

$$\Delta \log r_{gas} = \log(0.7) = -0.15 \tag{4.17}$$

So we see that the SFR increase is consistent with a decrease in the fraction of gas relative to stars, i.e. in the gas content, that is what we would expect for the simple closed box model calculated above.

Variation in Z

To estimate the variation in metallicity, the approach is very similar to what was done previously with r_{gas}. On the basis of the closed-box model for metal evolution we can write the metallicity as a function of the gas abundance as:

$$\mathrm{Z} = \mathrm{y}\ \ln \mathrm{r}_{\mathrm{gas}}^{-1} \tag{4.18}$$

and, for simplicity, assume the variation in r_{gas} to be similar to a function f_r:

$$\frac{\mathrm{r}_{\mathrm{gas,t}}}{\mathrm{r}_{\mathrm{gas,0}}} \approx \mathrm{f}_{\mathrm{r}} \tag{4.19}$$

The difference in metallicity between galaxies in a merger and isolated galaxies can therefore be written as:

$$\frac{\mathrm{Z_t}}{\mathrm{Z_0}} = \frac{\mathrm{y}_* \ \ln \mathrm{r}_{\mathrm{gas,t}}^{-1}}{\mathrm{y}_0 \ \ln \mathrm{r}_{\mathrm{gas,}}^{-1}} = \frac{\ln \mathrm{r}_{\mathrm{gas,0}}^{-1}}{\ln \mathrm{r}_{\mathrm{gas,0}}^{-1}} + \frac{\ln \mathrm{f}_{\mathrm{r}}^{-1}}{\ln \mathrm{r}_{\mathrm{gas,0}}^{-1}} \tag{4.20}$$

$$= 1 + \frac{\ln \mathrm{f}_{\mathrm{r}}}{\ln \mathrm{r}_{\mathrm{gas,0}}} \tag{4.21}$$

Then, to calculate the difference in metallicity, combining the r_{gas} which is equal to 0.14, and f_r that is calculated to be 0.7, Equation 4.21 becomes:

$$\Delta \log \mathrm{Z} = 0.072 \tag{4.22}$$

This result is consistent with the trend found in Figure 4.4, of an increase in metallicity for small projected distances.

Variation in T_R

Finally, for the variable T_R, we estimate the variation between merger and isolated galaxies assuming that T_R is given by

$$\mathrm{T_R} = \frac{\mathrm{M_{gas}}}{\mathrm{SFR}} \tag{4.23}$$

and after a time Δt_m, T_R becomes,

$$\mathrm{T_{R,t}} \approx \frac{\mathrm{M_{gas,0}} - \mathrm{SFR_0}\,\dfrac{\Delta\mathrm{SFR}}{2}\,\dfrac{1}{2}\,\Delta\mathrm{t_m}}{\mathrm{SFR_0}\,\Delta\mathrm{SFR}} \tag{4.24}$$

which gives, for the ratio between T_R for galaxies in mergers and isolated galaxies, the following relation :

$$\frac{\mathrm{T_{R,t}}}{\mathrm{T_{R,0}}} = \frac{1}{\Delta\mathrm{SFR}} - \frac{1}{4}\,\frac{\Delta\mathrm{t_m}}{\mathrm{T_{R,0}}} \tag{4.25}$$

Assuming that the median T_R for a galaxy of $M_* = 10^{10} M_\odot$ from the SDSS DR6, i.e. $T_{R,0}$, is $\sim 1.12 \times 10^9$ yr, then Equation 4.25 holds:

$$\frac{\mathrm{T_{R,t}}}{\mathrm{T_{R,0}}} = \frac{1}{3} - \frac{1}{4}\,\frac{0.5 \times 10^9}{1.11 \times 10^9} \tag{4.26}$$

and, consequently,

$$\Delta \log \mathrm{T_R} = -0.63 \tag{4.27}$$

which is in accordance with the result found for the variation in the Roberts time shown in Figure 4.6, for galaxies with projected distances below 10 kpc.

Summarizing, assuming a closed box model in the central region of galaxies, the predicted results for the different quantities as calculated analytically, are:

$$\Delta \log \mathrm{r_{gas}} = -0.15 \tag{4.28}$$

$$\Delta \log \mathrm{Z} = 0.072 \tag{4.29}$$

$$\Delta \log \mathrm{T_R} = -0.63 \tag{4.30}$$

The three results are consistent with the trends shown in Figures 4.5, 4.4 and 4.6, respectively.

Under the assumption of a simple closed box model for the central regions of galaxies, the predictions from the SFR regarding what the gas content will be, what trend would the metallicity and gas consumption time scales reveal, are consistent with our results. The blind projections concerning the change in r_{gas}, Z and T_R using analytical estimates have been shown to be consistent with each other. This lends some credibility to the notion that the central regions can be modeled as closed boxes.

Regarding previous studies, the main object of study for interacting and/or merging galaxies has been the entire galaxy where the profiles of metallicity gradients are taken into account as well as the in-falls of metal-enriched gas that produce diverse stellar populations (e.g. Kewley et al. 2006a; Michel-Dansac et al. 2008; Rupke et al. 2010; Kewley et al. 2010). Our study, being focused solely in the central regions of the galaxy, represents, to the best of our knowledge, a first approach to this subject and therefore is not possible direct a comparison between the two methods - central region vs. entire galaxy.

Future Work

Given the experimental nature of this study on the gas and metal content of merging galaxies, there is certainly more work to be done in order to establish this closed box behaviour of the central regions of merging galaxies. The first approach would be to apply this analysis to other samples of merging galaxies and investigate whether this behaviour holds. However, the lack of gas estimates, and the difficulty to get reliable measurements specially for large surveys, is a major obstacle.

A possible starting point would be to select a small sample of some nearby systems of galaxies used in this project and obtain reliable measurements - through both radio observations to map the H_I content and integrated field unit spectroscopy (IFU) to assess their SFR rigorously. This procedure could then robustly confirm the particular dynamics of the central regions of merging galaxies that, given the results presented here, seem to be quite oblivious to its surroundings.

Chapter 5

Probing single mergers

The advantages of investigating a large sample of mergers are manifold but, most importantly, such samples are crucial to build a theory for galaxy formation and evolution in the now prevailing ΛCDM cosmology, where structure grows hierarchically through mergers of ever growing clumps of matter.

Nonetheless, the exact processes behind a merger event between any two, or more, galaxies can only be understood in detail through the inspection of individual examples of merging galaxies. For instance, as referred in Chapter 1, the first clue for the importance of dry merging in building up massive galaxies was revealed by the discovery of a triple red merger at z=1.27 in the cluster RX J0848+4453 in a work by (van Dokkum et al. 2001). There is a lack of well known mergers between gas-poor galaxies, due to their almost unperturbed morphologies during the merger process and to the recent interest in this type of mergers, but other individual merger systems have been exhaustively studied specially gas-rich interacting galaxies – e.g. the Antennae, Stephan's Quintet, Whirlpool galaxy (e.g. Nikola et al. 2001; Read 2003; O'Sullivan et al. 2009). Such focused investigation allowed a better understanding of phenomena like the internal processes leading to triggered star formation or the merger dynamics causing features like tidal tails and bridges. The case for dry mergers is no different.

5.1 A subset of dry mergers

During the course of this work, in particular during the visual inspection, several interesting systems were found. At a rather low redshift (to note that the high redshift limit of the merger sample is $z = 0.2$), some of the systems in this subset of mergers consist of more than two, and possibly as many as five, elliptical galaxies with small separations. These systems were detected because at least two of the objects had spectroscopic information from the SDSS and were within the conditions for a merger mentioned in Chapter 2, with a projected distance $r_p \leq 30\,h^{-1}$kpc and velocity offset $v_{sep} \leq 800$ km/s. However, probably due in part to the limitation imposed by the placement of the fibers and to the selection of photometric targets for spectroscopic observations, most of these systems lack the spectroscopic redshift needed to assess their merging status.

Some of these systems are illustrated in Figure 5.1. The available spectra for these galaxies show no emission lines, indicative of an absence of active star formation, and the remaining galaxies have colours consistent with ellipticals at the same redshift. Our estimations point towards each of these merger candidates enclosing a total stellar mass in excess of $2.5 \times 10^{11} M_{\odot}$. The redshifts of these systems range from $z = 0.10$ to $z = 0.15$ and their projected separations are $\lesssim 20$ kpc and their velocity offsets $\leq$ 400 km/s. They may constitute key examples of the build-up of the massive end of the mass function, in particular at low redshifts.

5.2 The quintuple dry merger

One particularly interesting dry merger example is the case for a possible merger of up to five galaxies, shown in Figure 5.2 (*top*). The objects in this system have been classified by the SDSS as four galaxies and one star. However, that is most probably an incorrect classification due to the compactness of the object. This group has spectra for two of the galaxies, as indicated in Figure 5.2 *bottom*, that show no signs of star formation and place this sytem at $z \sim 0.18$. All galaxies in the image have similar r-band fluxes and colours consistent with being ellipticals at the same redshift. The galaxies with spectroscopic data are at a projected separation of <12 kpc and have a velocity offset < 410 km/s. Radio data from the Faint Images of the Radio Sky at Twenty-cm (FIRST) survey, has shown a clear detection of one of the sources (the

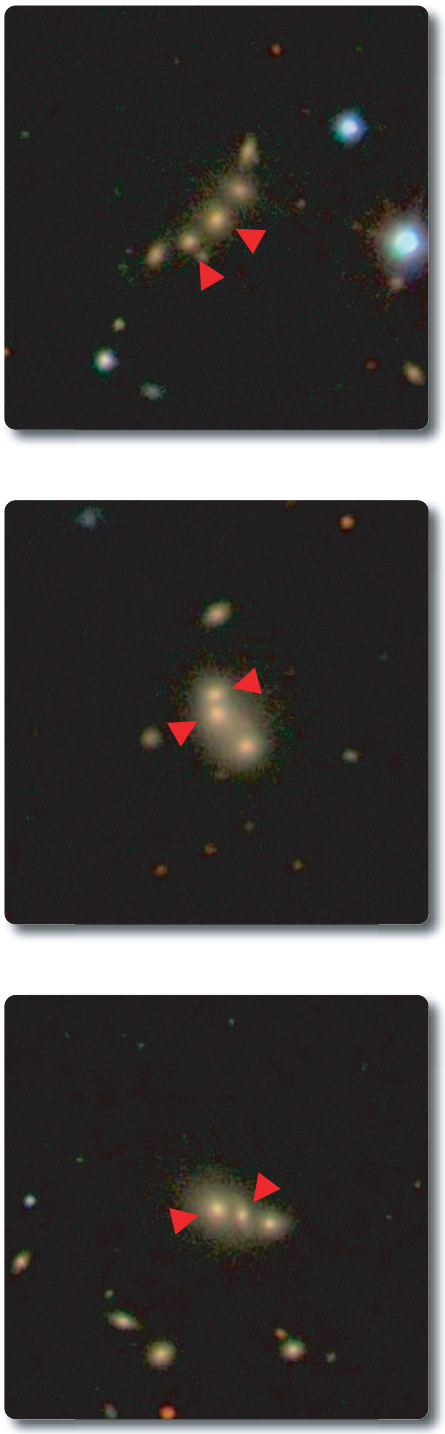

Figure 5.1: Three potential merging systems taken from the merger sample. The galaxies with existing SDSS spectra are identified by the red arrows. The images are 1' x 1' in size and are oriented with north up and west to the right.

highlighted galaxy in the left in Figure 5.2) and a possible extended region towards the direction of the other four galaxies.

Assuming a merger of four galaxies and that all sources are in fact at the same redshift, the total stellar mass for each of the elliptical galaxies in slightly below $10^{11} M\odot$ and the total mass of the merger is $\sim 3 \times 10^{11} M\odot$. There is no known overdensity around this merger, but Best et al. (2006) find that radio-loud galaxies with stellar masses $< 10^{11} M\odot$ are almost exclusively brightest central galaxies, thus there may be an undetected group around this merger, in which case we might in fact be looking at a forming brightest central galaxy. Therefore, this system may be an excellent example of the build-up of the massive end of the elliptical mass function and it should offer a number of insights into the mechanics of gas-poor mergers and how they proceed.

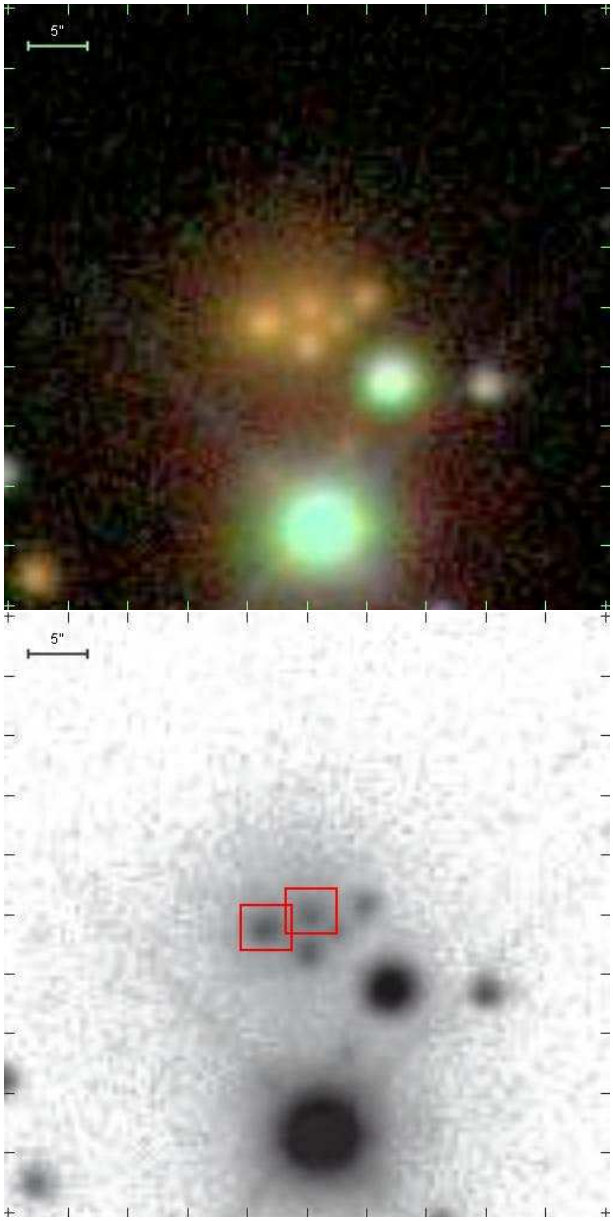

Figure 5.2: The merging system image from the SDSS DR6. The five objects are clearly seen, with the one in the right being the possibly misclassified galaxy. The green objects in top image are classified as stars by the SDSS. The red squares in the bottom image indicate the galaxies with spectroscopic information.

Chapter 6

Conclusions and Future Work

The study of merging galaxies started more than a half a century ago and even today, while some questions have been answered, our knowledge of this phenomenon is still far from complete. This holds particularly true for dry mergers, since their role in galaxy formation and evolution was recognized only a decade ago. Building the largest sample of dry mergers to date was the core of this work and analysing in detail all the information enclosed in this sample with close to 4000 merging systems, with approximately 20% being dry mergers, represents an endeavor that extends far beyond this PhD thesis.

6.1 Assembling galaxies via mergers

As galaxies come closer together during a merger event, the changes in their properties are affected, more or less severely, throughout the time-scale that the merger encompasses. During the encounter, as they approach and even collide, various processes take place from mild morphological changes, usually starting in the first stages of the merger, to violent triggering of nuclear activity in what is possibly the last stage before the galaxies have combined and no longer can be identified as two, or more, separate systems. Meanwhile, during this time, not only their shapes are changed dramatically but both the stellar and gas content of the individual galaxies can be affected, more or less strongly, at the different stages of the interaction. Having a sample of galaxies

at several stages of the merger event is then key to have an insight into how different processes change over time.

6.1.1 Star formation and nuclear activity

The enhanced star formation activity is probably the most immediate consequence of galaxy interaction. Due to tidal forces playing during the interaction, the perturbed gas in the galaxies is quickly transformed into stars, often in violent merger induced star-bursts. Benefiting from the spectroscopic information, the EW(Hα) was used as a proxy for star formation activity and that very phenomenon was observed in the galaxies of the merger sample gathered to this work. A strong relation between galaxy separation within a group and star formation activity was found and, for very close galaxies (in their late merger stages), i.e. for projected separations below 10 kpc, an enhancement up to a factor of three was found.

The nuclear activity, on the other hand, did not show the same behaviour as the star formation activity. Theoretical work has frequently proposed that a galaxy-galaxy collision may trigger the AGN activity in the galaxies in a very late stage of the merger, which could be translated into an increase of the AGN fraction towards small projected distances. Even though we have no such galaxies in our sample, we could explore the progress towards this stage, usually where the nuclei of the galaxies have coalesced into an apparently single object, were not present in our merger sample, a decrease of the fraction of AGN in the merger sample towards small separations was found. As mentioned, we make use of the classification as AGN-host galaxy, based on spectroscopic data, as described in Kauffmann et al. (2003), where a set of spectroscopic indexes classify a galaxy in star-forming, AGN or composite. The decrease of the AGN fraction was considered to be the result of the lack of detection of this AGN classifying emission lines, since the triggered star formation activity seems to veil the presence of the AGN.

6.1.2 Major and minor mergers

The role of major mergers in building up massive galaxies is expected to be more significant when compared with minor mergers, since they would be more efficient to assemble galaxies with higher masses. Our merger sample consisted of roughly the

same number of major and minor mergers, where we defined minor mergers to be those with mergers with stellar mass ratios $\geq \frac{1}{3}$ or $< \frac{1}{3}$, respectively, and major mergers have been found to play a bigger role especially above $M_* \sim 10^{11} M_\odot$.

6.1.3 Dry and non-dry mergers

Approximately 80% of the mergers in the merger sample used in this work are indeed mergers where at least one of the galaxies is gas-rich. Establishing a limit on the amount of gas that would divide the mergers into gas-poor or gas-rich is rather arbitrary since the overall properties of these galaxies has been shown to be a continuum – consequently, there is a gradual transition from dry to non-dry mergers. According to our criteria to define dry and non-dry mergers, the latter were found to be important in the intermediate and low mass parts of the galaxy mass function. The main question motivated by this work was then:

What is the role of dry-mergers in building up the most massive end of the mass function?

The fraction of galaxies in potential dry mergers in the spectroscopic SDSS DR6 sample constitutes more than 2% of the galaxies. In fact, 20% of the merger sample is made up by a large sample of mergers between gas-poor galaxies – which translates to $\sim$ 700 systems. Dry mergers have been shown to be particularly important for masses greater than $5 \times 10^{11} M_\odot$, revealing their status as building blocks for very massive galaxies - the role of dry mergers in building up the massive end of the galaxy mass function was found to be not negligible: up to 7% of the stellar mass in galaxies with masses $11.0 < \log(M_*/M\odot) < 11.6$ has been involved in this type of mergers.

This result seems to reconcile the different views on the importance of dry mergers in building up the high mass end of the galaxy mass function. Considering both major and minor dry mergers (whose importance was highlighted by López-Sanjuan et al. (2010)) we have shown that some early-type galaxies have indeed been assembled at late times, at least since $z = 0.2$, in accordance with numerous works pointing towards an increase of stellar mass enclosed in early-types for $z < 1$. Without questioning that the massive end of the mass function was mostly in place at $z \sim 1$, some evolution

appears necessary.

Even though there are a number of points to consider when comparing in detail the results of several studies – e.g. different surveys, redshift intervals, merger timescales – which can hinder a direct comparison and, therefore, the possibility of getting a clear picture of the role of dry mergers, the general directions can be patched together shaping up a new scenario for galaxy assembly through this type of mergers. To note:

- The bulk of the massive end of the mass function being already in place by $z \sim 1$ (e.g Abraham et al. 2007; Le Fevre et al. 2003; Scarlata et al. 2007)
- The increase of stellar mass enclosed in early-types since $z = 1$ (e.g. Brinchmann & Ellis 2000; Hogg et al. 2002; Renzini 2006; Scarlata et al. 2007; Bundy et al. 2009)
- The mergers between gas-rich spirals not able to reproduce the observed properties of very massive ellipticals (e.g. Bell et al. 2005; Naab et al. 2006)
- Dry mergers at late epochs are observed (e.g. van Dokkum et al. 2001; Bell et al. 2006; Masjedi et al. 2006)

These findings can be brought together by the small, yet significant, fraction of galaxies assembled via dry mergers found in this work, in particular for galaxies with stellar masses above $\log(M_*/M_\odot) > 11.0$. The increase in stellar mass in early-type galaxies is likely to come from two sources, dry mergers at very high masses and a mixture of dry and non-dry mergers at lower masses. Even though there is much work to be done in disentangling the time-scales of the mergers themselves – it seems to be the key, and probably the last major, obstacle to determine the place of dry mergers (e.g. Bundy et al. 2009; De Propris et al. 2010; Chou et al. 2011; Tojeiro & Percival 2011) – the importance of this type of mergers in building very massive galaxies is definitely significant within the sampled low redshift interval of $0.005 < z < 0.2$.

6.1.4 Environment

It could be naively expected that mergers in high density environments would be more frequent when compared with low density regions. The common understanding that

spiral, gas-rich galaxies, populate less dense regions whereas the fraction of early-type galaxies grows with density, also places mergers between early-types more probable in these regions. But of course, the higher relative velocities between the galaxies in these regions does reduce the likelihood of merging somewhat again. Using criteria outlined by Barton et al. (2007), 18% of dry mergers have been found to be truly isolated, an *ideal* setting for the merger to actually take place.

6.1.5 Gas in galaxies

Despite the gas-dependent merger classification used exhaustively throughout the literature for the past decades, obtaining reliable gas measurements is still a complex task. Moreover, gas measurements are generally available for galaxies classified as being star forming galaxies, making the analysis of the continuum of properties mentioned before even harder. Therefore, we applied the analysis of the gas in merging systems to galaxies classified as star-forming and investigated what happened in their central regions during the merger process by answering the following questions:

1. Is low-metallicity gas channelled to the center during a merger?
2. Are merging galaxies more gas rich in the center than similar isolated galaxies?
3. Is the time-scale for the consumption of the available gas to form stars identical between galaxies in mergers and isolated galaxies?

The answers to these questions led us to an unexpected scenario for the dynamics of the central regions of merging galaxies with projected separations below 10 kpc – with an increase in metallicity, coupled with a decrease in the gas to stars ratio and a decrease in the gas consumption time-scale, plus the increased star formation rate which has been studied in-depth in various studies – a simple closed box scenario is proposed, as illustrated in Figure 6.1. The central regions of galaxies seem to be quite insensitive to their surroundings, at least during the stages of the mergers up to a separation of a $\sim$ 10 kpc, without significant exchanges between the two regions. At a later stage, their central regions will most probably merge and give rise to other phenomena such as AGN feedback and/or halted star formation activity. However, the potential merging galaxies seem to start experiencing the presence of a neighbour at their very cores before the merger itself takes place.

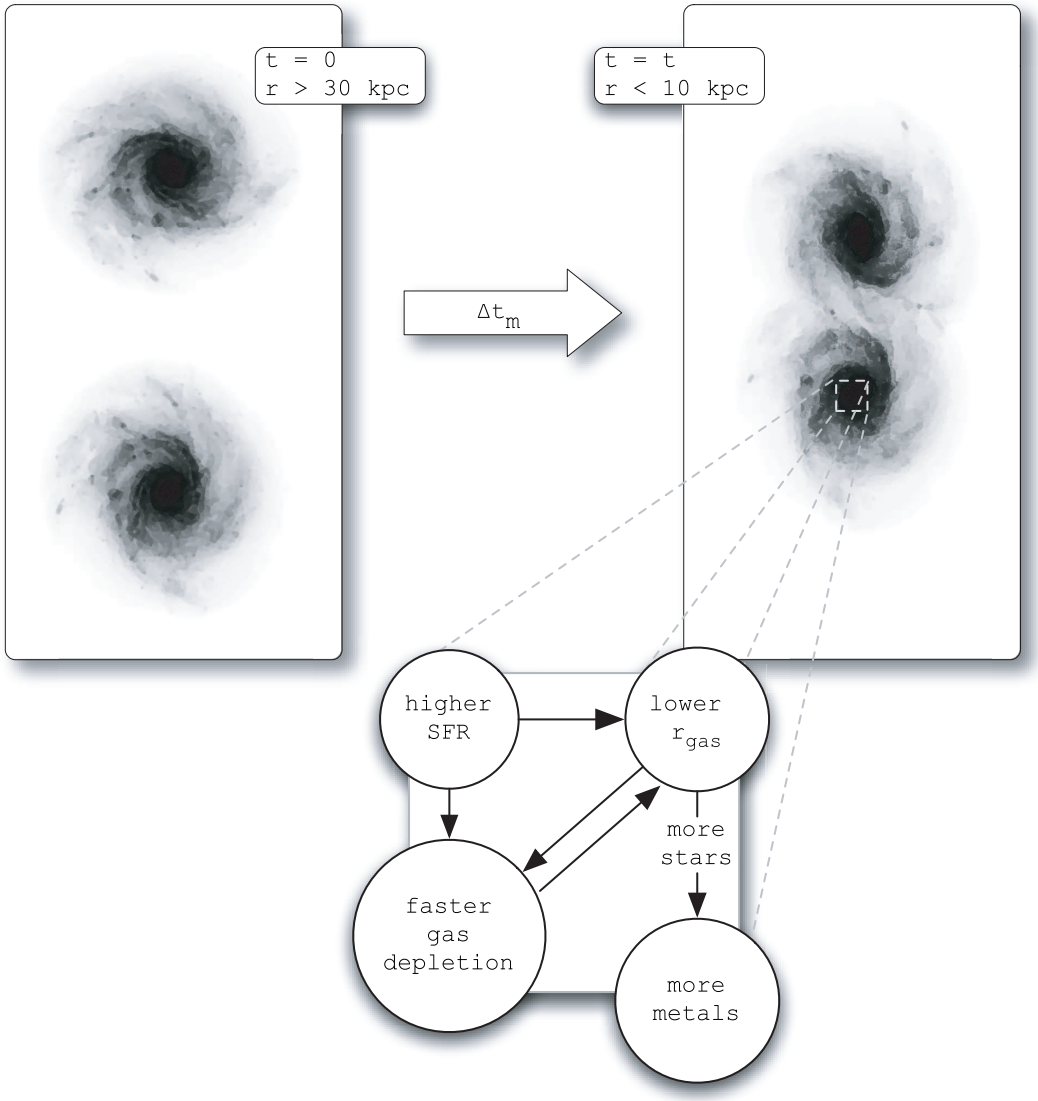

Figure 6.1: The simple closed box model for the central regions of galaxies.

6.1.6 Probing single mergers

Probably as important as the statistics of a large and complete sample of mergers of galaxies, is to understand the intrinsic processes and dynamics of the merger phenomenon. To that end, analysing in detail single mergers representative of what it is observed in the present day universe and even at higher redshifts, brings valuable information to disclose the galaxy merging process.

During the course of this work, several particularly interesting systems were identified. In particular, a possible quadruple, or even quintuple, merger of elliptical galaxies, for the moment dubbed *The Quintuplet*. This group has spectra for two of the galaxies that show no signs of star formation and place this sytem at $z \sim 0.18$. All galaxies in the image have similar colours and are consistent with being ellipticals at the same redshift. This merger candidate is estimated to enclose a total stellar mass in excess of $2 \times 10^{11} M\odot$. Thus, it may be an excellent example of the build-up of the massive end of the elliptical mass function and a confirmation of its merger status would provide observational evidence to the recent claims based on semi-analytic techniques that brightest central galaxies do evolve significantly at $z < 1$ De Lucia & Blaizot (2007).

6.2 Future work

6.2.1 Building larger merger samples

Even though the merger sample assembled in the work is among the biggest samples of mergers to date, sampling a even wider range of galaxies masses and mergers stages will inevitably lead us a step forward. Therefore, making use of the last release of the SDSS, Data Release 7, to update this merger sample is the natural course of action.

As shown in Chapter 2, upgrading the spectroscopic sample of galaxies with the photometric catalogue increases dramatically the number of potential merging systems. However, the lack of a spectroscopic redshift may pose a problem when defining what systems may be potentially merging. Because photometric redshifts are still not completely reliable and galaxies undergoing a merger have their photometry sometimes significantly altered, developing techniques to make use of photometric data only, is

critical.

6.2.2 Building smaller merger samples

Maybe as important as the statistics that only large samples of galaxies can provide, is the precision of the measurements – such as stellar mass, gas content, metallicity, dust, AGN activity – used to assess their properties. With smaller samples of potential merging galaxies, getting the necessary data is naturally less complicated (e.g. gas content) and much more information can be obtained probing other regions of the spectra – from radio to X-rays.

Furthermore, by combining data of different surveys – e.g. COSMOS (Scoville et al. 2007), GEMS (Rix et al. 2004) – smaller samples can more easily be matched, adding up more data for analysis. Another advantage of smaller, more strictly constrained, merger samples is the ability of following up on a representative set of systems that would be intimately linked to the overall sample. The complete analysis of potential merging galaxies could therefore be taken to a higher level and their details fully understood.

6.3 Final remarks

The importance of dry mergers in making up massive galaxies is nowadays under great debate. The work done in this project contributes significantly to that discussion by giving dry mergers a non-negligible role in assembling new galaxies, possibly being the only path to give rise to very massive galaxies. Future work, to which this project contributed to set the foundations of, will certainly settle the importance in building new galaxies from mergers between galaxies that are old, red and dead.

Appendix A

Volume Correction

As mentioned in Chapter 2, Section 2.1, the Main Galaxy Sample has a faint magnitude cut-off at an r-band Petrosian magnitude of 17.77 and, at the bright end, a r-band Petrosian magnitude, r_p, cut-off for objects with $r_p < 15.0$ or fiber magnitudes brighter than 15.0 in g- or r-band, or 14.5 in the i-band. Observing up to redshifts of z$\sim$ 1 and mapping close to a quarter of the entire sky, the SDSS was indeed unprecedented on the number of objects observed. However, in order to build accurate galaxy luminosity, or mass, functions, it is necessary to account for probability of a galaxy being detected in a survey and to apply the necessary corrections to guarantee that the luminosity function is not dependent on the limits of the survey but, instead, is a reliable measure of the actual space distribution of galaxies within a given luminosity interval.

The correction technique used in this work was developed by Schmidt (1968) and is usually known as the $1/V_{max}$ method. The volume V_{max} is defined by a maximum and minimum redshifts, z_{max} and z_{min}, within which a given galaxy can be detected - more luminous galaxies can be detected within larger volumes when compared to low luminosity galaxies. The z_{max} value is the maximum redshift at which a galaxy could be observed given the faint magnitude limit of the survey, and z_{min} is, similarly, the minimum redshift determined by the bright magnitude cut-off. The volume V_{max} is therefore the volume between z_{min} and z_{max} and the correction consists of weighting each galaxy by the inverse of its V_{max}, as shown in Equation A.1, where ρ_L is the space density at a given luminosity L and N_L is the total number of galaxies with that luminosity. The A term corrects for the surveyed area of the spectroscopic sample of the SDSS DR6.

$$\rho_{\rm L} = \sum_{\rm i=1}^{\rm N_L} \frac{1}{\rm V_{max}^{i}} \times {\rm A} \tag{A.1}$$

$$\rm A \;=\; \frac{Area_{\,sky}}{Area_{\,SDSS\,DR6}} \;=\; \frac{41252\ deg^2}{7425\ deg^2} \;=\; 5.56$$

Appendix B

An illustrative set of mergers from the merger sample

Table B.1: A set of potential mergers drawn from the merger sample.

Image	Merger ID	Projected Distance (kpc)	Velocity Offset (km/s)
	00022	21.877	85.889
	00037	9.201	346.231
	00061	26.616	87.963
	00062	21.274	39.920

Continued on next page

Table B.1 – *continued from previous page*

Image	Merger ID	Projected Distance (kpc)	Velocity Offset (km/s)
	00069	29.490	211.101
	00080	10.636	181.094
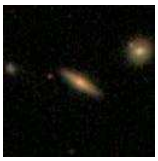	00081	31.395	176.284
	00083	22.633	111.964
	00108	14.347	322.907
	00109	26.772	353.160
	00114	24.831	26.842
	00161	15.980	44.008
	00163	5.507	112.765

Continued on next page

Table B.1 – *continued from previous page*

Image	Merger ID	Projected Distance (kpc)	Velocity Offset (km/s)
	00201	27.423	443.597
	00202	9.977	168.349
	00276	5.708	56.957
	00315	31.947	206.257
	00370	26.375	239.251
	00371	10.382	50.602
	00374	12.869	120.903
	00396	30.726	108.053
	00407	21.748	484.181

Continued on next page

Table B.1 – *continued from previous page*

Image	Merger ID	Projected Distance (kpc)	Velocity Offset (km/s)
	00446	22.056	588.132
	00447	27.634	1.030
	00449	19.734	66.814
	00477	11.959	495.274
	00478	29.508	451.612
	00508	25.958	310.611
	00509	27.286	142.705
	00543	4.758	40.553
	00560	23.439	169.670

Continued on next page

Table B.1 – *continued from previous page*

Image	Merger ID	Projected Distance (kpc)	Velocity Offset (km/s)
	00593	19.874	427.178
	00697	14.638	226.001
	00825	12.655	444.648
	00833	29.179	143.903
	00839	22.342	234.443
	00862	12.766	520.892
	00863	19.356	266.656
	00868	4.757	132.244
	00872	26.335	260.713

Continued on next page

Table B.1 – *continued from previous page*

Image	Merger ID	Projected Distance (kpc)	Velocity Offset (km/s)
	00912	3.627	122.076
	00977	4.577	43.217
	00981	19.416	53.684
	01000	16.964	16.558
	01046	3.085	78.122
	01050	26.814	510.715
	01053	13.916	794.253
	01054	30.589	1.931
	01055	17.805	191.778

Continued on next page

Table B.1 – *continued from previous page*

Image	Merger ID	Projected Distance (kpc)	Velocity Offset (km/s)
	01082	27.480	94.007
	01136	25.791	620.160
	01154	6.442	69.277
	01249	17.048	53.854
	01298	30.677	25.313
	01334	27.947	135.163
	01345	25.871	209.557
	01383	20.358	41.071
	01384	4.602	508.428

Continued on next page

Table B.1 – *continued from previous page*

Image	Merger ID	Projected Distance (kpc)	Velocity Offset (km/s)
	01391	23.681	246.879
	01395	9.124	321.235
	01414	5.871	363.509
	01458	27.807	636.625
	01591	6.550	251.647
	01595	7.203	218.423
	01599	22.146	509.197
	01621	11.750	267.854
	01624	5.840	339.326

Continued on next page

Table B.1 – *continued from previous page*

Image	Merger ID	Projected Distance (kpc)	Velocity Offset (km/s)
	01625	14.987	185.747
	01626	19.759	115.239
	01634	4.034	106.314
	01635	11.580	53.412
	01641	21.992	182.786
	01647	6.997	48.897
	01651	11.602	15.648
	01660	15.528	53.890
	01758	28.276	3.449

Continued on next page

Table B.1 – *continued from previous page*

Image	Merger ID	Projected Distance (kpc)	Velocity Offset (km/s)
	01766	12.856	95.341
	01772	16.604	322.276
	01774	6.489	20.443
	01778	7.150	37.971
	01791	17.124	389.222
	01801	7.073	103.368
	01802	28.237	166.002
	01877	22.795	57.165
	01892	24.105	67.717

Continued on next page

Table B.1 – *continued from previous page*

Image	Merger ID	Projected Distance (kpc)	Velocity Offset (km/s)
	01923	27.773	93.287
	01964	23.489	317.878
	01974	13.423	110.976
	01996	20.676	171.883
	02015	31.611	45.542
	02068	7.382	8.357
	02185	26.222	20.186
	02194	24.597	94.640
	02230	17.868	126.026

Continued on next page

Table B.1 – *continued from previous page*

Image	Merger ID	Projected Distance (kpc)	Velocity Offset (km/s)
	02295	28.490	55.497
	02314	13.228	137.034
	02315	11.034	153.353
	02323	29.913	67.142
	02353	8.184	561.476
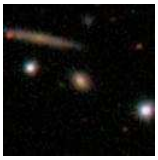	02385	27.447	65.274
	02410	12.301	144.631
	02411	6.554	160.166
	02426	9.756	13.945

Continued on next page

Table B.1 – *continued from previous page*

Image	Merger ID	Projected Distance (kpc)	Velocity Offset (km/s)
	02447	2.133	4.106
	02532	24.251	321.724
	02533	9.518	263.337
	02534	13.711	162.868
	02543	15.375	34.066
	02567	16.940	500.080
	02589	24.985	31.337
	02602	22.360	58.479
	02609	22.557	724.337

Continued on next page

Table B.1 – *continued from previous page*

Image	Merger ID	Projected Distance (kpc)	Velocity Offset (km/s)
	02675	10.916	159.969
	02731	10.723	248.659
	02798	12.217	543.581
	02803	31.020	46.992
	02918	22.473	407.515
	02944	30.653	82.677
	02947	29.747	81.045
	02949	27.940	79.519
	02950	16.912	85.752

Continued on next page

Table B.1 – *continued from previous page*

Image	Merger ID	Projected Distance (kpc)	Velocity Offset (km/s)
	02955	31.068	142.977
	03008	23.665	27.848
	03016	21.666	394.859
	03065	27.671	178.405
	03067	26.143	14.459
	03123	31.333	173.530
	03240	12.987	100.306
	03248	18.450	138.339
	03260	16.445	339.874

Continued on next page

Table B.1 – *continued from previous page*

Image	Merger ID	Projected Distance (kpc)	Velocity Offset (km/s)
	03263	8.559	126.077
	03264	15.335	589.968
	03265	25.231	207.393
	03266	3.776	172.862
	03269	8.513	196.353
	03276	13.112	443.628
	03285	13.648	144.772
	03307	18.149	229.834
	03313	16.367	148.483

Continued on next page

Table B.1 – *continued from previous page*

Image	Merger ID	Projected Distance (kpc)	Velocity Offset (km/s)
	03342	20.482	208.969
	03350	31.537	35.955
	03362	8.978	392.709
	03489	26.217	255.020
	03497	4.904	39.411
	03522	8.171	105.288
	03538	9.828	26.277
	03543	23.477	277.461
	03618	28.327	179.788

Continued on next page

Table B.1 – *continued from previous page*

Image	Merger ID	Projected Distance (kpc)	Velocity Offset (km/s)
	03631	20.849	237.785
	03633	24.574	210.158
	03646	27.019	140.485
	03650	25.993	191.434
	03673	15.086	92.071
	03693	10.064	146.779
	03698	19.103	123.741
	03729	12.242	13.418
	03782	20.776	29.243

Continued on next page

Table B.1 – *continued from previous page*

Image	Merger ID	Projected Distance (kpc)	Velocity Offset (km/s)
	03832	21.441	145.271
	03941	20.296	35.655

References

Abadi, M. G., Moore, B., & Bower, R. G. 1999, MNRAS, 308, 947

Abazajian, K. N., Adelman-McCarthy, J. K., Agüeros, M. A., et al. 2009, ApJS, 182, 543

Abraham, R. G., Glazebrook, K., McCarthy, P. J., et al. 2004, AJ, 127, 2455

Abraham, R. G., Nair, P., McCarthy, P. J., et al. 2007, ApJ, 669, 184

Adelman-McCarthy, J. K., Agüeros, M. A., Allam, S. S., et al. 2008, ApJS, 175, 297

Adelman-McCarthy, J. K., Agüeros, M. A., Allam, S. S., et al. 2006, ApJS, 162, 38

Baldry, I. K., Glazebrook, K., Brinkmann, J., et al. 2004, ApJ, 600, 681

Baldwin, J. A., Phillips, M. M., & Terlevich, R. 1981, PASP, 93, 5

Barazza, F. D., Wolf, C., Gray, M. E., et al. 2009, A&A, 508, 665

Barnes, J. E. 1988, ApJ, 331, 699

Barnes, J. E. & Hernquist, L. 1992, ARA&A, 30, 705

Barnes, J. E. & Hernquist, L. 1996, ApJ, 471, 115

Barton, E. J., Arnold, J. A., Zentner, A. R., Bullock, J. S., & Wechsler, R. H. 2007, ApJ, 671, 1538

Beckwith, S. V. W., Stiavelli, M., Koekemoer, A. M., et al. 2006, AJ, 132, 1729

Bekki, K., Couch, W. J., & Shioya, Y. 2002, ApJ, 577, 651

Bell, E. F., Naab, T., McIntosh, D. H., et al. 2006, ApJ, 640, 241

Bell, E. F., Papovich, C., Wolf, C., et al. 2005, ApJ, 625, 23

Bell, E. F., Wolf, C., Meisenheimer, K., et al. 2004, ApJ, 608, 752

Belokurov, V., Zucker, D. B., Evans, N. W., et al. 2006, ApJ, 642, L137

Bennett, C. L., Bay, M., Halpern, M., et al. 2003, ApJ, 583, 1

Bertone, G., Hooper, D., & Silk, J. 2005, Phys. Rep., 405, 279

Best, P. N., Kaiser, C. R., Heckman, T. M., & Kauffmann, G. 2006, MNRAS, 368, L67

Binggeli, B., Sandage, A., & Tammann, G. A. 1988, ARA&A, 26, 509

Binney, J. & Tremaine, S. 1987, Galactic Dynamics, Princeton Series in Astrophysics (Princeton, U.S.A.: Princeton University Press)

Blanton, M. R., Eisenstein, D., Hogg, D. W., Schlegel, D. J., & Brinkmann, J. 2005, ApJ, 629, 143

Blanton, M. R., Lin, H., Lupton, R. H., et al. 2003, AJ, 125, 2276

Boulanger, F., Baud, B., & van Albada, G. D. 1985, A&A, 144, L9

Bouwens, R. J., Illingworth, G. D., Labbe, I., et al. 2011, Nature, 469, 504

Bouwens, R. J., Illingworth, G. D., Oesch, P. A., et al. 2010, ApJ, 709, L133

Bower, R. G., Benson, A. J., Malbon, R., et al. 2006, MNRAS, 370, 645

Brinchmann, J., Charlot, S., White, S. D. M., et al. 2004, MNRAS, 351, 1151

Brinchmann, J. & Ellis, R. S. 2000, ApJ, 536, L77

Brocklehurst, M. 1971, MNRAS, 153, 471

Bruzual, G. & Charlot, S. 2003, MNRAS, 344, 1000

Bundy, K., Ellis, R. S., & Conselice, C. J. 2005, ApJ, 625, 621

Bundy, K., Ellis, R. S., Conselice, C. J., et al. 2006, ApJ, 651, 120

Bundy, K., Fukugita, M., Ellis, R. S., et al. 2009, ApJ, 697, 1369

Bundy, K., Treu, T., & Ellis, R. S. 2007, ApJ, 665, L5

Carlberg, R. G., Cohen, J. G., Patton, D. R., et al. 2000, ApJ, 532, L1

Catinella, B., Schiminovich, D., Kauffmann, G., et al. 2010, MNRAS, 403, 683

Charlot, S. & Fall, S. M. 2000, ApJ, 539, 718

Charlot, S., Kauffmann, G., Longhetti, M., et al. 2002, MNRAS, 330, 876

Chou, R. C. Y., Bridge, C. R., & Abraham, R. G. 2011, AJ, 141, 87

Cimatti, A. 2007, in Astronomical Society of the Pacific Conference Series, Vol. 380, Deepest Astronomical Surveys, ed. J. Afonso, H. C. Ferguson, B. Mobasher, & R. Norris, 51–+

Cimatti, A. 2009, in American Institute of Physics Conference Series, Vol. 1111, American Institute of Physics Conference Series, ed. G. Giobbi, A. Tornambe, G. Raimondo, M. Limongi, L. A. Antonelli, N. Menci, & E. Brocato, 191–198

Ciotti, L., Lanzoni, B., & Volonteri, M. 2007, ApJ, 658, 65

Colless, M., Dalton, G., Maddox, S., et al. 2003, VizieR Online Data Catalog, 7226, 0

Connolly, A. J., Szalay, A. S., Bershady, M. A., Kinney, A. L., & Calzetti, D. 1995, AJ, 110, 1071

Cowie, L. L. & Barger, A. J. 2008, ApJ, 686, 72

Cowie, L. L., Songaila, A., Hu, E. M., & Cohen, J. G. 1996, AJ, 112, 839

Croton, D. J., Springel, V., White, S. D. M., et al. 2006, MNRAS, 365, 11

Dame, T. M., Hartmann, D., & Thaddeus, P. 2001, ApJ, 547, 792

Darg, D. W., Kaviraj, S., Lintott, C. J., et al. 2010, MNRAS, 401, 1043

de Grijs, R., Lee, J. T., Mora Herrera, M. C., Fritze-v. Alvensleben, U., & Anders, P. 2003, New Astronomy, 8, 155

De Lucia, G. & Blaizot, J. 2007, MNRAS, 375, 2

De Lucia, G., Springel, V., White, S. D. M., Croton, D., & Kauffmann, G. 2006, MNRAS, 366, 499

De Propris, R., Driver, S. P., Colless, M., et al. 2010, AJ, 139, 794

de Ravel, L., Le Fèvre, O., Tresse, L., et al. 2009, A&A, 498, 379

Dekel, A. & Silk, J. 1986, ApJ, 303, 39

Di Matteo, T., Springel, V., & Hernquist, L. 2005, Nature, 433, 604

di Serego Alighieri, S., Lanzoni, B., & Jørgensen, I. 2006, ApJ, 647, L99

Diemand, J. & Moore, B. 2009, ArXiv e-prints

Domingue, D. L., Xu, C. K., Jarrett, T. H., & Cheng, Y. 2009, ApJ, 695, 1559

Dopita, M. A. 1985, ApJ, 295, L5

Eggen, O. J., Lynden-Bell, D., & Sandage, A. R. 1962, ApJ, 136, 748

Eisenstein, D. J., Annis, J., Gunn, J. E., et al. 2001, AJ, 122, 2267

Eliche-Moral, M. C., Balcells, M., Aguerri, J. A. L., & González-García, A. C. 2006, A&A, 457, 91

Eliche-Moral, M. C., Prieto, M., Gallego, J., & Zamorano, J. 2010, ArXiv e-prints

Ellison, S. L., Patton, D. R., Simard, L., & McConnachie, A. W. 2008, AJ, 135, 1877

Emsellem, E., Cappellari, M., Krajnović, D., et al. 2007, MNRAS, 379, 401

Faber, S. M., Willmer, C. N. A., Wolf, C., et al. 2007, ApJ, 665, 265

Franx, M., Labbé, I., Rudnick, G., et al. 2003, ApJ, 587, L79

Gallazzi, A., Charlot, S., Brinchmann, J., & White, S. D. M. 2006, MNRAS, 370, 1106

Garnett, D. R. 2002, ApJ, 581, 1019

Garnett, D. R. & Shields, G. A. 1987, ApJ, 317, 82

Gunn, J. E., Carr, M., Rockosi, C., et al. 1998, AJ, 116, 3040

Gunn, J. E. et al. 2006, AJ, 131, 2332

Haehnelt, M. G. 1995, MNRAS, 273, 249

Hammer, F., Flores, H., Puech, M., et al. 2009, A&A, 507, 1313

Hausman, M. A. & Ostriker, J. P. 1978, ApJ, 224, 320

Heyl, J. S., Cole, S., Frenk, C. S., & Navarro, J. F. 1995, MNRAS, 274, 755

Hogg, D. 2006, in The Fabulous Destiny of Galaxies: Bridging Past and Present, ed. V. Le Brun, A. Mazure, S. Arnouts, & D. Burgarella, 41–+

Hogg, D. W., Blanton, M., Strateva, I., et al. 2002, AJ, 124, 646

Hopkins, P. F., Hernquist, L., Cox, T. J., Keres, D., & Wuyts, S. 2009a, ApJ, 691, 1424

Hopkins, P. F., Somerville, R. S., Cox, T. J., et al. 2009b, MNRAS, 397, 802

Huang, S. & Gu, Q. 2009, MNRAS, 398, 1651

Jarosik, N., Bennett, C. L., Dunkley, J., et al. 2011, ApJS, 192, 14

Jesseit, R., Naab, T., Peletier, R. F., & Burkert, A. 2007, MNRAS, 376, 997

Jorgensen, I., Franx, M., & Kjaergaard, P. 1996, MNRAS, 280, 167

Jurić, M., Ivezić, Ž., Brooks, A., et al. 2008, ApJ, 673, 864

Kauffmann, G. & Charlot, S. 1998, MNRAS, 297, L23+

Kauffmann, G. & Haehnelt, M. 2000, MNRAS, 311, 576

Kauffmann, G., Heckman, T. M., Tremonti, C., et al. 2003, MNRAS, 346, 1055

Kauffmann, G., White, S. D. M., & Guiderdoni, B. 1993, MNRAS, 264, 201

Kaviraj, S., Khochfar, S., Schawinski, K., et al. 2008, MNRAS, 388, 67

Kawata, D. & Mulchaey, J. S. 2008, ApJ, 672, L103

Kennicutt, Jr., R. C. & Kent, S. M. 1983, AJ, 88, 1094

Kennicutt, Jr., R. C., Tamblyn, P., & Congdon, C. E. 1994, ApJ, 435, 22

Kereš, D., Katz, N., Weinberg, D. H., & Davé, R. 2005, MNRAS, 363, 2

Kewley, L. J., Geller, M. J., & Barton, E. J. 2006a, AJ, 131, 2004

Kewley, L. J., Groves, B., Kauffmann, G., & Heckman, T. 2006b, MNRAS, 372, 961

Kewley, L. J., Rupke, D., Jabran Zahid, H., Geller, M. J., & Barton, E. J. 2010, ApJ, 721, L48

Khochfar, S. & Burkert, A. 2003, ApJ, 597, L117

Khochfar, S. & Silk, J. 2009, MNRAS, 397, 506

Kolb, E. W. & Turner, M. S. 1990, The early universe

Kormendy, J. & Bender, R. 1996, ApJ, 464, L119+

Lake, G. & Moore, B. 1999, in IAU Symposium, Vol. 186, Galaxy Interactions at Low and High Redshift, ed. J. E. Barnes & D. B. Sanders, 393–+

Larson, R. B. 1975, MNRAS, 173, 671

Le Fevre, O., Vettolani, G., Maccagni, D., et al. 2003, in Society of Photo-Optical Instrumentation Engineers (SPIE) Conference Series, Vol. 4834, Society of Photo-Optical Instrumentation Engineers (SPIE) Conference Series, ed. P. Guhathakurta, 173–182

Lequeux, J., Combes, F., Dantel-Fort, M., et al. 1998, A&A, 334, L9

Lequeux, J., Peimbert, M., Rayo, J. F., Serrano, A., & Torres-Peimbert, S. 1979, A&A, 80, 155

Leroy, A. K., Walter, F., Bigiel, F., et al. 2009, AJ, 137, 4670

Li, C., Kauffmann, G., Heckman, T. M., Jing, Y. P., & White, S. D. M. 2008, MNRAS, 385, 1903

Lilly, S. J., Le Fevre, O., Crampton, D., Hammer, F., & Tresse, L. 1995, ApJ, 455, 50

Lin, L., Koo, D. C., Willmer, C. N. A., et al. 2004, ApJ, 617, L9

Liu, F. S., Mao, S., Deng, Z. G., Xia, X. Y., & Wen, Z. L. 2009, MNRAS, 396, 2003

López-Sanjuan, C., Balcells, M., Pérez-González, P. G., et al. 2010, ApJ, 710, 1170

Lotz, J. M., Davis, M., Faber, S. M., et al. 2008a, ApJ, 672, 177

Lotz, J. M., Jonsson, P., Cox, T. J., & Primack, J. R. 2008b, MNRAS, 391, 1137

Lotz, J. M., Jonsson, P., Cox, T. J., & Primack, J. R. 2010, MNRAS, 404, 575

Maller, A. H., Katz, N., Kereš, D., Davé, R., & Weinberg, D. H. 2006, ApJ, 647, 763

Mannucci, F., Cresci, G., Maiolino, R., Marconi, A., & Gnerucci, A. 2010, MNRAS, 408, 2115

Mapelli, M. & Moore, B. 2009, ArXiv e-prints

Marchesini, D., van Dokkum, P. G., Förster Schreiber, N. M., et al. 2009, ApJ, 701, 1765

Marzke, R. O., da Costa, L. N., Pellegrini, P. S., Willmer, C. N. A., & Geller, M. J. 1998, ApJ, 503, 617

Masjedi, M., Hogg, D. W., Cool, R. J., et al. 2006, ApJ, 644, 54

Mateus, A. 2008, ArXiv e-prints

Michel-Dansac, L., Lambas, D. G., Alonso, M. S., & Tissera, P. 2008, MNRAS, 386, L82

Mihos, C. 2003, ArXiv Astrophysics e-prints

Mihos, J. C. 1995, ApJ, 438, L75

Mihos, J. C., Richstone, D. O., & Bothun, G. D. 1992, ApJ, 400, 153

Minchev, I., Quillen, A. C., Williams, M., et al. 2009, MNRAS, 396, L56

Moore, B., Katz, N., Lake, G., Dressler, A., & Oemler, A. 1996, Nature, 379, 613

Moore, B., Lake, G., & Katz, N. 1998, ApJ, 495, 139

Moran, S. M., Kauffmann, G., Heckman, T. M., et al. 2010, ApJ, 720, 1126

Morganti, R., de Zeeuw, P. T., Oosterloo, T. A., et al. 2006, MNRAS, 371, 157

Naab, T. & Burkert, A. 2003, ApJ, 597, 893

Naab, T., Khochfar, S., & Burkert, A. 2006, ApJ, 636, L81

Naab, T. & Ostriker, J. P. 2009, ApJ, 690, 1452

Navarro, J. F., Frenk, C. S., & White, S. D. M. 1996, ApJ, 462, 563

Negroponte, J. & White, S. D. M. 1983, MNRAS, 205, 1009

Newberg, H. J., Yanny, B., Rockosi, C., et al. 2002, ApJ, 569, 245

Newberg, H. J., Yanny, B., & Willett, B. A. 2009, ApJ, 700, L61

Niederste-Ostholt, M., Belokurov, V., Evans, N. W., & Peñarrubia, J. 2010, ApJ, 712, 516

Nikola, T., Geis, N., Herrmann, F., et al. 2001, ApJ, 561, 203

O'Sullivan, E., Giacintucci, S., Vrtilek, J. M., Raychaudhury, S., & David, L. P. 2009, ApJ, 701, 1560

Park, C. & Hwang, H. S. 2009, ApJ, 699, 1595

Patton, D. R. & Atfield, J. E. 2008, ApJ, 685, 235

Patton, D. R., Carlberg, R. G., Marzke, R. O., et al. 2000, ApJ, 536, 153

Patton, D. R., Pritchet, C. J., Carlberg, R. G., et al. 2002, ApJ, 565, 208

Patton, D. R., Pritchet, C. J., Yee, H. K. C., Ellingson, E., & Carlberg, R. G. 1997, ApJ, 475, 29

Peng, Y.-j., Lilly, S. J., Kovač, K., et al. 2010, ApJ, 721, 193

Penzias, A. A. & Wilson, R. W. 1965, ApJ, 142, 419

Petrosian, A., McLean, B., Allen, R. J., et al. 2002, AJ, 123, 2280

Pozzetti, L., Bolzonella, M., Lamareille, F., et al. 2007, A&A, 474, 443

Purcell, C. W., Bullock, J. S., Tollerud, E. J., Rocha, M., & Chakrabarti, S. 2011, Nature, 477, 301

Read, A. M. 2003, MNRAS, 342, 715

Renzini, A. 2006, ARA&A, 44, 141

Richard, S., Brook, C. B., Martel, H., et al. 2010, MNRAS, 402, 1489

Rix, H.-W., Barden, M., Beckwith, S. V. W., et al. 2004, ApJS, 152, 163

Roberts, M. S. 1963, ARA&A, 1, 149

Rupke, D. S. N., Kewley, L. J., & Chien, L.-H. 2010, ApJ, 723, 1255

Ryder, S. D. & Dopita, M. A. 1993, ApJS, 88, 415

Sanchez-Blazquez, P., Gibson, B. K., Kawata, D., Cardiel, N., & Balcells, M. 2009, ArXiv e-prints

Scarlata, C., Carollo, C. M., Lilly, S. J., et al. 2007, ApJS, 172, 494

Schechter, P. 1976, ApJ, 203, 297

Schlegel, D. J., Finkbeiner, D. P., & Davis, M. 1998, ApJ, 500, 525

Schmidt, M. 1968, ApJ, 151, 393

Schweizer, F. 1986, Science, 231, 227

Schweizer, F. & Seitzer, P. 1992, AJ, 104, 1039

Schweizer, F., Seitzer, P., Faber, S. M., et al. 1990, ApJ, 364, L33

Scoville, N., Abraham, R. G., Aussel, H., et al. 2007, ApJS, 172, 38

Shimasaku, K., Fukugita, M., Doi, M., et al. 2001, AJ, 122, 1238

Silk, J. 1997, ApJ, 481, 703

Silk, J. & Rees, M. J. 1998, A&A, 331, L1

Springel, V., Di Matteo, T., & Hernquist, L. 2005a, ApJ, 620, L79

Springel, V., Di Matteo, T., & Hernquist, L. 2005b, MNRAS, 361, 776

Springel, V., Frenk, C. S., & White, S. D. M. 2006, Nature, 440, 1137

Springel, V., Wang, J., Vogelsberger, M., et al. 2008, MNRAS, 391, 1685

Springel, V., White, S. D. M., Jenkins, A., et al. 2005c, Nature, 435, 629

Stoughton, C., Lupton, R. H., Bernardi, M., et al. 2002, AJ, 123, 485

Strateva, I., Ivezić, Ž., Knapp, G. R., et al. 2001, AJ, 122, 1861

Strauss, M. A., Weinberg, D. H., Lupton, R. H., et al. 2002, AJ, 124, 1810

Strigari, L. E., Bullock, J. S., Kaplinghat, M., et al. 2008, Nature, 454, 1096

SubbaRao, M., Frieman, J., Bernardi, M., et al. 2002, in Society of Photo-Optical Instrumentation Engineers (SPIE) Conference Series, Vol. 4847, Society of Photo-Optical Instrumentation Engineers (SPIE) Conference Series, ed. J.-L. Starck & F. D. Murtagh, 452–460

Thomas, D., Maraston, C., Bender, R., & Mendes de Oliveira, C. 2005, ApJ, 621, 673

Tinsley, B. M. 1980, Fund. Cosmic Phys., 5, 287

Tojeiro, R. & Percival, W. J. 2011, MNRAS, 417, 1114

Toomre, A. 1977, in Evolution of Galaxies and Stellar Populations, ed. B. M. Tinsley & R. B. Larson, 401–+

Toomre, A. & Toomre, J. 1972, apj, 178, 623

Tran, K., van Dokkum, P., Franx, M., et al. 2005, ApJ, 627, L25

Tremonti, C. A., Heckman, T. M., Kauffmann, G., et al. 2004, ApJ, 613, 898

van Dokkum, P. G. 2005, AJ, 130, 2647

van Dokkum, P. G., Franx, M., Fabricant, D., Kelson, D. D., & Illingworth, G. D. 1999, ApJ, 520, L95

van Dokkum, P. G., Stanford, S. A., Holden, B. P., et al. 2001, ApJ, 552, L101

White, S. D. M. & Frenk, C. S. 1991, ApJ, 379, 52

White, S. D. M. & Rees, M. J. 1978, MNRAS, 183, 341

Williams, R. E., Baum, S., Bergeron, L. E., et al. 2000, AJ, 120, 2735

Williams, R. E., Blacker, B., Dickinson, M., et al. 1996, AJ, 112, 1335

Yagi, M., Kashikawa, N., Sekiguchi, M., et al. 2002, AJ, 123, 87

Yip, C. W., Connolly, A. J., Szalay, A. S., et al. 2004, AJ, 128, 585

York, D. G., Adelman, J., Anderson, Jr., J. E., et al. 2000, AJ, 120, 1579

Young, J. S., Allen, L., Kenney, J. D. P., Lesser, A., & Rownd, B. 1996, AJ, 112, 1903

Zaritsky, D. 1993, PASP, 105, 1006

Zwicky, F. 1953, Physics Today, 6, 7